TOWARDS IMPROVED INSECT MONITORING SYSTEMS USING UHF RFID AND OTHER PASSIVE ASYMMETRIC DIGITAL RADIO TECHNOLOGIES

DIPL.-PHYS. PASCAL HIRSCH (UNIVERSITÄT BONN)

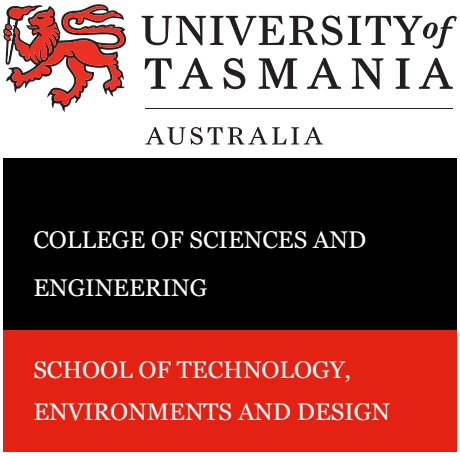

Submitted in fulfilment of the requirements for the degree of

Doctor of Philosophy

School of Technology, Environments and Design
Department of Information & Communication Technology

University of Tasmania

2019-04-08

TABLE OF CONTENTS

LIST OF FIGURES

LIST OF TABLES

ACRONYMS

AC Alternating Current

bps Bits per Second

dBm Decibels relative to 1 mW (i.e.: 0 dBm = 1 mW, 10 dBm = 10 mW, 20 dBm = 100 mW)

DC Direct Current

EC-FDTD Equivalent Circuit Finite Difference Time Domain

EPC Electronic Product Code

FDTD Finite Difference Time Domain

GIHH Global Initiative for Honeybee Health

GNSS Global Navigation Satellite System

IC Integrated Circuit

ISO International Organization for Standardization

ITV Instituto Tecnológico Vale

PCB Printed Circuit Board

PIT Passive Integrated Transponder

RFID Radiofrequency Identification

RSSI Received Signal Strength Indicator

SSH Secure Shell

UART Universal Asynchronous Receiver-Transmitter

UHF Ultra High Frequency

USB Universal Serial Bus

VHF Very High Frequency

ABSTRACT

Radio technology has been used as a tool to gain insights into animal behaviour since the 1960s when it was first used to monitor animal locations using animal-mounted transmitters. Since then, ongoing miniaturisation accompanied by cost reduction has enabled new applications in this area, e.g. detecting large numbers of individually tagged insects in a few selected locations using RFID technology or tracking the location of a small number of tagged insects (typically less than 10) over distances of more than 100 m using harmonic radar. It is however still impossible to track a large number of individually tagged small animals over distances exceeding a few cm. Yet exactly this combination would be required to gain more insight into the behaviour of honey bees *(Apis mellifera)*, which are crucial for human food production but whose populations have declined steeply in many areas of the world.

Presented in two parts, this thesis investigates different aspects of using asymmetric digital radio technology for automatically monitoring a large number of individually tagged small social animals such as honey bees *(Apis mellifera)*.

The first part focuses on the prospects and challenges of using UHF RFID as a cost effective automatic monitoring technology.

The second part addresses the limitations in detection range inherent to UHF RFID as demonstrated in the first part. It presents a roadmap to developing a new class of digitally modulating passive radio tags combining ideas from harmonic radar and RFID, which allows to suppress unwanted reflections of the interrogation signal from the environment (also called 'clutter'), aiming to increase tag detection range.

Below, I describe both parts in more detail.

In the first part, as part of the research a very affordable first prototype monitoring system based on a compact off-the-shelf USB RFID reader module equipped with a single internal antenna was developed and built. Field trials testing this prototype on honey bees showed that this system is able to capture RFID tag detection data which allows to detect temporal variations in hive activity levels. This

data also provides some information about tag recapture and tag reading longevity rates. However, it quickly became apparent that the data quality achievable by this system was limited. For example, with just a single antenna the system could not detect whether the tagged bees were entering or leaving the hive.

This problem was addressed by another field trial using two of these RFID reader modules in tandem connected to a single control computer, operating alternatingly. Analysis of this data revealed that the reader modules only achieved low detection rates. Unfortunately, both trials frequently suffered from system failures due to overheating and some unknown technical issues, further reducing data quality.

To better understand the low detection rates observed in the field experiments, a lab-based robotic measurement system to scan the spatial structure of the detectability range of our tags in the near field of a reader antenna was developed. Measurements performed with this system revealed that the detection range of the RFID reader modules in combination with our tags was limited to less than 10 mm.

These insights lead to the development of an improved detection system based on a more capable industrial RFID reader module supporting up to 4 antennas which addresses the needs of CSIRO's Global Initiative for Honeybee Health.

Based on detection range measurements and electromagnetic simulations, an optimized arrangement of four commercially available RFID antennas was devised. Consisting of two opposing pairs of compact ceramic patch antennas, this arrangement lead to dramatically improved detection rates which were confirmed in further field trials using this new system in the course of an honours thesis within our group.

The second part addresses the tight detection range limits inherent to UHF RFID while maintaining the ability to distinguish a large number of individual tag IDs by developing ideas for a new concept for passive transponders combining concepts from RFID technology and harmonic radar. As a first step towards this new development, a compact dual band parasitic dipole antenna was developed using electromagnetic simulations, manufactured as a prototype and tested in the laboratory.

ACKNOWLEDGEMENTS

I would like to thank my supervisory team for supporting me throughout the course of my PhD project. Without the guidance and resources provided by my primary supervisor Professor Paulo de Souza including the initial offer to participate in a world class research project and the organisation of scholarships, the project would not have been possible in the form presented in this thesis. I am particularly grateful for his generosity during the very hard time early in my candidature when I lost my dad to cancer. I want to thank Dr Robert Ollington for many inspiring and fruitful discussions of methods and ideas. The same is true for Associate Professor Geoff Allen who was always happy to talk about ideas and whose good sense of humour made these discussions particularly enjoyable. Associate Professor Arko Lucieer also provided scientific guidance and supported me wherever he could.

For organisational support and help with logistics I would like to thank Associate Professor Leonie Ellis, Associate Professor Paul Turner, and Mandy Fenlon from UTas as well as Jan Ellis and Janine Stewart from CSIRO Sandy Bay.

I am grateful to the Commonwealth Scientific and Industrial Research Organisation (CSIRO) for supporting my work through a base scholarship as well as an additional top-up scholarship from CSIRO's Office of the Chief Executive (OCE) program, to Vale Institute of Technology for providing funding for the base scholarship to CSIRO and to the University of Tasmania for waiving tuition fees and also for providing general support throughout my candidature.

Particular thanks go to Ryan Warren for invaluable contributions to the outcome of this thesis by rigorously testing variations of our simulated antenna configurations in the field and providing data for a comparative analysis of the old and new systems' sucess ratios.

Likewise, I would like to thank Dr Gustavo Pessin, Helder Arruda and Leon Cardoso for conducting experiments with *Apis mellifera* in Brazil.

I would also like to thank the members of CSIRO's Swarm Sensing Team with whom it was a pleasure to work, including Dr Se-

tia Budi, Dr Ferry Susanto, Leandro Disiuta, Dr Benita Vincent, Peter Marendy, Dr Ray Williams, Dr Auro Almeida, Dr Stephen Quarrell, Dale Worledge, Dr Selim Mahbub, Dr Andojo Ong, Dr Huyen Nguyen, Dr Ulrich Engelke, and Tom Gillard.

Special thanks go to Dr Diet Ostry, Dr Andrew Weily and Mark Johnson from CSIRO's Wireless Laboratory whom I had the privilege and pleasure to collaborate with for a few months and who provided me with invaluable support and insights.

Also at CSIRO I enjoyed many interesting and fruitful discussions with Dr Shane Richards, Dr Pascal Craw, David Biggins, Daniel Hugo, Maciej Matuszak, Dr Andrew Davie, Dr Andrew Hellicar, Dr Charlotte Sennersten, Dr Craig Lindley, Dr Philip Smethurst, Dr Gregory Timms, Andrew Terhorst, Dr Martin Lochner and Dr Andreas Duenser.

I also value the opportunities I was given by Paulo de Souza, Ulrich Engelke and Angela Davis to participate in the local organising committees for the International Conference on Digital Image Computing: Techniques and Applications (DICTA) conference 2013 as well as the 2015 IEEE International Symposium on Big Data Visual Analytics.

I also miss the inspiring discussions about Bioinformatics I had with Dr Michael Charleston – which I would love to continue in the future!

During my time in Hobart, it was a pleasure to be part of and contribute to the Hobart Hackerspace (a Makerspace), resulting in many friendships and lots of intriguing discussions in the spirit of our motto 'Make, Learn, Inspire'. Speaking of enjoyable times in Hobart, it was a pleasure to be able to contribute a little bit to setting up the Greenhill Observatory at Bisdee Tier as well as to the decommisioning of the Mt Canopus Observatory, working with Dr John Greenhill, Dr Tony Sprent, Mike Emery, Keith Bolton, Dr Andrew Cole, and Professor John Dickey, who enthusiastically encouraged me to undertake a PhD with Paulo's Swarm-Sensing team.

Of course, special thanks also go to my family and friends who provided me with tremendous support throughout my candidature. My mum Margarete Buzasi-Farsch and dad Karl-Heinz Hirsch as well as my step-father Professor Nikolaus Buzasi always encouraged and supported me to pursue my interests in science and technology ever since I was fascinated by nature and its workings in my early childhood. I am also immensely grateful to my partner Anke who brought me to Australia in the first place, and also to my close friends Harald

Ketzer, Norbert Heußer, Thorsten Wendt, Pit Linnartz, Brian Marriott, Cliff Senkbeil and family, and Anja Jess-Hempen – who have always been there for me in times of need as well as in times of joy. I aspire to be to all of you what you are to me! Special thanks also go to Dr Jenny Sprent, Chris Edie and Hamish – not just for making the best Sticky Date pudding and providing the laptop I later used for controlling my measurement setup, but also for a wonderful time and making Anke and me feel very welcome in Hobart. A really special thank you is due to Hamish who gave us Buzzing Chicken, my PhD project mascot!

DECLARATION OF ORIGINALITY

This thesis contains no material which has been accepted for a degree or diploma by the University or any other institution, except by way of background information and duly acknowledged in the thesis, and to the best of my knowledge and belief no material previously published or written by another person except where due acknowledgement is made in the text of the thesis, nor does the thesis contain any material that infringes copyright.

September 2018

AUTHORITY OF ACCESS

Pascal Hirsch
September 2018

LIST OF PUBLICATIONS

Work undertaken as part of this thesis has been published as:

1) **P. Hirsch**, A. R. Weily, and P. de Souza, **'Compact Dual-Band Parasitic Dipole Antenna for Harmonic Transponders,'** in *2015 International Symposium on Antennas and Propagation (ISAP),* Hobart, Australia, 2015, pp. 1–3.

I co-authored the following manuscripts during the course of the thesis project:

1) P. de Souza, P. Marendy, K. Barbosa, S. Budi, **P. Hirsch,** N. Nikolic, T. Gunthorpe, G. Pessin, A. Davie, **'Low-Cost Electronic Tagging System for Bee Monitoring,'** *Sensors,* vol. 18, no. 7, p. 2124, Jul. 2018.

2) F. Susanto, T. Gillard, P. de Souza, B. Vincent, S. Budi, A. Almeida, G. Pessin, H. Arruda, R. N. Williams, U. Engelke, P. Marendy, **P. Hirsch,** J. He, **'Addressing RFID Misreadings to Better Infer Bee Hive Activity,'** *IEEE Access,* vol. 6, pp. 31935–31949, 2018.

The following manuscript is work in progress:

1) P. de Souza, R. Williams, S. Budi, F. Susanto, B. Vincent, S. Quarrell, G. Allen, A. Almeida, D. Worledge, L. Disiuta, **P. Hirsch,** G. Pessin, H. Arruda, P. Marendy, L. dos Santos, T. Gillard, A. O. Ong, **'Agent-based Modelling of Honey Bee Forager Flight Behaviour for Swarm Sensing Applications,'** *IEEE Access* (Under Review)

STATEMENT OF CO-AUTHORSHIP

The following people and institutions contributed to the publication of work undertaken as part of this thesis:

Name	Institution	Role
Pascal Hirsch	University of Tasmania, School of Technology, Environments and Design; Data61, CSIRO	Candidate, Author 1
Andrew R. Weily	Data61, CSIRO	Author 2
Paulo de Souza	Data61, CSIRO	Author 3, Supervisor

Manuscript 1, **P. Hirsch**, A. R. Weily, and P. de Souza, **'Compact Dual-Band Parasitic Dipole Antenna for Harmonic Transponders,'** in *2015 International Symposium on Antennas and Propagation (ISAP)*, Hobart, Australia, 2015, pp. 1–3:
Located in Chapter 6.
Candidate was the primary author and contributed approximately 75% to the planning, execution, and preparation of the research project and subsequent paper through modeling, simulation, optimisation, and analysis, visualisation, and interpretation of results, and writing the bulk of the paper.
Author 2 contributed to the conception and initial design as well as to analysis and interpretation of the simulation results and contributed to the interpretation of the work by critically revising the paper.
Author 3 contributed to the initial conception of the research and was involved in proofreading the manuscript.

We the undersigned agree with the above stated 'proportion of work undertaken' for the above published peer-reviewed manuscript contributing to this thesis:

Professor Paulo de Souza	Professor Mark Hunt
Supervisor	Head of School
Data61, CSIRO	School of Technology, Environments and Design
18.04.2019	9/5/19
Date	Date

THESIS CONTEXT & TEAM CONTRIBUTIONS

The work presented in this thesis was undertaken as part of an ongoing larger research project at CSIRO focused on environmental sensing, ultimately aiming to develop energy-autonomous sensors for environmental properties which are small enough to be deployed on insects. This encompassing research project involves international collaborations with many partners, such as Vale Institute of Technology (Brazil), CSIRO's Wireless Laboratories (Sydney, Australia), and other international research groups and scientists which work on honey bees.

Work done in the context of this overarching research project addresses theoretical (framework development) and practical aspects (ranging from sensing and data acquisition system design to data processing, visualisation and analysis).

Some topics covered in the wider project — excluding that of my thesis:

- Development of a theoretical framework to describe environmental phenomena using entropy theory (Mahbub et al., 2017).
- Development of an energy harvesting device for exploiting wing-beat induced vibrations in insects (Ong and De Souza Junior, 2016).
- Development and energy optimisation of an RFID bee monitoring system (de Souza et al., 2018; Marques dos Santos, 2016).
- Integrated data management of RFID based individual bee detection and weather data (Arruda, 2016).
- Simulation and visualisation of honey bee flight paths and associated simulated sensing results (Williams, 2016; Engelke, Hutson et al., 2016; Engelke, Marendy et al., 2016; Nguyen, Wang et al., 2017; Nguyen, Ketchell et al., 2017).
- Improving understanding of bee behaviour based on RFID detection data (Gama et al., 2017; Gomes et al., 2017).
- Mitigation of missed tag detections in an RFID bee monitoring system (Susanto et al., 2018).

During the time of my PhD project, I have additionally contributed to some developments within the wider project. My contributions included developing parts of the control software for the RFID reader

systems (particularly regarding low-level hardware access), support with setting up and running some of the Tasmanian field sites (Figure 2.4), contributions to data analysis, and creating a 3D model of the reader housing suitable for 3D printing (Figure 2.3), as well as taking part in discussions and in some cases as a co-author (de Souza et al., 2018; Susanto et al., 2018). At the same time, collaboration partners within our team contributed to my thesis by providing bee detection data collected in field experiments which I analysed in Chapters 2 and 4 as well as by performing electromagnetic measurements of the antenna/transponder prototypes manufactured according to the design which I simulated and optimised (Chapter 6).

All other work in this thesis is my own except where otherwise referenced or acknowledged.

Part I

DEVELOPMENT OF A COST EFFECTIVE, ENERGY AUTONOMOUS MONITORING SYSTEM FOR RFID TAGGED INSECTS BASED ON COMMODITY HARDWARE

1

INTRODUCTION

RFID TECHNOLOGY

The term RFID (Radio Frequency Identification) refers to a whole range of short-range radio frequency communication technologies that typically employ simple, low-cost transponders ('tags') on one side and more complex devices ('readers') on the other (Figure 1.1). Tags can either be self-powered ('active') or purely rely on harvesting energy from the interrogation signal sent by the reader ('passive') (Finkenzeller, 2010). Since passive RFID tags do not require batteries, they are not limited by battery life and thus can operate much longer and are also cheaper to produce. This allows many more individuals to be tagged and monitored at lower additional cost once the initial costs for the RFID readers have been covered. Generally, only a small amount of digital data is transmitted by a tag in response to an inquiry signal from the reader (most commonly unique ID numbers, usually up to a few 1000 bits – although Thomas et al. (2013) were able to demonstrate that it is possible to continuously stream data at sustained data rates of up to 5 Mbps using passive RFID technology). According to Landt (2005), RFID systems have been using frequencies from 100 kHz up to 10 GHz. RFID tags capable of transmitting multiple bits have been commercially available since the 1980s (ibid.).

Today, RFID is a mature technology and there are multiple standards for RFID systems. The most frequently used systems operate in the LF (low-frequency: 3 kHz – 300 kHz), HF (high frequency: 3 MHz – 30 MHz), and UHF (ultra-high frequency: 30 MHz – 300 MHz) frequency bands (see Table 1.1, Finkenzeller (2010)).

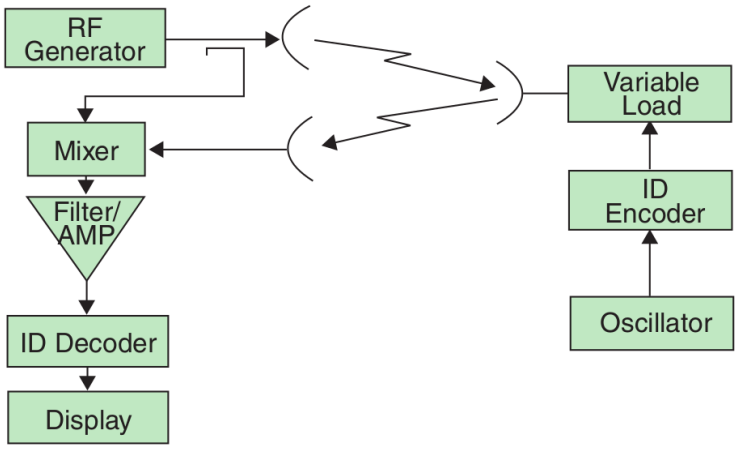

Figure 1.1: Schematic diagram of an RFID system using passive tags. Source: Landt (2005). Copyright © 2005, IEEE

Table 1.1: Commonly used RFID systems (see Finkenzeller, 2010). Note: LF Tags conforming to ISO 14223-1 are also known as 'Passive Integrated Transponders', or PIT-tags.

Band	Frequency Range	Read Range	Typical Use	References
LF	125–134 kHz	a few cm	Animal Identifica-tion	ISO 14223-1 (2011)
HF	13.56 MHz	$\leq$ 1 m	Access Control, Credit Cards	ISO 16593-2 (2006)
UHF	860–960 MHz	< 1 cm – > 100 m	Inventory Tracking, Manufacturing, Medical Tagging	ISO 18000-63 (2013)

RFID technology allows one to achieve low tag weights (less than 3 mg, e.g. Figure 1.2) by passively powering the tag (which acts as a transponder, since it receives as well as transmits signals) remotely from an RFID reader, thus requiring no battery power (Kissling et al., 2014). To this end, the RFID reader device emits an interrogation signal that is received by the tag's antenna. This received signal is then rectified and used to power the tag's circuitry. The tag transmits information back to the reader (e.g. its unique identification number (ID)) by modulating its reflectivity, e.g. through repeatedly shorting the antenna terminals for brief periods of time. These variations in the amount of scattered energy can be detected by the reader; accordingly, this mode of communication is also called 'backscatter communication'.

Figure 1.2: Honey bee *(Apis mellifera)* with an RFID tag glued to the dorsal thorax. Source: Streit et al. (2003)

RFID tags have been used for insect monitoring for more than a decade (Streit et al., 2003). They are available for diverse frequency bands, ranging from the low frequency band (LF: 30 kHz – 300 kHz) up to microwaves in the 10 GHz range. Achievable detection distances for insect monitoring applications are usually below 1 m, but for the smallest tags they can even be around 1 mm (Streit et al., 2003; Schneider et al., 2012).

UHF RFID

UHF RFID in its current form is a mature technology – its operation has been standardised by the International Organisation for Standardisation as ISO 18000-6C in 2006 (Dobkin, 2013). This standard was revised and renamed to ISO 18000-63 in 2013 (International Organization for Standardization, 2013).

UHF RFID tags operate in the frequency range between 860 MHz and 960 MHz (Nikitin, Rao and Lazar, 2007) – corresponding to wavelengths between 31 cm and 35 cm. In order to achieve the largest possible reading distance, an ideal half-wave dipole antenna would accordingly have to be around 13 cm to 14 cm long, and a rectangular patch antenna would have to have a side length of similar size (Finkenzeller, 2010). Passive UHF RFID tags equipped with such dipole antennas can achieve reading distances of more than 100 m if used with a standard compliant RFID reader. Advanced antenna design

techniques allow to reduce the size of the tag antennas down to a few cm in length while maintaining long reading ranges (Marrocco, 2008).

The tag designs described above strive to maximize the reading distance and thus necessarily couple to the far field of the RFID reader antenna (Nikitin and Rao, 2008). UHF RFID can however also be used as a near-field technology (Nikitin, Rao and Lazar, 2007). In this case, the antenna size can be further reduced down to a few mm, albeit at the expense of reduced reading range (ibid.).

Any antenna whose dimensions fit into the radian sphere for a given wavelength λ (a sphere of radius $a = \frac{\lambda}{2\pi}$) is considered an electrically small antenna at this wavelength (Wheeler, 1947; Hansen, 1981). For UHF RFID (frequencies f between 865 MHz and 926 MHz in Australia and/or Europe), the radius of a radian sphere is between

$$a = \frac{\lambda}{2\pi} = \frac{c_0}{2\pi f} \approx \frac{32\text{–}35\,\text{cm}}{2\pi} \approx 5.2\text{–}5.5\,\text{cm}$$

(where c_0 denotes the speed of light in vacuum). Consequently, the antennas of mm-sized UHF RFID tags are electrically small at these frequencies. Therefore, they can only radiate or receive a small fraction of the power of a half-wave dipole antenna (McLean, 1996; Nikitin, Rao and Lazar, 2007; Shahpari, 2015).

A typical use for such small near-field UHF RFID tags is item-level tagging for tracking goods in commercial settings, i.e. for tagging expensive jewelery items or pharmaceuticals as an anti-counterfeiting measure (Dobkin, 2013; Wamba et al., 2013). Such small near-field UHF RFID tags have been available commercially for some time (Nikitin, Rao and Lazar, 2007).

High market volume in combination with high maturity of the technology lead to low cost and good availability of UHF RFID readers and tags.

The technology of both readers and tags has been continuously improving in the past: readers have become more sensitive (according to Occhiuzzi and Marrocco (2016) by roughly 3 dB every 2 years) and tag chips need less power to activate (Figure 1.3) and can thus operate in weaker fields, resulting in increased reading ranges (Duroc and Tedjini, 2018; Nikitin, Rao and Lam, 2012; Occhiuzzi and Marrocco, 2016). Figure 1.3 suggests that this trend is likely to continue for some time into the future.

Anti-collision algorithms being part of the protocol allow UHF RFID to handle the presence of a large number of simultaneously readable

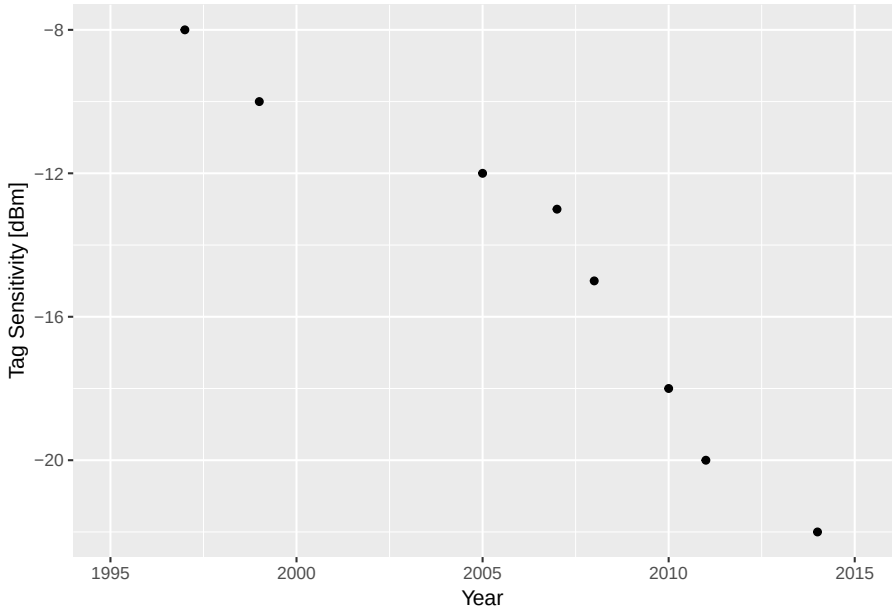

Figure 1.3: Evolution of UHF RFID tag sensitivity (minimum operating power using a dipole antenna) over time. Data source: Duroc and Tedjini (2018).

tags, which is required to support item-level tagging scenarios using far-field tags with large maximum reading distance (Klair et al., 2010).

UHF RFID can also work at higher communication speeds than LF or HF RFID, allowing to read more tags within the same amount of time and / or to read additional information that could be stored in the tag memory (ibid.). Finally, many countries implement regulations that allow UHF RFID to be used without requiring individual operating licenses (GS1 AISBL, 2016).

Due to its versatility and cost effectiveness, RFID technology has also been applied in other fields. For example, it has been of particular interest to researchers monitoring animals ranging from birds in the sky (Hou et al., 2015) to fish in the water (Zydlewski et al., 2006), and animals as large as elephants to insects as small as wasps (Sumner et al., 2007) and ants (Robinson et al., 2009).

Monitoring insects is of particular interest, because they play big ecological roles – as pollinators, commercial crop pests, or as vectors for diseases (between plants and animals, including humans). Of particular importance for global food production is the European honeybee *(Apis mellifera)* which has suffered from colony collapses in many parts of the world for which the reasons have not been fully resolved (Klein et al., 2017). Without increasing our knowledge of the movement of bees, these collapses could become a global problem.

In 2003, Streit et al. introduced the use of RFID tags to individually mark bees (Streit et al., 2003). Since then, this method to mark insects has been applied and refined in a number of studies. For example, RFID has been used to monitor impacts of pesticides on individual bee survival rates (Decourtye et al., 2011; Gill et al., 2012; Henry et al., 2012), sub-lethal effects of insecticides (Schneider et al., 2012; Berenbaum, 2016), the influence of colony nutritional status on role allocation in bees (Molet et al., 2008; Tenczar et al., 2014), as well as the large scale homing ability of honey bees (Pahl et al., 2011; Thompson et al., 2016). Perry et al. (2015) used this method to investigate how stress could play a role in colony collapse disorder of honey bees.

Due to the many advantages of RFID technology (simple, small, lightweight, robust, long-lived, and cheap tags as well as globally available mature technology), we chose near-field UHF RFID tags for our goal to develop a cost-effective monitoring system that can be used globally.

This development project focused on keeping cost and power requirements of the system to a minimum, aiming to make it available at a lower cost than less optimised systems currently available, for example by building fixtures for holding the RFID readers using 3D printing techniques and using recent cheap single board computers like the Intel Edison as control computers.

2

FIELD TESTS OF FIRST SYSTEM PROTOTYPES BASED ON COMMODITY HARDWARE (SINGLE & DUAL READER)

2.1 INTRODUCTION

In recent years, RFID tags and readers have become commodity hardware items (Duroc and Tedjini, 2018). However, animal researchers typically use rather expensive devices offered by well-known research equipment companies (see for example Vinatier et al., 2010; Beyaert et al., 2012; Moreau et al., 2011).

As a first step towards exploring the options of implementing a cost effective, energy autonomous and robust system for tracking large numbers of RFID tagged bees which can be deployed in the field, a first, minimal prototype was built in our research group using off-the-shelf hardware components. This prototype consisted of a single UHF RFID reader module equipped with an internal antenna in the form of a USB peripheral which is powered by the USB connection (i.e. it does not need any additional power supply) and which is so small and light weight that it would even be suitable for hand-held operation. This RFID reader was connected to a small single-board computer running a custom written control program we implemented in Python (Rossum, 1995) on a Linux operating system. This system was tested in a first field trial.

After trialling this first prototype, we improved the monitoring system by adding a second, identical RFID reader module. This second prototype was also tested in the field.

Figure 2.1: Bee with attached RFID tag (Hitachi IM-PK2525, dimensions: 2.5 mm × 2.5 mm × 0.4 mm). Photo: CSIRO

2.2 MATERIALS AND METHODS

2.2.1 *Choice of RFID tag and reader*

As an RFID tag suitable for tagging bees we selected the Hitachi 'IM5-PK2525 Ultra Small Package Tag' (Figure 2.1), because it is one of the smallest (2.5 mm × 2.5 mm × 0.4 mm) and lightest (5.4 mg) commercially available tags, is available a low price (less than AUD 0.50 per piece), and is mechanically and chemically robust thanks to its epoxy composite body with gold plated embedded antenna (Hitachi Chemical Co., Ltd., 2012a,b). The tag contains an ImpinJ Monza 5 chip with a die size of 465 µm x 465 µm and a spiral coil antenna combined in one package. It conforms to the RFID standard ISO/IEC 18000-6 Type C EPCglobal Class1 Generation2 (International Organization for Standardization, 2013). Some additional information about the internal structure of the tag is available in a related US patent held by Hitachi (Endou et al., 2015).

The embedded spiral coil antenna of this tag measures less than 2.5 mm along each side and thus exhibits limited efficiency at UHF frequencies (Dobkin, 2013). It couples mainly to the magnetic field of the reader and its operational mode is better characterised as an inductor than an antenna (Dobkin, 2013; Cole et al., 2003; Lehpamer, 2012; Nikitin, Rao and Lazar, 2007). The data sheet for IM-PK2525 specifies a typical read range of 10 mm for this tag (Hitachi Chemical

Co., Ltd., 2012b). This type of tag therefore operates only in the near field of a reader antenna.

Since tags any larger than this particular type would be unsuitable for use in long-term monitoring of honey bees, the main challenge of our project is to make the detection system work under the constraints imposed by this particular type of antenna.

While it is possible to significantly increase the read range of this tag by wirelessly coupling its antenna to a larger booster antenna, this method effectively increases the size of the tag antenna to the size of the booster antenna, making this approach unsuitable for our intended use case (Pachler et al., 2013).

For the RFID readers, we decided to work with MTI RU-824 UHF RFID USB desktop readers (Microelectronics Technology Inc., 2012) because of their low cost ($\approx$ USD 250.00), compact form factor, and since they only need a USB connection, which makes them easy to integrate with a single board control computer.

The control computer (Ledato Nanos G20, later also Intel Edison) was running a custom written control program which we implemented in Python version 2.7 on a Linux operating system.

2.2.2 *Field test setup for first, single antenna prototype*

In two locations, similar experiments with tagged bees were set up – one in Geeveston, Tasmania (S 43°09′, W 146°55′), and another one at Santa Bárbara do Pará in the Brazilian Amazon (S 1°14′, E 48°16′). The Tasmanian experiment comprises four similar Langstroth bee hives which each have been equipped with a modified entrance tunnel containing an MTI RU-824 USB RFID reader module (see Figure 2.2). The RFID readers were mounted to the entrances using custom designed 3D printed housings containing a height-restricted section forcing the bees closer to the reader antenna while passing through (Figure 2.3). The readers were connected via USB cables to small battery powered computers (Intel Edison) located in an electronics box placed next to the hive (Figure 2.4). These boxes also contain rechargeable batteries which are re-charged through solar panels located next to them (Figures 2.2, 2.4). Two artificial feeder stations were positioned at distances of 5 m and 15 m from the hives, each with their own RFID reader and computer system. Each of the four hives was also equipped with an automatic scale (BeeWatch Professional 2.0) that tracked the hive weight as well as the temperature and humidity of

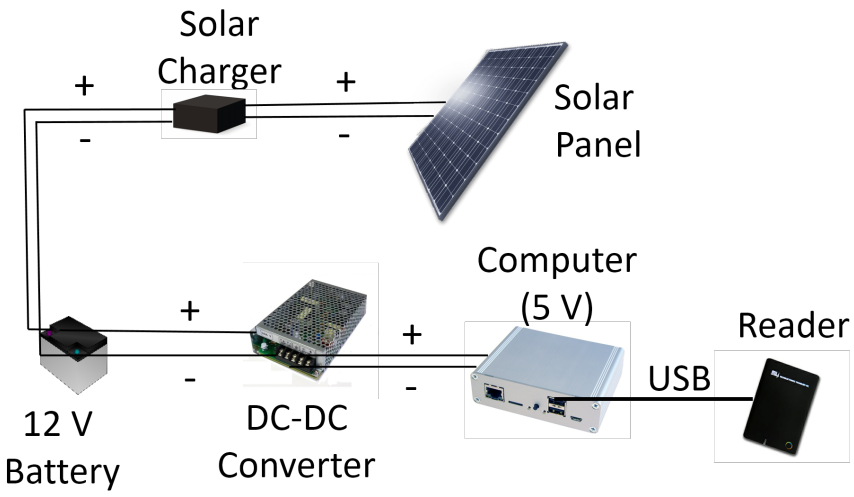

Figure 2.2: Schematic diagram of the RFID reader set-up at each monitoring station.

the brood chambers inside the hive. The site has also been equipped with an automatic weather station (see Table 2.1) in order to monitor temperature, humidity, atmospheric pressure, wind speed and direction, precipitation as well as illumination. The weather station as well as the automatic scales were equipped with internal GSM radio modems to wirelessly transmit the recorded data into online databases at CSIRO. The data from our RFID reader system was downloaded manually via cable to a notebook computer (DELL Latitude Rugged) on-site twice a week, as the weather allowed.

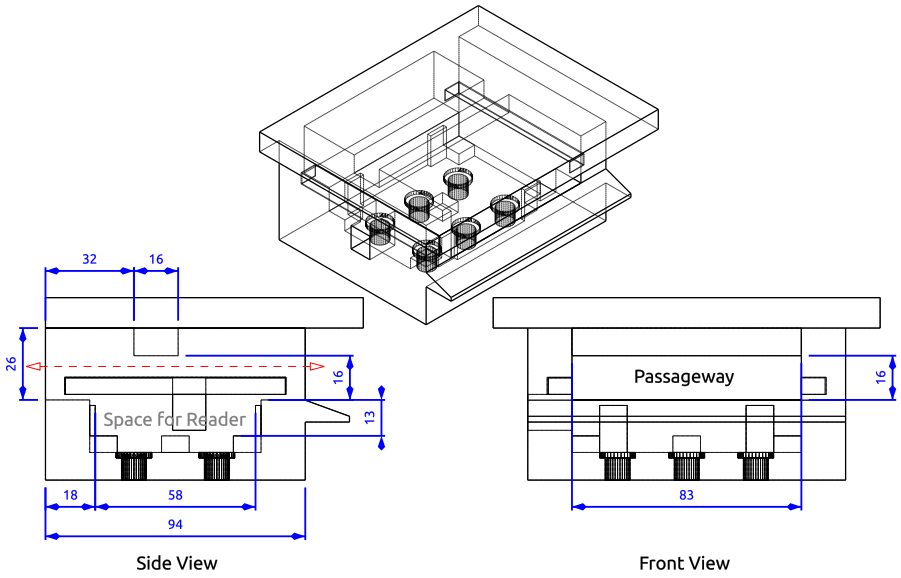

Figure 2.3: Housing used to attach the RFID modules to entrance tunnels (3D CAD model after a custom design by CSIRO). Relevant dimensions are indicated in mm. A bar protruding from the ceiling of the passageway, spanning the full width of the tunnel, forces the bees to pass closer to the internal antenna of the reader. With the height of the reader being 12 mm (see Figure 2.6), the remaining maximum height of the passageway between the top surface of the reader and this bar is 17 mm. To increase weather robustness, the design includes a protruding lid and stand-offs and drainage holes in the bottom part. A protrusion on the front side provides a landing pad. The rectangular cut-out on the side is sealed around the USB cord of the reader once it is installed. The 3D printed housing consists of two parts (top and bottom) which separate right above the landing pad. The back side of the housing is attached to the front face of the hive or feeding station (see Figure 2.4). Bees enter or leave the hive by passing though the reader housing front-to-back or vice-versa along the indicated passageway (parallel to the dashed red line). Figure 2.6 shows an inside view of a wooden prototype of the reader housing with a reader installed and the lid removed (right hand side, mounted next to a second, slightly modified reader housing containing a second reader).

Figure 2.4: Two hives of the experimental field set-up near Geeveston, South-Eastern Tasmania (Hives, Scales, Electronics boxes, and Solar Panels). The reader housings containing the RFID readers (Figure 2.3) are mounted in front of the original entrance openings at the bottom of the hives. Source: CSIRO

A complete list of components used in our field setup for these RFID experiments is presented in Table 2.1.

Table 2.1: Components of RFID field experiment set-up.

Bee Hives	Standard Langstroth Bee Hive
RFID Reader	MTI RU-824 (based on Impinj Indy R1000 Chip)
RFID Tags	Hitachi IM5-PK2525 (2.5 mm × 2.5 mm × 0.4 mm)
Control Computer	Original version: Ledato NanosG20 (ARM based CPU, 32 Bit, 396 MHz) Newer version: Intel Edison compute module (Dual-Core Intel Atom Processor, 500 MHz, 1 GB RAM, 4 GB Flash) on Intel Edison Breakout Board
Solar Panels	BP3125J, 17.4 V, 125 W
Solar Charger	GSL Electronics, MPPT12-1
DC-DC Converter	Mean Well SD-25A-5
Battery	Panasonic LC-R1233 (12 V, Deep Cycle)
Hive Scales	BeeWatch Professional 2.0 (Biene & Natur GmbH)

Table 2.1: Components of RFID field experiment set-up.

Weather Station	Data logger: CR800 (Campbell Scientific Australia) Installed Sensors: • Air temperature, relative humidity: model CS215 • Precipitation: High-end tipping bucket rain gauge, model CS700 • Wind speed and direction: RM Young sensor, model 03002 • Global solar radiation: Pyranometer LI2000X

The described experiment set-up became operational in March 2014. In order to establish a data baseline, the bee hives were characterised in mid 2014. Since then, we tagged more than 5000 honey bees and collected baseline data for use in subsequent experiments.

In August of 2015, CSIRO/Data61 officially launched the Global Initiative for Honey Bee Health (GIHH) to foster international collaboration (CSIRO, 2015). Since then, a number of collaborative experiments involving international researchers have been set up as a result, and we have been working towards improving the experimental set-up. These improvements have been achieved by outfitting the hive entrances with two or four antennas to improve the data quality by lessening our reliance on heuristics to infer the direction (entering or leaving the hive) of detected tagged bees, although the heuristics do not become completely obsolete since missed readings can still occur (Susanto et al., 2018).

We have also been working towards replacing the MTI RU-824 USB RFID readers used in the first and second prototype system by a custom built RFID reader to reduce the number of missed readings through the use of a different antenna setup as well as by eliminating the need for reader downtime because of thermal issues.

2.3 RESULTS AND DISCUSSION FOR FIRST, SINGLE ANTENNA PROTOTYPE

Field trials testing the first single-antenna prototype on honey bees showed that this system is able to capture RFID tag detection data which allows to detect temporal variations in hive activity levels (Figure 2.8, Susanto et al. (2018)).

This data also provided some information about tag recapture and tag reading longevity rates. However, it quickly became apparent that the data quality achievable by this system was limited.

One limitation of this first prototype system was that the RFID readers were incapable of actively running 100% of the time because of overheating issues causing the system to fail. To mitigate this issue of overheating, the readers regularly had to be put into an inactive state, in which they were unable to detect the presence of any RFID tag. We empirically found that an interruption of 0.5 s every 2 s was necessary to achieve stable operation. This operating mode obviously caused missed readings in addition to those caused by other reasons like interference or insufficient signal strength due to tag-reader distance or tag orientation.

Despite operating the readers at this reduced duty cycle, we still encountered occasional system crashes, prompting us to implement the following measures to improve the robustness of the monitoring system:

- To reduce system downtime due to unknown technical reasons, we introduced watchdog timers which automatically restart the system by temporarily cutting power when communication with the reader modules stalls for longer than a configurable limit.
- Power usage of the monitoring system was optimised using fuzzy logic to determine optimal reader downtime settings for different times of day according to bee activity levels (Marques dos Santos, 2016).

A further limitation of the first prototype system was that with only one single-antenna RFID detector at each monitoring location (hive entrance and artificial feeder station), we were only able to sense the presence and IDs of tagged bees at these particular locations, but it was impossible to determine in which direction they were moving past the readers. If the system would reliably detect each passage of a tagged bee through the entrance tunnel, we could apply heuristics

based on detection time stamps to infer whether the recorded events are more likely to represent a bee leaving or entering the hive (or feeder station) or whether a detected bee was just staying close to the entrance area without actually entering or leaving.

Bazazi et al. (2016) resolved the issues related to missed readings by visually analysing simultaneously recorded video footage. Unfortunately, this was infeasible in our case because of the large number of bees and simultaneous continuous monitoring system operation at multiple sites. Van Geystelen et al. (2016) used twin reader configurations to minimise missed readings and also present a heuristic algorithm to correct for them. To add the capability to sense the bees' movement direction (into/out of the hive or feeder) to our system, we added a second, identical reader module to the entrance tunnels of the hives and feeding stations. This configuration was then tested in a second field trial discussed in the next section.

2.4 ANALYSING MISSED DETECTIONS USING A DUAL READER PROTOTYPE

To enable us to detect whether the bees were entering or leaving the hive or feeding station, we built an improved second prototype of the monitoring system similar to the first version described above, but this time using two RFID reader modules in tandem. The additional reader per system was connected to the existing control computer and operated alternatingly in order to minimize mutual interference. Like the first prototype, this system employed MTI RU-824 USB RFID reader modules equipped with a single internal antenna. The readers were placed inside the entrance tunnel of the bee hive such that bees entering or leaving the hive had to pass both readers in sequence: the *inner* reader closer to the hive and the *outer* reader closer to the exit side of the entrance tunnel, spaced 8.5 cm apart (Figures 2.5, 2.6).

This second prototype was tested in a field trial at Santa Bárbara do Pará, Brazil, between May and August 2015, in collaboration with Vale Institute of Technology. In this trial, we collected detection data on an africanised strain of *Apis mellifera* tagged with Hitachi IM-PK2525 RFID tags.

For each detection event, we recorded its timestamp, the ID of the detected tag (a unique 96 bit value which had previously been written to each deployed tag's EPC memory), and the hardware ID (serial number) of the detecting RFID reader module (see Table 2.2 for an example). We recorded the timestamps with a resolution of 1 s, since

Figure 2.5: Bee hive at Brazilian field site equipped with prolonged entrance tunnel housing two RFID readers. Photo: CSIRO/Instituto Tecnológico Vale (ITV)

Figure 2.6: Hive entrance tunnel outfitted with two MTI RU-824 RFID readers to detect whether bees enter or leave the hive. The outer dimensions of the reader modules are 80 mm × 57 mm × 12 mm. Annotations show the readers' serial numbers useful to identify reader position in the recorded data. Source: CSIRO/ITV

Table 2.2: Structure of RFID tag detection data.

filename	ReaderID	Timestamp	TagID	Reader
20150702_TESTING.csv	1446U2003	2015-07-02 04:07:10	1D0010100100104300001404	inner
20150702_TESTING.csv	1446U2003	2015-07-02 04:07:12	1D0010100100104300001404	inner
20150702_TESTING.csv	1446U2003	2015-07-02 04:07:20	1D0010100100104300001404	inner
20150702_TESTING.csv	1446U2003	2015-07-02 05:46:12	1D0010100100104300001404	inner
20150702_TESTING.csv	1446U2003	2015-07-02 06:08:04	1D0010100100104300001404	inner
20150702_TESTING.csv	1446U2003	2015-07-02 07:10:01	1D0010100100104300001410	inner

Table 2.3: The tagging log, listing tagging dates and used tag number ranges. Due to system failures, the first batch (2015-05-22) had to be excluded from the analysis.

Date	TimeIn	TimeOut	ID_num_low	ID_num_high
2015-05-22	2015-05-22 10:54:00	2015-05-22 12:24:00	1321	1370
2015-06-25	2015-06-25 09:49:00	2015-06-25 11:11:00	1371	1420
2015-07-16	2015-07-16 09:19:00	2015-07-16 10:58:00	1421	1520

personal observations confirmed that this time resolution was sufficient to reliably detect the presence of bees close to the RFID reader when they were entering or leaving the hive. In an effort to conserve storage space, we only recorded each unique tag ID once per timestamp, although we typically observed multiple detections per second whenever a tag was detected at all.

We also kept a tagging log, recording tagging dates along with tag number ranges used on that day (Table 2.3).

2.4.1 *Results and Discussion of the dual reader field trial*

Analysis of the data captured during the second field trial revealed that the reader modules we used only achieved low detection rates and therefore did not allow us to reliably detect whether a bee entered or left the hive. However, the distribution of inter-detection intervals for the same tag allowed us to estimate an upper bound on the rate of successful detections.

The second trial also suffered from system failures caused by overheating as well as unknown technical problems, sometimes failing for multiple days at a time.

Detailed results of this second trial will be given below.

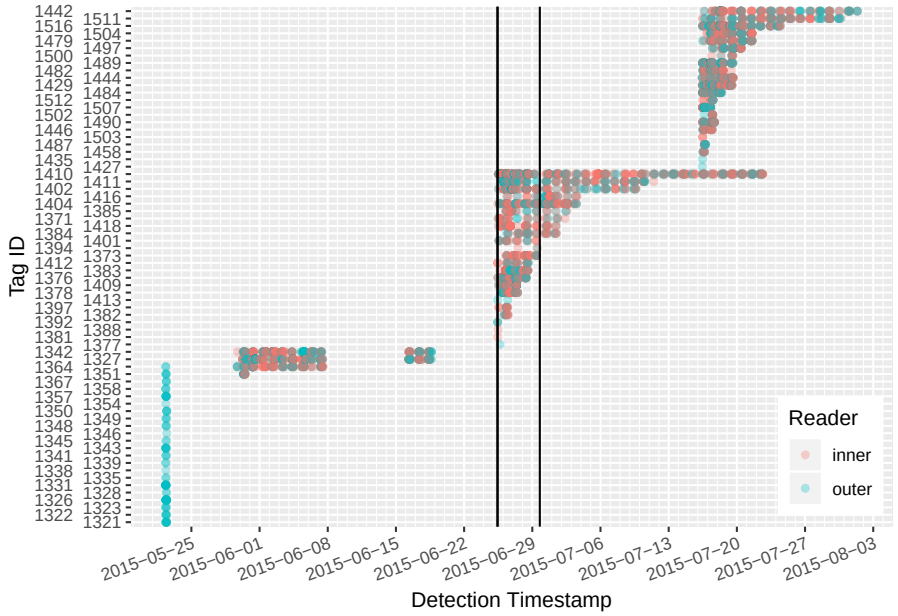

Figure 2.7: Overview of the RFID detection results from the dual reader field trial, showing when each individual bee's RFID tag was detected by inner or outer RFID reader. Individual dots appear translucent to mitigate overplotting and allow to get a rough sense of detection event density. The vertical black lines indicate logged system re-boot events. Note that a long lasting system failure right after deploying the first batch of tags together with another one about two weeks later lead to a loss of a significant of data for that batch so that it was excluded from further analysis. The tag IDs are ordered according to the time of their last detection event, resulting in a visual indication of tag longevity.

In total, 8610 detection events from 77 different tags were recorded during the course of this trial.

Because of a system failure, data from the first of three tagging batches had to be excluded from further analysis (Figure 2.7, Table 2.3). We also excluded data from the tagging days to minimize the effect caused by the disturbance. Data from two days on which the system had rebooted itself for unknown reasons (likely due to power failures) was also discarded. This left us with 4540 detection events from 42 tags used in the further analysis. The total number of deployed tags during the second and third batch was 148. This corresponds to a recapture rate of 28.4%.

Figure 2.8 shows the diurnal distribution of all recorded detection events of this trial for each reader. Both readers clearly show a broad activity maximum during the day and reduced activity levels during the night.

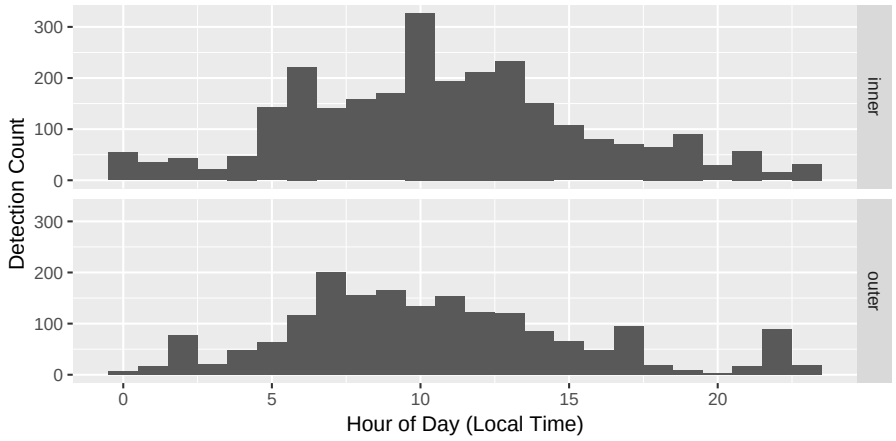

Figure 2.8: Total number of analysed accumulated detection events per hour of the day for each of the two RFID readers *(inner, outer)*, showing a broad activity maximum during the light hours of the day.

Exploratory data analysis revealed a pattern in the distribution of inter-detection intervals which could be used to heuristically estimate the ratio of missed to successful detections. Figure 2.9 shows histograms of the inter-detection intervals between successive detections of the same tag, pooled over all tags, conditioned by the reader location of the previous and current detection event on a logarithmic time scale.

All four of these distributions show a similar multimodal structure. A relatively narrow peak at short time spans of up to 30 s which is much higher in the graphs on the diagonal (implying that a detection by one reader was most often followed by another detection at the same reader within up to 30 s) is followed by a very long tail (note the logarithmic time axis), with at least one additional less well pronounced peak, roughly spanning intervals from 2 minutes up to 4 hours between consecutive detections. There also appears to be a much weaker peak corresponding to a delay of about 0.5 to 1 day, implying that a few tags have only been detected once or twice a day. Excluding data for one day on which a re-boot had occurred will have caused a few spurious detections with a delay of more than 1 day, corresponding to the small bar at 10^5 s (Figure 2.9).

All four distributions also show a marked minimum at around 30 s, suggesting that a particular bee is unlikely to be detected again by any reader after a delay of about 30 s after it has been detected by one of the readers; this pattern is particularly pronounced in the panels displaying consecutive detections by different readers (corresponding to in- or outbound transitions). It should be noted that this pattern has been observed on in-hive tagged bees and therefore is independent of the caste of the detected bees. If a bee is not detected again for

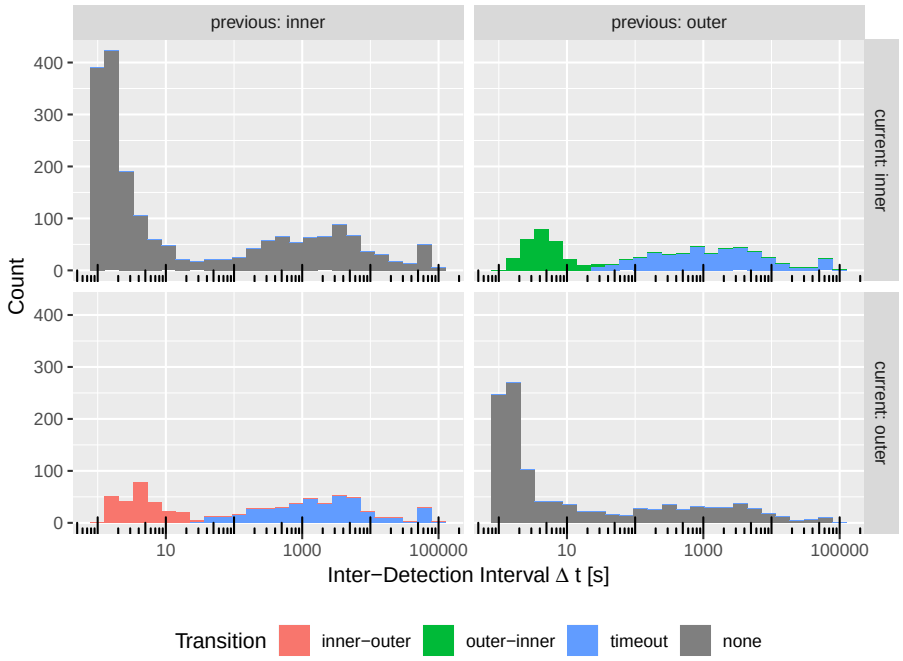

Figure 2.9: Histograms of inter-detection intervals for pairs of successive detections of the same tag, summed up for all tags. The panels correspond to the combination of the detection locations for the two detections of each pair (which can either be *inner* or *outer*, where *inner* corresponds to the reader located closer to the hive). Thus, the panels on the diagonal show subsequent detections which both occurred at the same end of the entrance tunnel, while the off-diagonal panels show *inner/outer* or *outer/inner* detection pairs. Colour represents the classification of the detection events into successfully detected inbound or outbound transitions, timeouts suggesting missed intermediate events, and successive detections by the same reader according to the heuristic described in section 2.4.1. Note the logarithmic scale of the x axis.

a longer period than 30 s, we can assume that it has been away from the entrance and could e.g. have been on a foraging trip or spent time inside the hive.

This observation allowed us to use the following heuristic to estimate the number of missed readings: we used 30 s (as suggested by Figure 2.9) as a cut-off point to decide whether a pair of successive detections of the same tag by different readers ('inner/outer' or 'outer/inner') was accepted as an actual in- or outbound transition of a bee and therefore the bee's location (inside or outside the hive) was considered known after the second detection event within this timespan. If a bee whose location was assumed known was detected next by the other reader (i.e. the *outer* reader if the bee was considered to be *inside* the hive or vice versa) after more than 30 s had passed, we inferred that we must have missed at least one detection event and classified

the respective detection pair as a timed-out transition. The histograms in Figure 2.9 are coloured according to this classification.

The empirically determined cut-off time of 30 s fits well with existing literature: in their 'Track-a-Forager' program for automated analysis of RFID tracking data, Van Geystelen et al. (2016) chose a default cut-off time of 20 s, but recommend to change it according to the separation of the RFID readers, and Tenczar et al. (2014) used a cut-off time of 40 s in a dual RFID reader setup with a similar separation (estimated from a figure), but connected by a narrow walkway.

Under these assumptions, we can estimate an upper bound on the probability to register a transition of a bee as a pair of detections at both readers given that we observed $n_{\text{success}} = 513$ successfuly detected transitions and $n_{\text{timeout}} = 900$ timeouts (see Figure 2.9):

$$p_{\text{trip}} = \frac{n_{\text{success}}}{n_{\text{success}} + n_{\text{timeout}}} = \frac{513}{1413} = 0.363$$

The probability for a transition to be detected by both readers is:

$$p_{\text{t}} = p_{\text{i}} p_{\text{o}}$$

Assuming that both readers have identical detection probabilities, we get:

$$p_{\text{i}} = p_{\text{o}} = \sqrt{p_{\text{t}}} = 0.603$$

Conversely, the probability to successfully detect all 4 events corresponding to a single foraging trip *(inner, outer, outer, inner)*, is:

$$p_{\text{trip}} = {p_{\text{trip}}}^2 = 0.132$$

This rather low detection rate is also apparent in a plot of the inferred state of detected bees (corresponding to the respective latest accepted transition as described above) versus time (Figure 2.10). This graph includes all bees which were detected on at least 6 different days during the study period. Although the expected number of daily foraging trips per bee varies with factors such as weather, forage availability and colony strength, it typically ranges between 5-15 trips per day for foragers and up to 100 trips per day for water collectors (British Columbia Ministry of Agriculture, 2015).

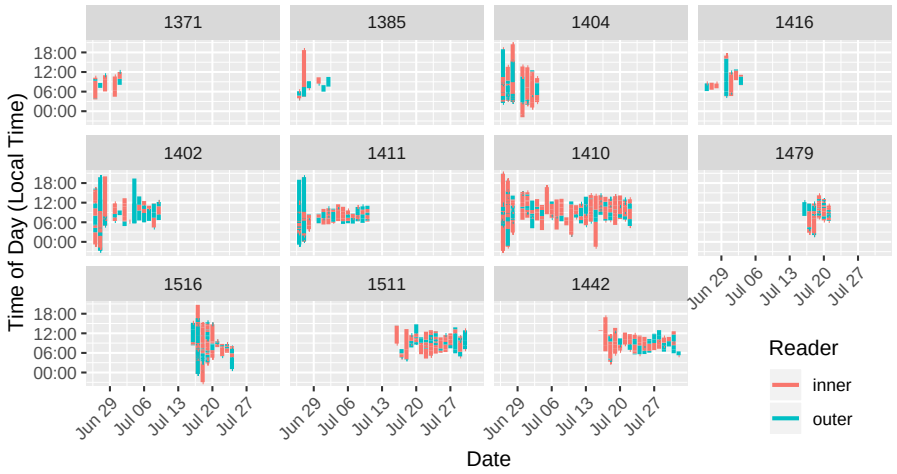

Figure 2.10: Timelines for individual bees showing which detector had registered the last accepted transition (i.e. two detections by different readers within 30s). The lines span the time between the first and last detected transition for the given individual bee per day. Each panel corresponds to an individual bee with the given (shortened) tag ID. Included are all bees which have each been detected on at least 6 different days during the study period. The rather low number of reconstructed daily foraging trips hints at a low detection rate / a high number of missed detections.

We also found that the ratio of missed readings between both readers varied strongly between different individual bees. This is evident in Figure 2.11, which depicts the balance of detected entering/leaving events for individual bees over time. The fact that the ratio of detected inward to outward movements also varies over time in a way that depends on the individual bee suggests that this is not inherent to the combination of tag and reader.

The limitations of the prototype systems based on the MIT RU-824 RFID readers as outlined above prompted the development of a more capable monitoring system which has since been ongoing as a joint venture between our research group at CSIRO and an external company (RFIT Pty Ltd).

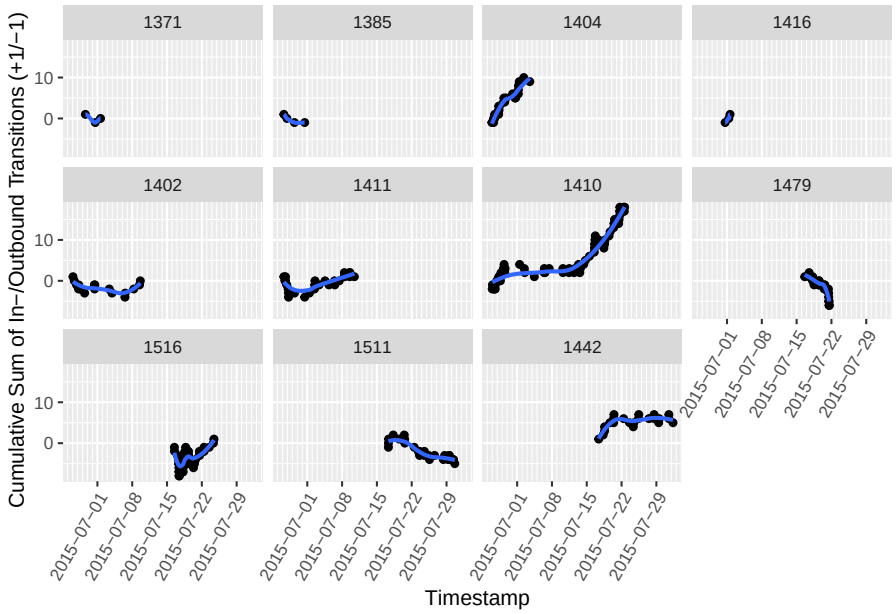

Figure 2.11: Cumulative sum of detected in-/outbound transitions per individual bee (counted as +1 for inbound and -1 for outbound). Identical probabilities of missing missing in- and outbound transitions would result in a cumulative sum fluctuating around 0. The observed pattern evidently deviates from this expected balanced pattern, revealing substantial inter-individual differences which could be caused by individual bees moving through the entrance tunnel in different ways (e.g. at different speeds or along different paths). Each panel corresponds to an individual bee with the given (shortened) tag ID. Only bees which have been detected on at least 6 days during the study period are included. The blue lines represent a LOESS smoothing interpolation (Cleveland and Devlin, 1988).

3

LABORATORY-BASED AUTOMATED SYSTEM FOR DETECTION RANGE MEASUREMENT OF NEAR-FIELD UHF RFID TAGS

3.1 INTRODUCTION

In the previous chapter, we report on the development of a first affordable prototype monitoring system based on one or two compact, off-the-shelf USB RFID reader modules equipped with a single internal antenna. Field trials testing this prototype on honey bees showed that it is able to capture RFID tag detection data which allows to detect temporal variations in hive activity levels. The data also provided some information about tag recapture and tag longevity rates. The dual reader prototype did not improve data quality sufficiently to reliably detect bees entering or leaving the hive which would be required to reconstruct the time line of a bee being inside or outside of the hive or feeder. Both trials also frequently suffered from system failures due to overheating and some unknown technical issues, further reducing data quality.

To better understand the low detection rates observed in the field experiments, we examined the spatial pattern of the detection probability and quality of our small RFID tags within the near field of selected RFID reader antenna configurations using one or more RFID tags as probes with which we scanned the volume of interest around or between the antennas by iteratively positioning the probe on all locations on a regular 3D grid covering that volume and recording successful tag detections.

Besides biotic factors such as angle and speed of tagged bees, there are a number of non-biotic factors which can influence the detection success rate:

- tag sensitivity

  - minimum operating power of tag IC
  - antenna efficiency
  - individual variations
- reader sensitivity
  - reader circuit
  - reader type, i.e. monostatic vs. bistatic, which would be better, but more expensive
- reader antenna configuration
  - antenna field structure
  - crosstalk / interference between antennas
- RFID protocol (Nikitin and Rao, 2009)
  - timing parameters / reader modes
  - number of tags (possible collisions)
- operating frequency (varies by country)
- dead time (resulting from reduced duty cycle to prevent overheating / or due to sequentially operated readers or antennas)

Using multiple approaches to analyse the detection performance of our RFID systems, we addressed the following questions:

1) How does detection rate depend on the relative position of the tag to the reader antenna?
2) How can we optimise an antenna arrangement to maximise the detection rate?

The goal of this sub-project was to quantify the read success ratio and its dependency on factors like reading distance, antenna configuration, signal power and available options in the RFID protocol.

3.2 METHODS AND MATERIALS

To examine how the detectability of our small IM-PK2525 RFID tag varies with the position of the tag relative to the reader antenna within its near field, a robotic system was developed which allows to position a tag at different locations within the near field of an antenna and to record detections reported by the RFID reader for each location. This system was then used to scan the antenna near field of the initial single-antenna setup employing the internal antenna of an MTI RU-824 Desktop USB RFID reader. We also measured the near field detection performance of three different commercially available UHF

RFID antennas, one specialised near-field antenna and two different circularly polarised ceramic patch antennas, which were connected to either the RU-824 RFID reader or to a newer multiple-antenna capable RFID reader prototype based on the commercial MTI RU00-M03X RFID module. The effect of interrogation signal power on tag detection performance was investigated by taking measurements at different power level settings. We finally measured the detectability pattern of a configuration of four ceramic patch antennas connected to the new RFID reader prototype.

Details pertaining to hardware and software of the developed measurement system will be described below.

3.2.1 *New RFID reader prototype*

As mentioned in section 2.4.1, the new custom-developed RFID reader system (Figures 3.1, 3.2) is based on a highly integrated industrial UHF RFID reader module, the MTI RU00-M03-X (Microelectronics Technology Inc., 2016), which is identical to the Impinj RS2000 module (Impinj, Inc., 2017b). The system also contains an Intel Edison module (Intel Corporation, 2017) as an embedded control computer along with a micro SD (Secure Digital) card slot for data storage and a GPS receiver which can provide accurate time and location, allowing the system to operate as an autonomous stand-alone unit, simplifying field deployment.

The RU00-M03-X comprises a single monostatic RFID reader backend combined with a four port antenna circulator allowing to connect up to four antennas which can be activated in a programmable sequence. Built around the Impinj R2000 integrated circuit, it provides an interrogation signal power of up to 31.5 dBm (1.41 W), which is 7.5 dBm higher than the maximum specified output power of the Impinj R1000 based RU-824 of 24 dBm, or 0.25 W (Microelectronics Technology Inc., 2012). The sensitivity of the RU00-M03-X module is specified at -74 dBm at 1% error rate with an antenna return loss of 15 dBm at 31.5 dBm output power using the default link profile (Impinj, Inc., 2017b).

3.2.2 *Measurement system hardware*

To find out how tag detection performance depends on the relative position of the tag to the reader antenna, we developed and built

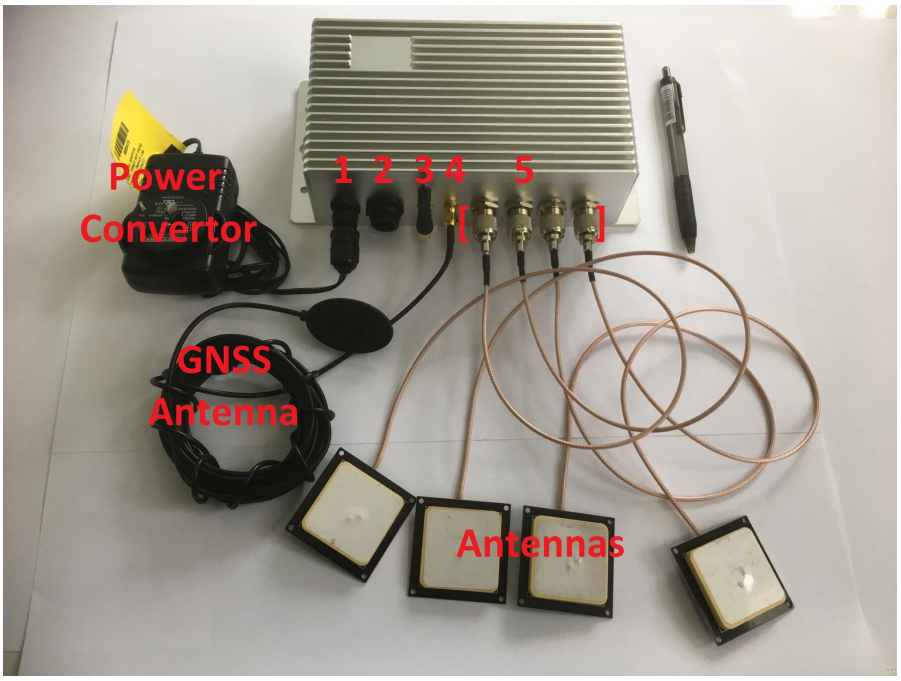

Figure 3.1: Custom-developed multi-antenna capable RFID reader prototype system (18.5 cm × 10.5 cm × 5.5 cm) based on the MTI RU00-M03-X commercial UHF RFID reader module, including peripherals. Numbered components: (1) power connector; (2) micro-USB port; (3) Wi-Fi-antenna; (4) Global Navigation Satellite System (GNSS) antenna; (5) RFID antenna connectors. Source: CSIRO

a cost effective measurement system based on a consumer grade off-the-shelf 3D printer (FlashForge Dreamer) serving as a 3D positioning stage (Figure 3.3). The tags were detected using

a) the same RFID readers which had also been used in the field experiments described above (MTI RU-824 RFID USB desktop readers), and later also
b) internal engineering prototypes of a new integrated, multi-antenna capable RFID reader system built around an a MTI RU00-M03-X module which was being developed in cooperation with an external company (RFIT Pty Ltd).

A laptop computer running Linux coordinated the automated measurement process.

Two slightly different system setups were developed for each of the two types of RFID reader we used: for measurements using the MTI RU-824, the reader modules were directly connected to the control computer via USB (see Figure 3.4). Since the RFID reader modules of the improved Impinj RS2000 / MTI RU00-M03-X based prototypes

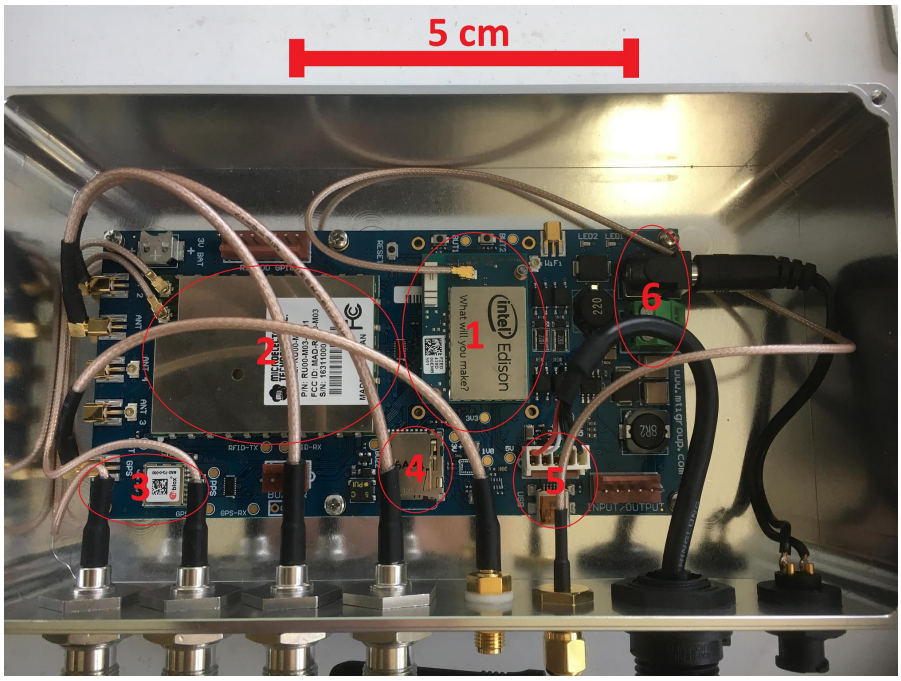

Figure 3.2: PCB of custom-developed multi-antenna capable RFID reader prototype system based on the MTI RU00-M03-X commercial UHF RFID reader module. Labelled components: (1) Embedded control computer module (Intel Edison); (2) MTI RU00-M03-X UHF RFID reader module; (3) GNSS receiver IC; (4) Micro-SD card connector; (5) external Micro-USB connector; (6) power connector. Source: CSIRO

are not directly accessible from the outside, because they are connected internally to the embedded Intel Edison control computer of the reader system via serial connection (UART – Universal Asynchronous Receiver Transmitter), the measurement system setup had to be adapted for this case. In this latter case, a secure shell (SSH) connection from the measurement system control computer to the embedded controller of the RFID system (which also runs Linux) was used to forward the embedded system's UART connection back to the control computer as a virtual device (Figure 3.5).

The measurement setup did not require any permanent modification of the 3D printer. The RFID reader antenna (or the whole reader module with its integrated internal antenna) was placed on the print bed of the 3D printer which can move up and down (i.e. in the 'Z' direction). To minimise the effect of any additional dielectric material within the near field of the tag antenna on its performance, the tags which were used as probes were glued to a plastic drinking straw (6 mm diameter) using the same cyanacrylate based glue which was also used in the field experiments to attach a tag to a bee (Cyberbond 2610 instant cyanoacrylate adhesive). Drinking straws are sufficiently

Figure 3.3: Experimental set-up for measuring the spatial pattern of detection probability depending on the position of a tag within the near field of a reader antenna using an off-the-shelf 3D printer as a positioning device. Here, an MTI RU-824 RFID reader is positioned a few cm above the print bed of a FlashForge Dreamer 3D printer used as a positioning stage. A Hitachi IM-PK2525 RFID tag is positioned just above the housing (and thus the antenna) of the RFID reader. It is attached to the print head carriage using custom designed 3D printed clamps holding a straw. Cling wrap was used to prevent the RFID reader from moving on the smooth surface of the print bed due to motion induced vibrations during the measurement. See Figure 3.9 for an example measurement result.

strong to allow accurate positioning of the tag (without bending too much depending on orientation as a result of gravity or acceleration forces during positioning) while having a very thin shell. The straw was then attached to the print head using custom designed 3D printed adapters which were clipped onto the print head carriage, which can be positioned in the (x, y) plane.

3.2.3 *Software*

The measurements were controlled using a custom-written Python (Rossum, 1995) program which accessed the RFID reader modules through their native USB or UART protocols for which the documen-

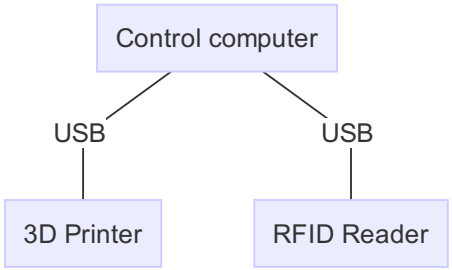

Figure 3.4: Measurement system for antenna dependent detection pattern using USB RFID reader modules (schema).

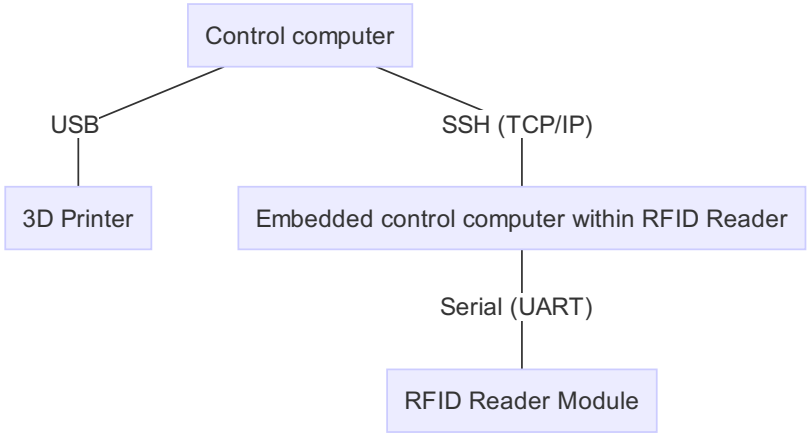

Figure 3.5: Measurement system for antenna dependent detection pattern using RFID reader system with embedded controller (schema).

tation is publicly available (Microelectronics Technology Inc., 2014; Impinj, Inc., 2016b).

3.2.3.1 *Scanning algorithm*

Initially, a very simple algorithm was used which just performed an exhaustive grid scan (Figure 3.6). Figure 3.7 shows a sequence diagram of the interactions between the components of the measurement system.

3.2.3.2 *Improved (adaptive) scanning algorithm*

The run time of an exhaustive grid scan is proportional to the covered volume, i.e. it grows according to $\mathcal{O}(\ell^3)$ with the linear dimensions ℓ of the volume, making it quite costly to add a sufficient margin around the volume of interest. Making sure that the full extent of an antenna's detection volume is covered by a scan requires to include a fair margin around the antenna.

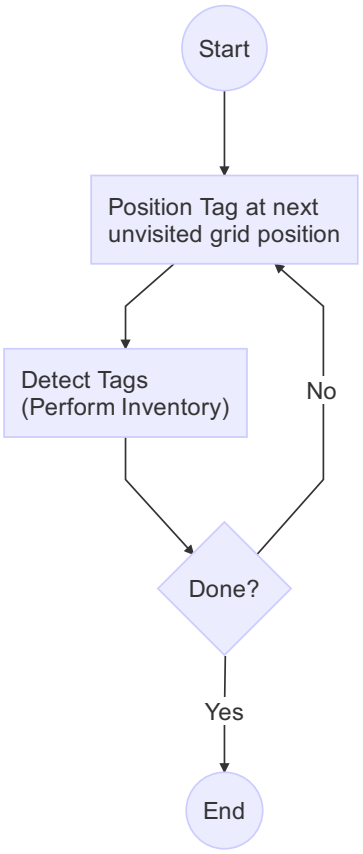

Figure 3.6: High level grid scanning measurement control algorithm.

The FlashForge 3D printer only supports asynchronous positioning commands, i.e. it does not report when the print head (x, y-axis) and the print bed (z-axis) have reached their target positions after a positioning command has been issued. Therefore, the measurement control software added a computed delay including a safety margin after each positioning command to allow the print head to reach its target position before starting the RFID inventory process for that location.

Given that probing a single point can take $t_p = 5\,\mathrm{s}$, scanning even a moderately sized single patch antenna measuring $x = 50\,\mathrm{mm}$ by $y = 50\,\mathrm{mm}$ using a step width of $\Delta\ell = 1\,\mathrm{mm}$ in each direction, resulting in a resolution of $\Delta\ell^3_{\mathrm{fine}} = 1\,\mathrm{mm}^3$, can take quite a long time. Assuming an overscan buffer of $b = 20\,\mathrm{mm}$ on each side and a maximum distance from the antenna plane of $z = 30\,\mathrm{mm}$, we are scanning every cubic millimeter of a volume of $V = (x + b)(y + b)z = 243\,000\,\mathrm{mm}^3$, amounting to

$$t_{\mathrm{total}} = \frac{T_p V}{\Delta\ell^3_{\mathrm{fine}}} = 337.5\,\mathrm{h},$$

which equals more than 14 days for a single parameter set (e.g. one particular power level for the interrogation signal).

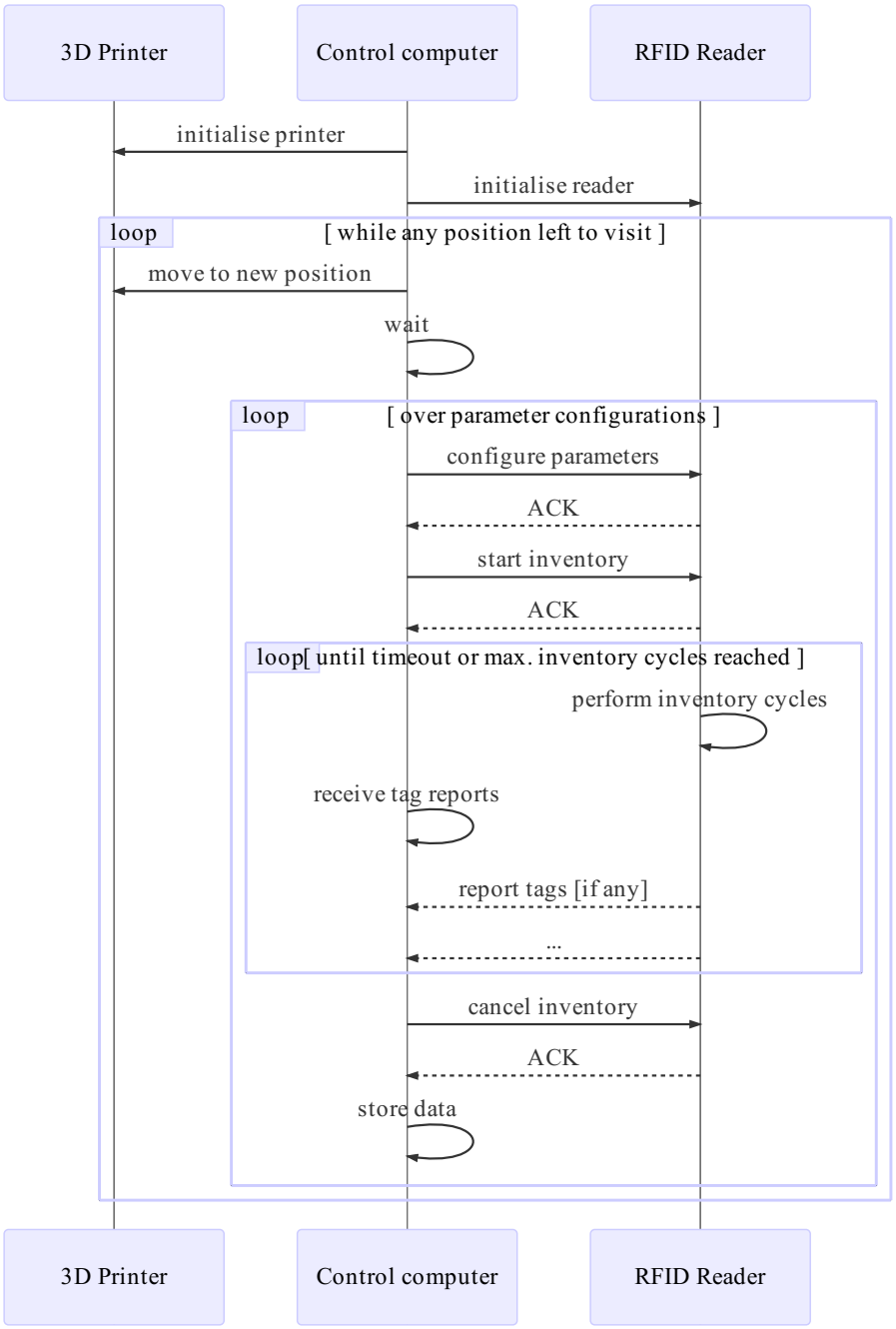

Figure 3.7: Sequence diagram of measurement control system.

Because the scan volume includes the beforementioned safety margin around the antenna, there is typically a considerable fraction of the scanned locations without any detection (which can be more than 50% depending on the shape of the detection pattern, see for example Figure 3.18). Given the rather coarse shape of the contiguous regions with detections, it suffices to reduce the scanning resolution within the no-detection regions. This allows to reduce the scanning effort and thus the time it takes to complete a measurement run.

To this end, we implemented an improved, adaptive scanning algorithm (Figure 3.8). It starts out with a coarse grid of regularly spaced 'seed locations' (typically using an isotropic step size of 5 mm) which it starts to scan. If a tag is detected at any location during a scan, the surrounding cells of that location up to the next coarse grid cell will be scanned using the full resolution (i.e. with a step size of 1 mm). Given the smooth shape of the contiguous regions within which detections occur, this ensures that these regions and their boundaries separating them from the non-detectable regions are fully covered (Figure 3.3). I chose a step width of $\Delta\ell_{\text{coarse}} = 5\,\text{mm}$ for the initial (seed) grid. This results in a reduction of the scanning effort and thus a speed-up of

$$R = \frac{\Delta\ell_{\text{fine}}^3}{\Delta\ell_{\text{coarse}}^3} = 125$$

within detection-free regions of the scanning volume, making it much more affordable to add a comfortable scanning margin. The achievable overall speed-up depends on the relative size of the detection-free volume.

3.2.3.3 *Measurement grid resolution*

The antenna of the Hitachi IM5-PK2525 RFID tags serving as probes in this experiment measures 2.5 mm by 2.5 mm. Spatial changes in the magnetic field on a smaller scale than this area would be smoothed out, because according to the Maxwell-Faraday equation

$$\oint_{\partial\Sigma} \mathbf{E} \cdot \mathrm{d}\ell = -\frac{\mathrm{d}}{\mathrm{d}t} \iint_{\Sigma} \mathbf{B} \cdot \mathrm{d}\mathbf{S}$$

(where $\mathbf{E}$ is the electric field vector, Σ the enclosed surface, and $\mathbf{B}$ the magnetic field) a coil antenna integrates the time-varying magnetic flux over the enclosed area. We thus chose a step size for the scanning grid of 1 mm in each direction. First measurements confirmed that this step size was sufficiently small, since any position at which a tag could be detected almost always belonged to a contiguous subvolume of surrounding grid positions at which the tag could also be detected and which showed smooth boundaries (Figure 3.3). This

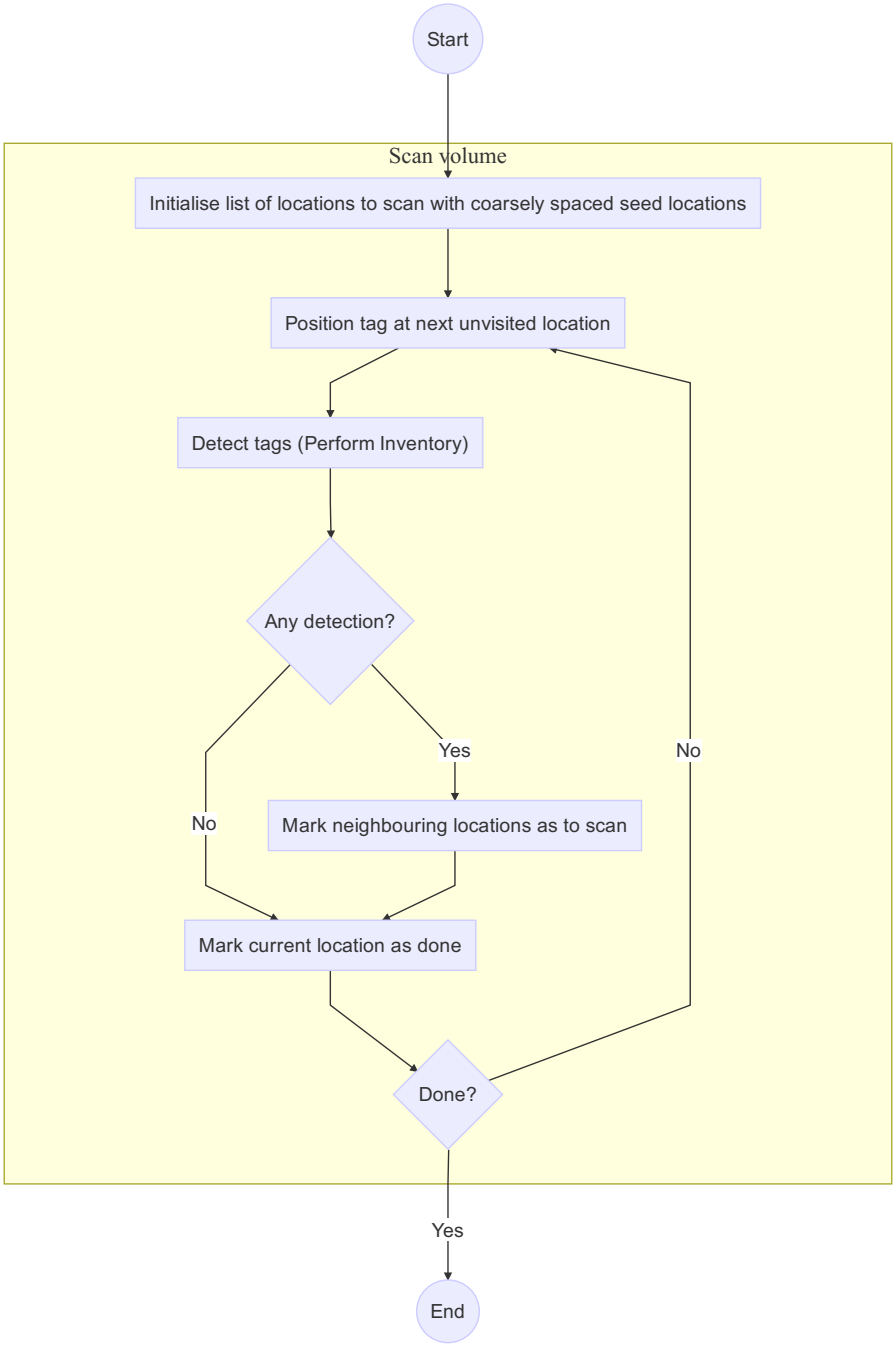

Figure 3.8: Adaptive grid scanning algorithm.

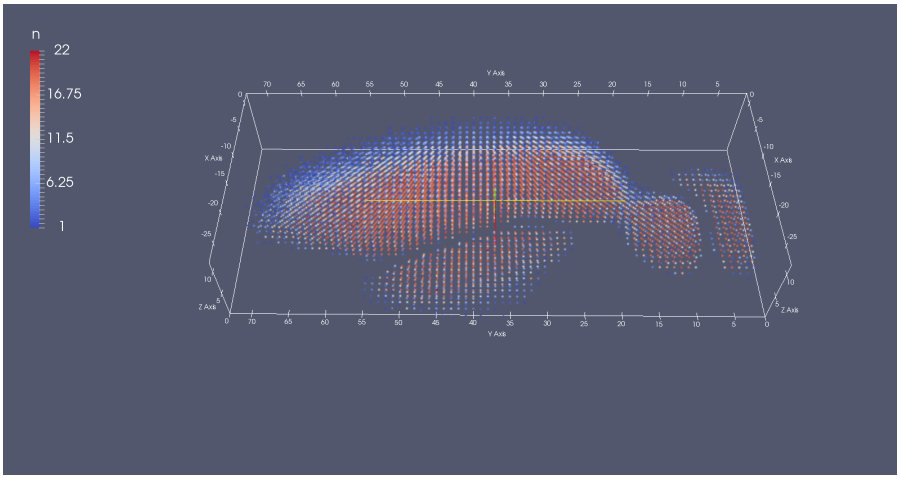

Figure 3.9: Measured detectability pattern for a Hitachi IM-PK2525 RFID tag positioned in the near field of an MTI RU-824 RFID reader equipped with an integrated antenna at +21 dBm interrogation signal power setting as measured with our 3D printer based measurement system. All axis units are mm. The (x, y) plane corresponds to the horizontal plane in Figure 3.3. Colour represents the number of detections which occurred at the respective tag position within an active detection period of max. 1 s during which the tag was interrogated up to 20 times while being stationary. The fact that sometimes more than 20 detections were counted could be caused by the way the detection cycle limit is implemented within the reader firmware.

figure also shows that the step size should not be much larger than 1 mm either, because then it would not be possible to resolve the volume separating different contiguous subvolumes from each other.

3.3 RESULTS AND DISCUSSION

3.3.1 *Single Antenna System Measurements*

A near field scan of the single antenna RFID detection system based on the MTI RU-824 USB RFID reader with integrated internal antenna which was used in the first field trials revealed an elongated irregular and asymmetric detection pattern extending up to 12 mm above the top surface of the reader (Figures 3.9, 3.10). This measurement result is consistent with the low detection rates observed in our field trials (see section 2.4.1).

Along the z direction (height), the detection profile quickly falls off, such that 75% of the detection volume lies below $z = 6$ mm (Figure

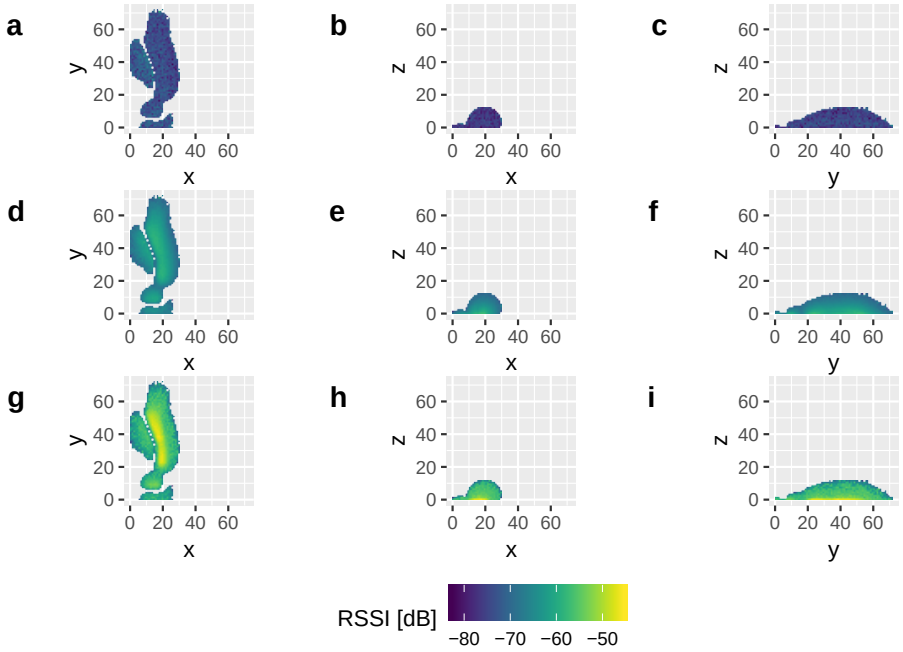

Figure 3.10: 2D projections of the measured detectability pattern for the internal antenna of an MTI RU-824 RFID reader, corresponding to Figure 3.9. Colour indicates signal strength (Received Signal Strength Indicator, RSSI): a) to c) show the minimum, d) to f) the mean, and g) to i) the maximum RSSI throughout the volume projected onto to the plot plane. Note that the pattern is offset along the x-axis compared to Figure 3.9 to reduce the required axis range while maintaining an aspect ratio of 1:1.

3.11), which explains the overall low detection rates, because reader and tag were typically separated by at least the height of a bee, even for a bee walking directly on top of the reader module.

Since there is evidence for individual lateral preferences in some bee species (Kells and Goulson, 2000; Goulson, Park et al., 2013), the profile's asymmetry along the y direction (parallel to the long side of the reader module) could explain the in/out detection asymmetry for individual bees as shown in Figure 2.11.

Since the IM-PK2525 RFID tag is inherently a near-field tag coupling predominantly to the magnetic field of the antenna, we assumed that a specialised near-field antenna designed to generate a high-intensity and relatively homogeneous magnetic field in its vicinity would be suited well to our application. We therefore measured the detection pattern of an Impinj A0303 Mini Guardrail Antenna (Impinj, Inc., 2017a), depicted in Figure 3.12. This antenna employs a segmented loop design similar to the one described in Qing et al. (2009) to achieve a constant current phase around the loop, resulting in an increased magnetic component of the near field. The detectabil-

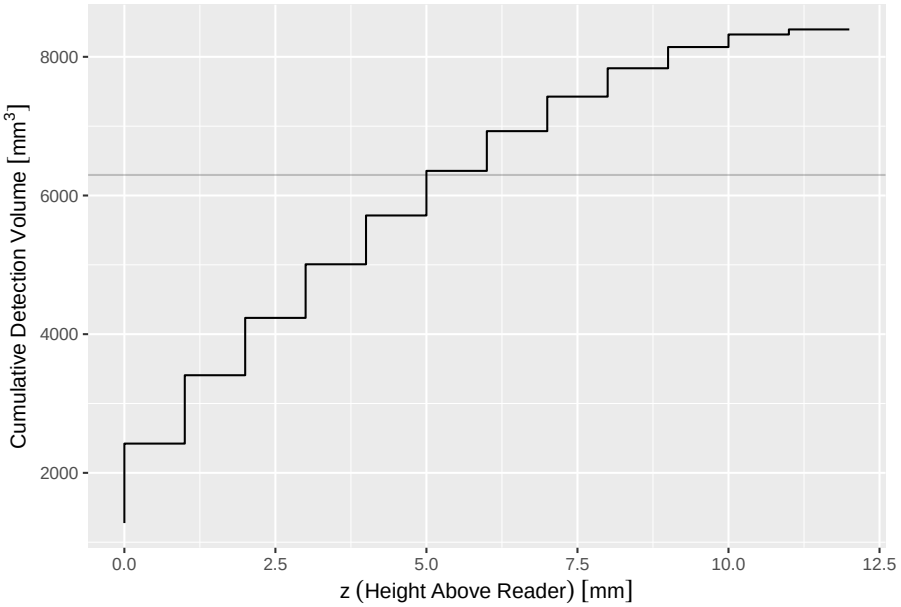

Figure 3.11: Cumulative distribution of measured detection volume from Figure 3.10 along the z-axis. The grey horizontal line represents the 75th percentile, indicating that over 75% of all detectable locations lie below $z = 5\,\text{mm}$.

ity pattern of this antenna indeed shows a relatively homogeneous magnetic field which results in a horizontally spread out, but very flat detectability region (Figure 3.14). The detectability region of this antenna was so flat that we could only detect the tag after removing the top cover (Figure 3.13). We concluded that antennas exhibiting a more localised magnetic field component are better suited to our application.

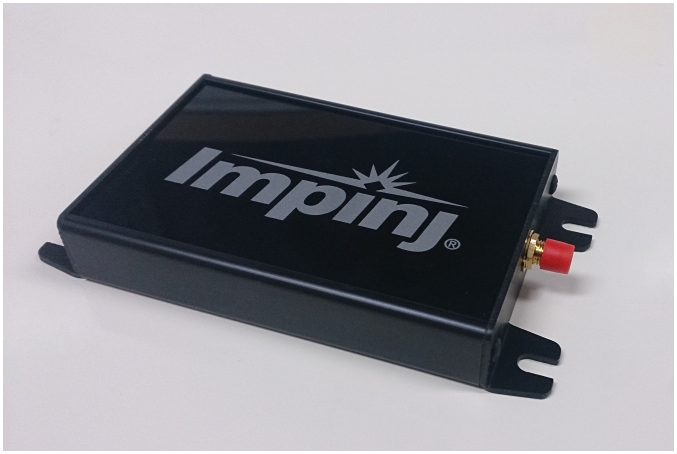

Figure 3.12: Impinj A0303 Mini Guardrail Antenna (133 mm × 70 mm × 19 mm). This antenna is designed to work well with predominantly magnetically coupled near-field UHF RFID tags in close proximity.

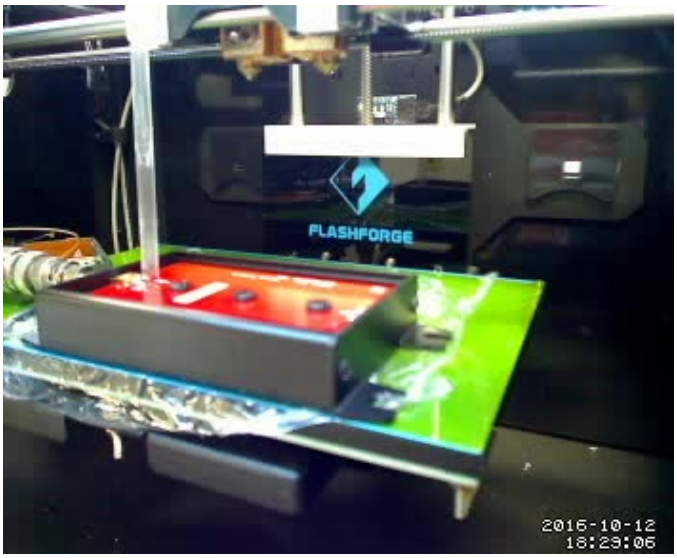

Figure 3.13: Detection pattern measurement of Impinj A0303 Mini Guardrail Antenna. For this measurement, the top cover of the antenna had to be removed to allow the tag to get close enough to the conducting traces of the printed circuit board (PCB) of the antenna to be detected at all. The probe RFID tag (Impinj IMPK2525) is located at the bottom of the drinking straw (transparent tube), with its surface normal parallel to the straw.

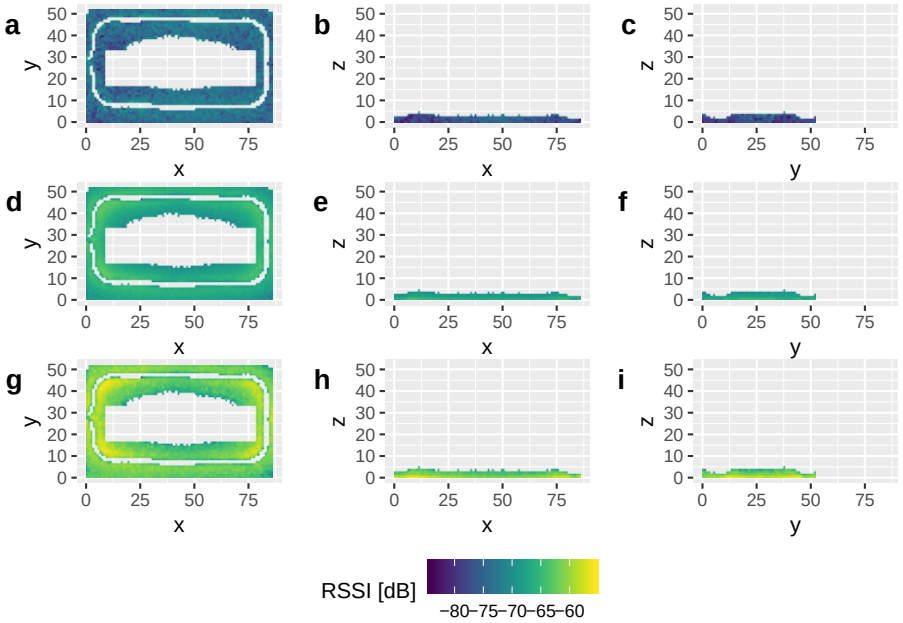

Figure 3.14: 2D projections of the measured detectability pattern for an Impinj A0303 Mini Guardrail Antenna connected to an MTI RU-824 RFID reader, measured at +27 dBm interrogation signal power. Colour indicates signal strength (Received Signal Strength Indicator, RSSI): a) to c) show the minimum, d) to f) the mean, and g) to i) the maximum RSSI throughout the volume projected onto to the plot plane. The horizontal scanning area was limited by the inner dimensions of the case of the antenna, because the tag could only be detected after removing the top cover of the antenna and probing close to the actual antenna PCB inside the case. The innermost region also had to be spared because of the presence of spacers in this location (see Figure 3.13).

Due to the small size of the antenna of the Hitachi IM-PK2525 RFID tag, we expected the detection range to be limited by the power the tag requires to operate, which it extracts from the interrogation signal emitted by the reader antenna. We therefore investigated the effect of increasing the interrogation signal power level up to the maximum level supported by the RFID reader module. The received signal strength as reported by the RFID reader in the RSSI (received signal strength indicator) field for each tag detection was averaged over all tag positions yielding at least one detection. The averaged RSSI exhibited a minimum at an interrogation power level of 18 dBm around which it close to linearly increased with changing interrogation power (on the logarithmic dB scale, thus correspondig to a product of exponentials with exponents of opposite sign), as can be seen in Figure 3.15. We found that an increase in RSSI did not correspond to the expected increase in detection volume: for interrogation signal power levels different from +18 dBm the detectable volume decreases with increasing power difference from +18 dBm (Figures 3.16 and 3.17).

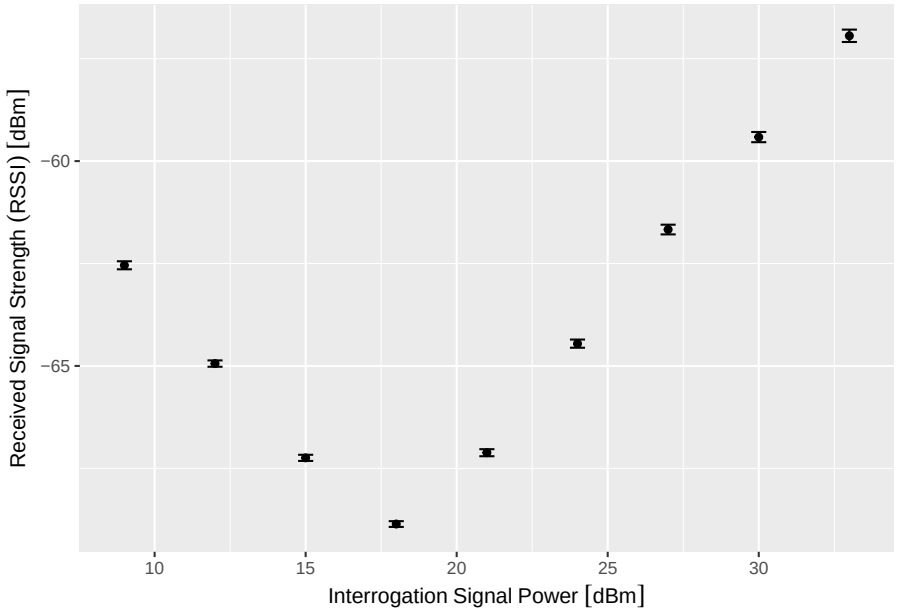

Figure 3.15: Signal strength reported by the detector as RSSI (Received Signal Strength Indicator) in units of dBm for all detections throughout the scanned near-field of an ARRUN5-915 ceramic patch antenna (Abracon Corporation, 2014b) connected to the new MTI RU00-M03-X based RFID reader prototype system using an IM-PK2525 tag as a probe.

This result is likely due to the fact that increased power of the reflected interrogation signal from the antenna reduces the effective sensitivity of the RFID reader at higher power levels, overcompensating the increase in received tag signal power which would otherwise suggest increased detectability, and reduced signal to noise ratio for lower power levels. In this power regime, the limiting factor for tag detectability is not the power required by the tag to operate, but the effective reader sensitivity at the given power level.

We therefore concluded that the optimum power level for use with an ABRACON ARRUN 915 MHz antenna is close to +18 dBm for both readers, the MTI RU-824 and the new MTI RU00-M03-X based prototype (Figures 3.16 and 3.17). To facilitate a meaningful comparison between the two reader modules, these measurements were conducted using an external ARRUN 915 MHz antenna connected to the internal antenna port of the RU-824 reader instead of using its internal antenna.

We further measured two commercial UHF RFID ceramic patch antennas of different sizes. The larger type, an ABRACON ARRUN5-915.000MHz antenna (Abracon Corporation, 2014b), has a ceramic substrate measuring 80 mm × 80 mm, while the smaller type, an ABRACON ARRSN5-915.000MHz (Abracon Corporation, 2014a)

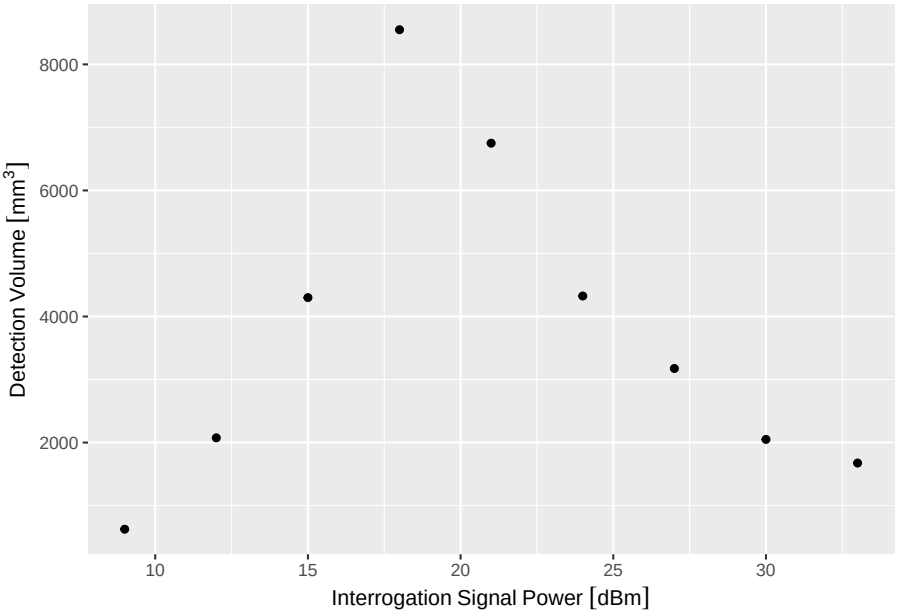

Figure 3.16: Detection volume (number of scanned grid locations yielding one or more detections) vs. interrogation signal power, measured using the new MTI RU00-M03-X based RFID reader prototype connected to an external ceramic patch antenna (ABRACON ARRUN5-915.000 MHz). Despite higher interrogation power levels leading to increased measured RSSI levels (see Figure 3.15), the actual detection volume / number of grid locations where the probe tag could be detected at all *decreases* with increasing interrogation power. This is likely due to the receiver input stage being overdriven into saturation.

employs a ceramic substrate of 45 mm × 45 mm. As expected, the larger antenna (ARRUN5) yielded a smaller vertical detection range of 9 mm at 18 dBm (Figure 3.18) than the ARRSN5, which achieved a maximum vertical range of 34 mm at 27 dBm (Figure 3.19). This difference in the optimal interrogation signal power is likely due to a lower reflection coefficient of the antenna, which enables us to exploit the benefits of using higher reader power to increase the reading range.

Based on these results, we decided to base our next steps on the ARRSN5 antenna, because the shape and size of its detection volume are well matched to using it as a detection antenna inside an entrance tunnel of a bee hive or artificial feeding station.

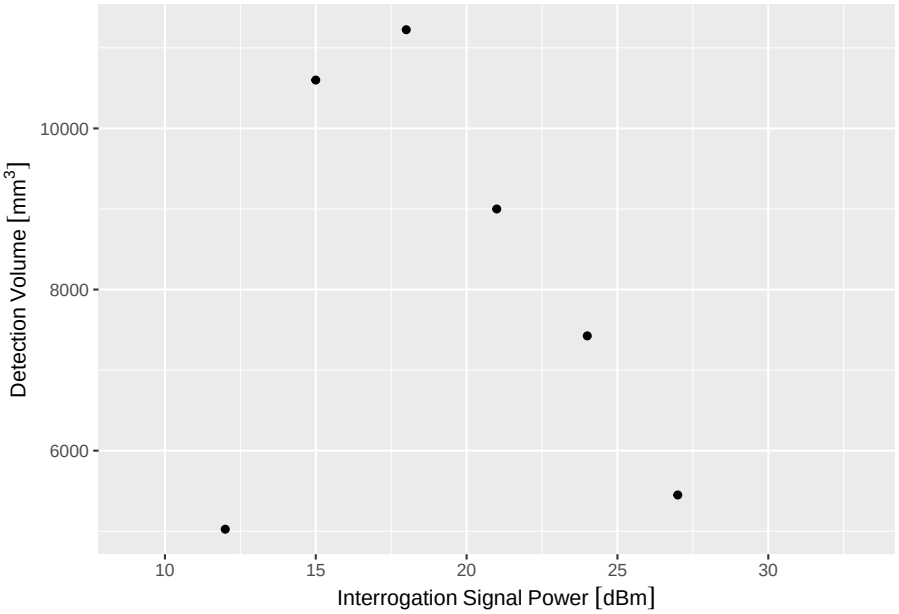

Figure 3.17: Detection volume (number of scanned grid locations yielding one or more detections) vs. interrogation signal power, measured using an MTI RU-824 RFID reader connected to an external ceramic patch antenna (ABRACON ARRUN5-915.000 MHz). This reader/antenna combination also achieves its maximum detection volume at around +18 dBm.

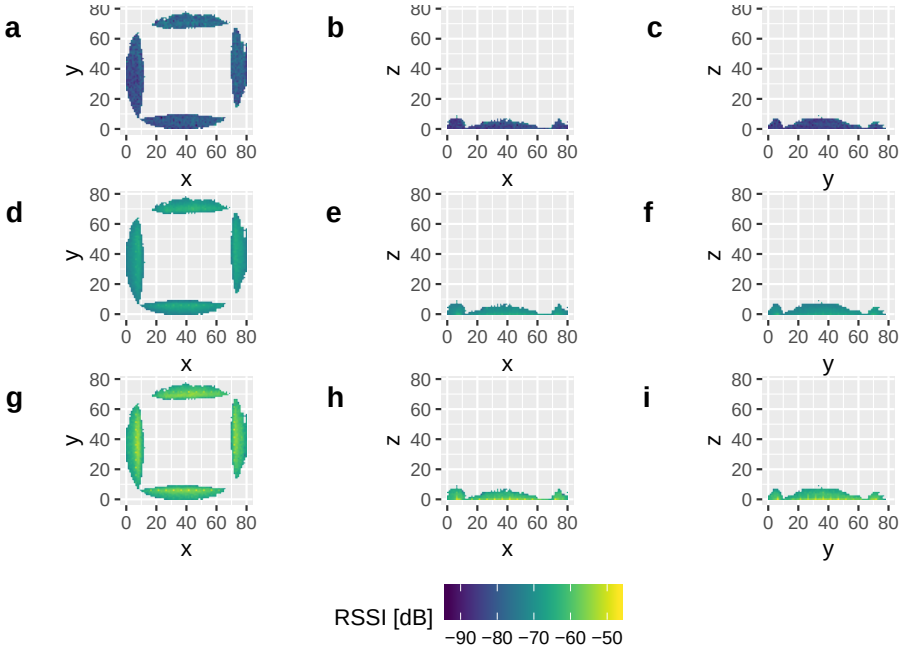

Figure 3.18: 2D projections of the measured detectability pattern for an ABRACON ARRUN5-915.000 MHz 80 mm × 80 mm ceramic patch antenna, measured at +18 dBm interrogation signal power where it exhibits the highest detection volume in combination with the MTI RU00-M03-X based RFID reader prototype. Colour indicates signal strength (Received Signal Strength Indicator, RSSI): a) to c) show the minimum, d) to f) the mean, and g) to i) the maximum RSSI throughout the volume projected onto to the plot plane.

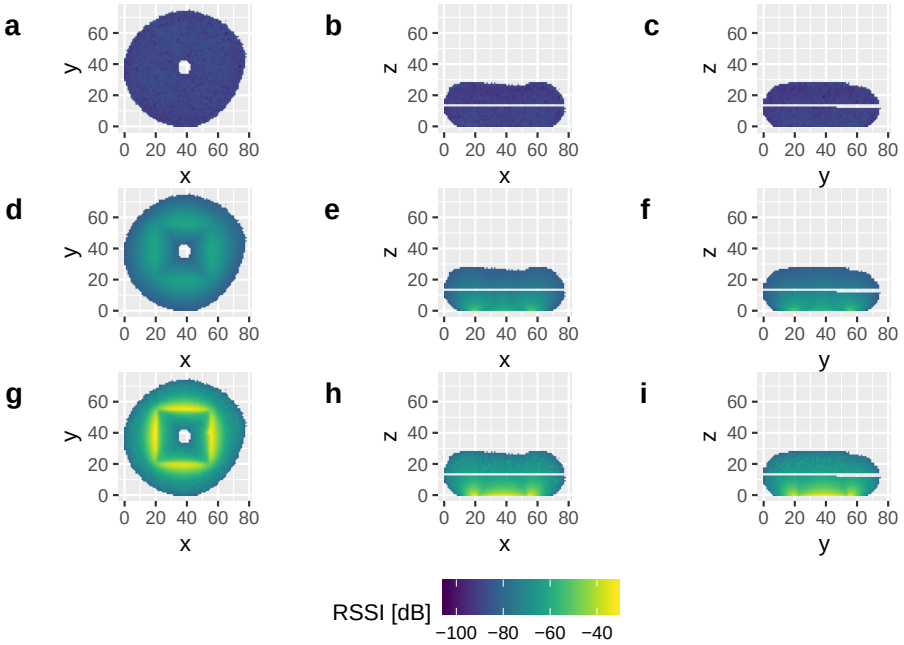

Figure 3.19: 2D projections of the measured detectability pattern for an ABRACON ARRSN5-915.000 MHz ceramic patch antenna with a ceramic substrate of 50 mm × 50 mm, measured at +27 dBm interrogation signal power (which yielded the maximum detection volume). Colour indicates signal strength (Received Signal Strength Indicator, RSSI): a) to c) show the minimum, d) to f) the mean, and g) to i) the maximum RSSI throughout the volume projected onto to the plot plane. The gaps at $z = 19$ mm and $z = 20$ mm are caused by missing data as a result of a technical problem during the measurement.

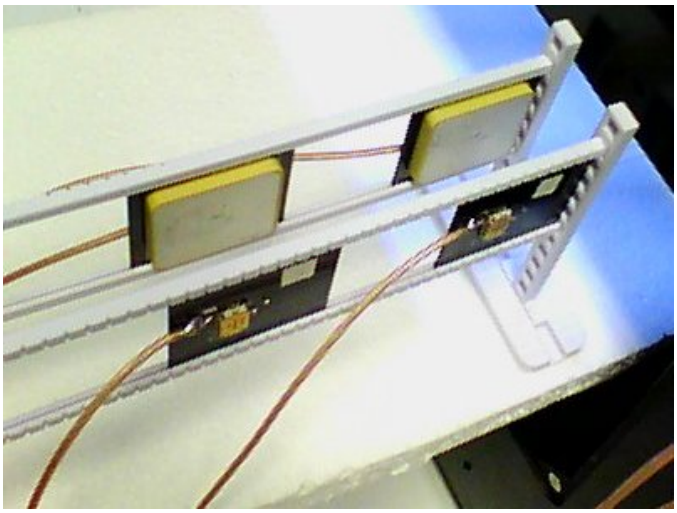

Figure 3.20: Custom-designed 3D printed adjustable measurement rig used for measuring detection pattern of four-antenna configuration. Gap between opposite antennas: 25 mm (surface to surface), separation between antenna pairs: 89 mm (center-to-center).

3.3.2 *Four-antenna configuration measurements*

In the last section, we demonstrated that the small IM-PK2525 RFID tags we use for tagging bees can be detected best within localised regions of high magnetic field strength inside the near-field of an antenna. We showed that the distribution of these regions in the near field structure of a patch antenna is well suited to detecting tagged bees moving past such an antenna placed within the entrance tunnel of a bee hive or an artificial feeding station. To further enhance the detection success rate and thus minimize the number of missed readings, we combined this insight with the fact that we are only interested in detecting tags in a confined space which is smaller than the wavelength of the RFID carrier frequency (which ranges from 31 cm to 35 cm for UHF RFID between 860 MHz and 960 MHz). In an effort to increase the volume of high-intensity magnetic field regions further away from the primary antenna (an ABRACON ARRSN5-915.000 MHz ceramic patch antenna), we placed an identical antenna, facing upside down, opposite to the primary one at a distance of a few cm (Figure 3.20). This secondary antenna was not actively driven, but parasitically coupled to the primary antenna, effectively forming a single antenna with a modified field configuration. Due to the requirement to sense whether the tagged bees enter or leave the hive (or feeding station), we placed a second such antenna pair next to the first pair, resulting in an antenna configuration as shown in Figure 3.20, which depicts the antennas mounted on a purpose-built 3D printed adjustable measurement rig.

All four antennas were simultaneously connected to the ports of the MTI RU00-M03-X based RFID reader prototype and operated in a round-robin sequence: each of the antennas was active as transmitter and receiver for a certain amount of time before switching to the next one. During the active period of one antenna, the other antennas were parasitically coupled to this active antenna.

First detectability measurement results obtained by scanning the volume between the antennas indicate that this approach works as expected, as can be seen in Figures 3.21, 3.22, and 3.23, each of which shows a different tag orientation. For this measurement, the two opposing antennas forming a pair were placed 25 mm apart (surface-to-surface distance), since this distance would provide sufficient clearance for the entrance tunnel which the bees use both for entering or leaving the hive and as a ventilation duct to maintain hive temperature by fanning air using their wings. The two pairs were placed at a distance of 89 mm from each other, the maximum feasible distance given the limited movement range of the 3D printer's print head carriage carrying the probe. As discussed in the next section (3.3.2.1), there is measurable crosstalk between the antenna pairs at this separation distance, indicating that a larger separation would be desirable for field deployments. However, even at this distance the tag was already predominantly detected by the correct antenna pair according to its position between the antenna pairs (see Figure 3.27).

The resulting detection pattern corresponds to a superposition of the individual detection patterns of the four constituent antennas with the received signal strength being highest in the high magnetic field regions close to the perimeter of the antenna patches of each antenna. For all tag orientations the detectable volume almost completely covers the cross-section of the scanned volume, as can be seen in the middle column (projection onto the (x, z)-plane) of Figures 3.21, 3.22, and 3.23.

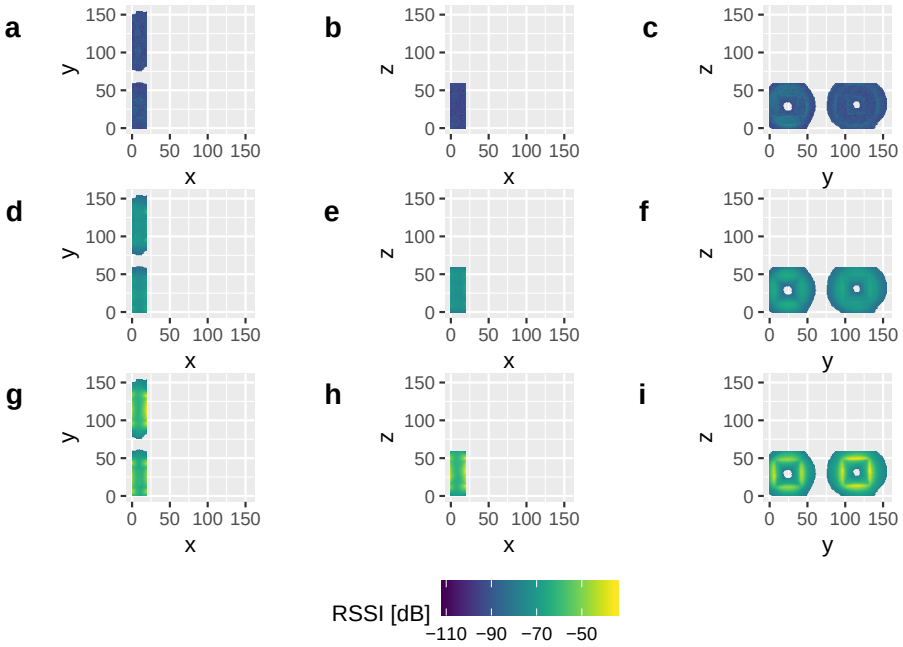

Figure 3.21: 2D projections of the measured detectability pattern for a configuration of four ABRACON ARRSN5-915.000 MHz 50 mm × 50 mm ceramic patch antennas, measured at +27 dBm interrogation signal power (which yielded the maximum detection volume) for tags oriented parallel to the antenna surfaces. Due to the movement limits of the 3D printer axes, the detectability pattern could not be fully covered and thus appears clipped. The results show that a tagged bee passing through the scanned volume (along the y-axis) would have a very high chance to pass through a detectable region. Colour indicates signal strength (Received Signal Strength Indicator, RSSI): a) to c) show the minimum, d) to f) the mean, and g) to i) the maximum RSSI throughout the volume projected onto to the plot plane.

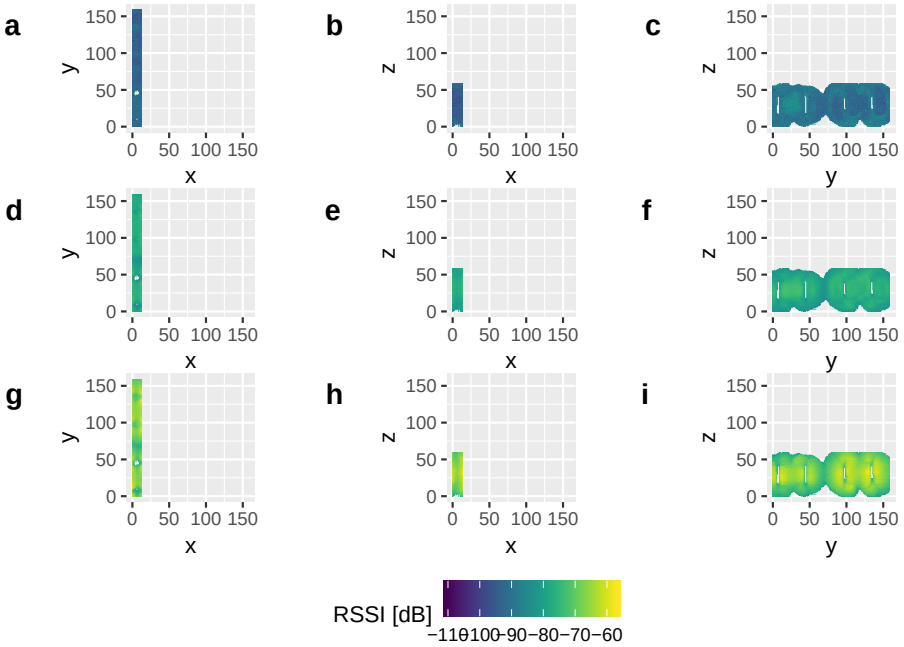

Figure 3.22: Measured detectability pattern of the four-antenna configuration shown in Figure 3.21 using identical parameters, but for tags oriented normal to the x-axis (perpendicular to the antenna surfaces). Colour indicates signal strength (Received Signal Strength Indicator, RSSI): a) to c) show the minimum, d) to f) the mean, and g) to i) the maximum RSSI throughout the volume projected onto to the plot plane.

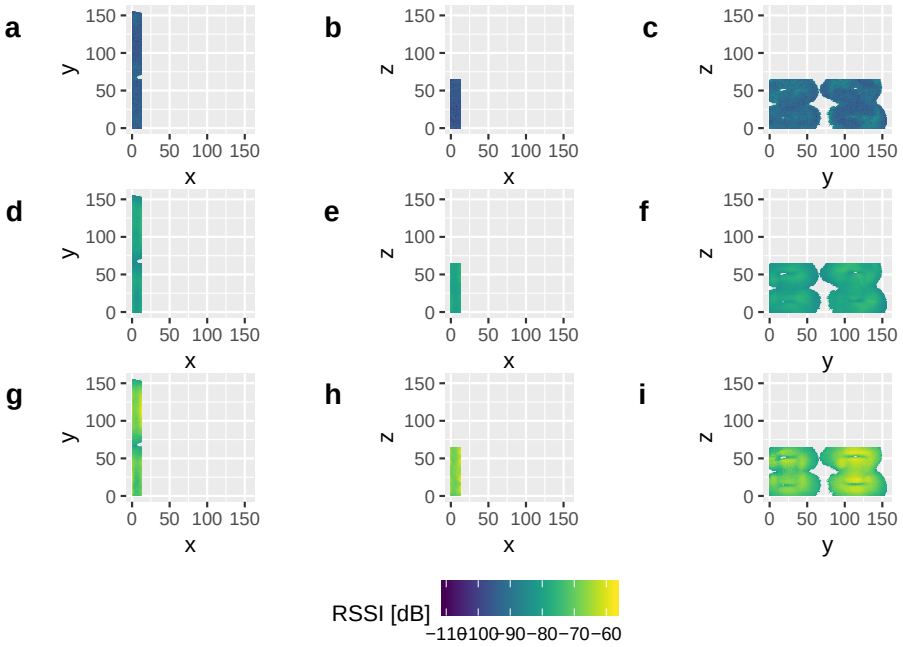

Figure 3.23: Measured detectability pattern of the four-antenna configuration shown in Figures 3.21 and 3.22 using identical parameters, but for tags oriented normal to the z-axis (perpendicular to the antenna surfaces). Colour indicates signal strength (Received Signal Strength Indicator, RSSI): a) to c) show the minimum, d) to f) the mean, and g) to i) the maximum RSSI throughout the volume projected onto to the plot plane.

3.3.2.1 *Antenna crosstalk*

Coupling between the antennas might cause tags to be detected by the currently active antenna although they are located outside of this antenna's detection range, but instead are within the detection range of another antenna coupled to the active one. In the context of detecting in which direction tagged bees passing through two antenna pairs located towards the ends of an entrance tunnel are moving through the tunnel, this would cause erroneous detection sequences yielding to possible misinterpretations of their movement direction.

Figures 3.24, 3.25, and 3.26 show the effects of this antenna coupling as measured in the four-antenna configuration described above (Section 3.3.2) for different orthogonal tag orientations from two perspectives. It can be seen that crosstalk is strongest between the two opposing antennas of each pair (which would not cause any issues with determining movement direction), but that there are also regions for which crosstalk to the currently inactive antenna pair would lead to erroneous detections as described and shown in Figure 3.27. Electromagnetic simulations indicate that this cross-pair coupling can be reduced by placing the two antenna pairs further apart (see Figure 4.4). Unfortunately, a larger pair separation distance would exceed the limits of the measurement system described above; we therefore turned to field experiments (Warren, 2017) and electromagnetic simulations (Chapter 4) to determine an optimal separation distance.

In addition to parasitic coupling of the antennas (i.e. the passive antennas receiving energy from the field generated by the active antenna), there could also be some additional coupling through the ports of the RFID reader (which are internally connected to a circulator IC), which we have not been able to measure yet.

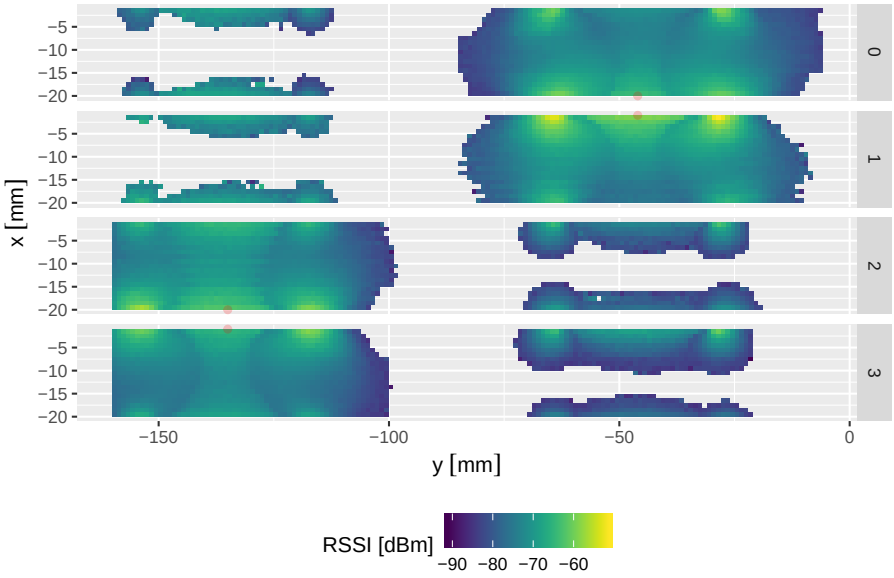

Figure 3.24: Visualisation of antenna crosstalk from the measurement shown in Figures 3.21 – 3.23 for tags oriented parallel to the antenna surfaces. Each row corresponds to one active antenna, as indicated by the row labels. The labels correspond to the following antenna positions (relative to this Figure): 0) bottom right, 1) top right, 2) bottom left, 3) top left. Colours correspond to the projection of the mean of the received signal strength (RSSI) for probe tags oriented parallel to the antenna surfaces, adjusted for their position offsets, averaged over all detections at each position through the scanned volume along the projection axis (z-axis). This figure shows that a tag oriented parallel to the antenna surfaces is most likely to be detected by the active antenna (marked with a red dot) if it is close to this antenna or the one opposite to that, but that it can also be detected by this active antenna if it is located close to one of the inactive antennas of the other antenna pair, albeit with a lower mean received signal strength.

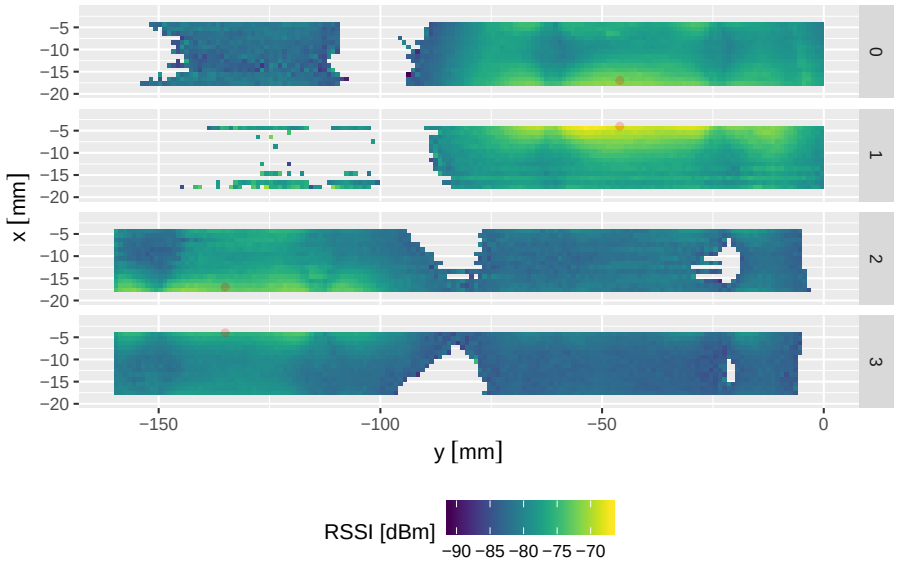

Figure 3.25: Visualisation of antenna crosstalk from the measurement shown in Figures 3.21 – 3.23 for tags oriented perpendicular to the antenna surfaces. Each row corresponds to one active antenna, as indicated by the row labels. The labels correspond to the following antenna positions (relative to this Figure): 0) bottom right, 1) top right, 2) bottom left, 3) top left. Colours correspond to the projection of the mean of the received signal strength (RSSI) of each of the 3 probe tags of the 5-tag probe which are oriented perpendicular to the antenna surfaces (adjusted for their position offsets) averaged over all detections at each position through the scanned volume along the z-axis. This figure shows that a tag oriented perpendicular to the antenna surfaces is most likely to be detected by the active antenna (marked with a red dot) if it is close to this antenna or the one opposite to that, but that it can also be detected by the active antenna if it is located close to one of the antennas of the other antenna pair, albeit with a lower mean received signal strength. Note that the probe tags of the shown orientations could not get any closer to the antenna surfaces than 3 mm due as a consequence of the probe geometry.

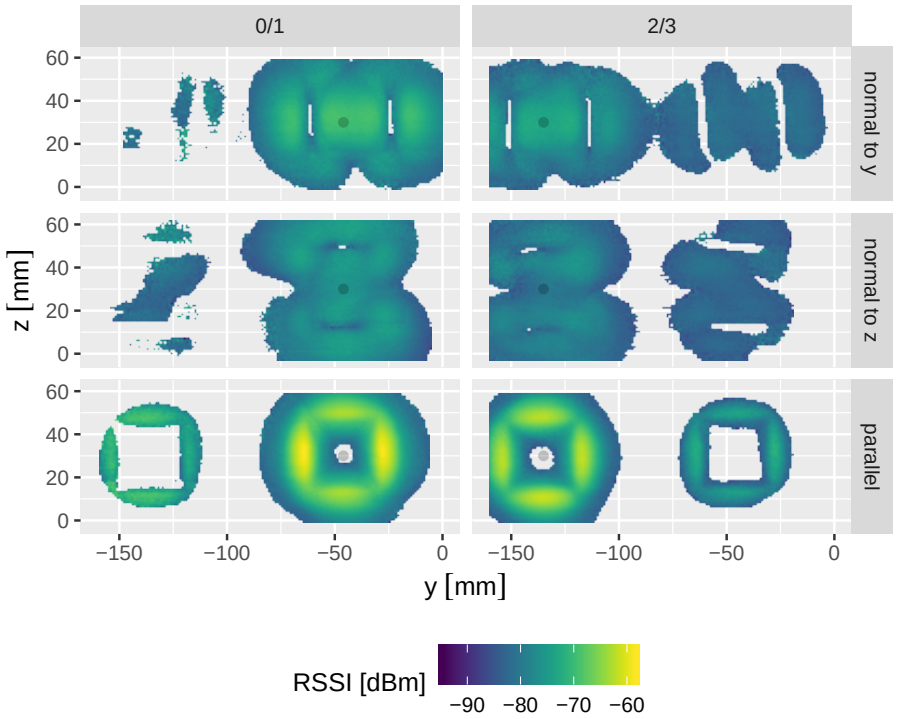

Figure 3.26: Visualisation of antenna crosstalk from the measurement shown in Figures 3.21 – 3.23. Each column corresponds to one active antenna, as indicated by the row labels. The labels correspond to the following antenna positions (relative to this Figure): 0/1) right, 2/3) left. Colours correspond to the projection of the maximum of the received signal strength (RSSI) of each of the 5 probe tags (adjusted for their position offsets) averaged over all detections at each position through the scanned volume along the z-axis (note that the probe tags in the top, bottom and front positions can not get closer to the antenna surfaces than 3 mm, which results in the blank areas at the lowest and highest y values). This figure shows that a tag is most likely to be detected by the active antenna (marked with a red dot) if it is close to this antenna or the one opposite to that, but that it can also be detected by the active antenna if it is located close to one of the antennas of the other antenna pair, albeit with a lower mean received signal strength.

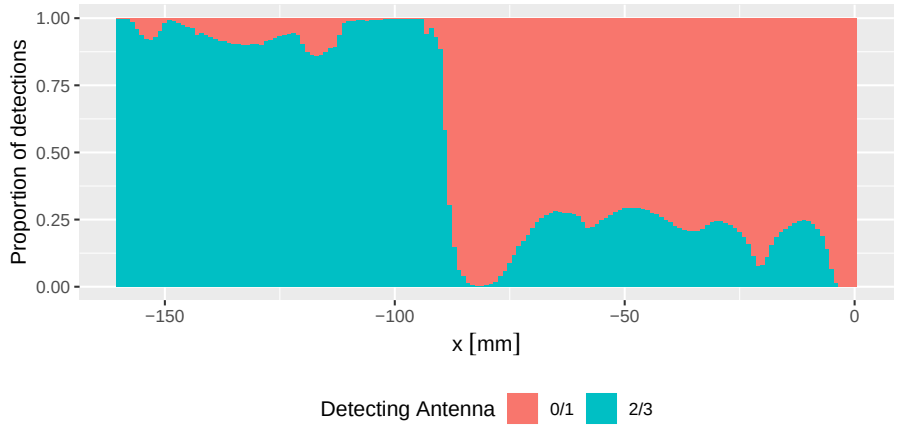

Figure 3.27: Proportions of the empirical marginal distribution of the detecting antenna conditioned on the position along the y-axis of the four-antenna configuration presented in the preceding figures. Bees moving through an entrance tunnel equipped with such an antenna configuration would have to pass through all points along the y-axis. If the bee can be detected multiple times during this passage, the higher probability of detection by the correct antenna pair could be exploited to infer the true direction of movement in the presence of misdetections.

3.3.2.2 *Detection timing*

For this measurement, the four antennas were operated sequentially: one antenna was active for up to 250 ms (or until 40 inventory rounds according to ISO-18000-63 had completed - whichever came first) before the reader would automatically switch to the next antenna in sequence (in field trials we used 125 ms and 20 inventory rounds). This means that each antenna was active (powered) and detecting tags at least once per second. For each tag detection, 144 bits of tag information were transmitted, as the tag's unique read-only ID (Tag-ID, or TID) of 48 bits was transmitted alongside the 96 bit EPC code in this case.

For a set of 5 tags simultaneously located within the detectable volume, the median time it takes for the full set to be detected is 50 ms (corresponding to a full-set detection rate of 20 times per second), the 95th percentile is 151 ms (corresponding to a full-set detection rate of 6.62 times per second).

3.3.3 *Conclusion and future optimisation opportunities*

In this chapter we demonstrated that it is possible to build a robotic measurement system capable of measuring the magnetic near-field of antennas at UHF RFID frequencies with a spatial resolution of 1 mm based on an off-the-shelf consumer-grade 3D printer in combination with an RFID reader capable of measuring received signal strength (RSSI) and inexpensive ultra-small package RFID tags.

We used this system to measure detection performance characteristics of two different RFID reader systems in combination with three commercially available UHF RFID antennas. We found that the size and shape of the detection volume of the stand-alone desktop UHF RFID reader with integrated antenna we used in the first field trials was not sufficient to reliably detect tagged bees walking past its antenna. We also found that two of the tested commercial antennas did not meet our requirements either: the detection patterns of both, a specialised near-field antenna, and a relatively large (80 mm × 80 mm substrate size) ceramic patch antenna, turned out to be spread out along the antenna surface but did not extend sufficiently far from the surface. In combination with the new RFID reader prototype, the third tested antenna, a smaller ceramic patch antenna (with a substrate sized 45 mm × 45 mm) showed the most promising detection pattern, extending vertically up to 30 mm from the antenna surface.

Based on this antenna, we designed a configuration of four identical antennas, arranged in two opposing pairs. Measurement results of the detection pattern of this antenna configuration suggest that it is well suited to our application of detecting RFID tagged bees.

Field tests of antenna arrangements of this kind with varying distances between the individual antennas, mounted within the entrance tunnel of an artificial feeding station for honey bees in the course of a Honours' thesis confirmed that using this antenna configuration effectively reduced the proportion of missed detections down to 2.7%, achieving a successful detection rate of 97.3% which is better than that of any previously published study (Warren, 2017).

All measurements were conducted using the (identical) default link profile of both readers (Table 3.1). The ISO 18000-63 standard includes provisions for using higher speed read modes which could potentially lead to further increases in detection performance. Buettner and Wetherall (2008) found in an empirical study on RFID detection performance that the achievable tag detection performance depends on many factors. Although their results suggest that using one of the higher speed reader modes or altering other protocol parameters would be unlikely to increase the net detection performance significantly in our case, this still needs to be examined. Another aspect which should be addressed in future research is the influence of the number of simultaneously readable tags on the detection performance. Here, again, Buettner and Wetherall's results (ibid.) suggest that numbers of tags ranging up to a few tens are not likely to cause any problem in terms of detection performance limits. They were able to show that they could read a full set of 16 tags at least seven times per second at a tag data rate of 26.7 kbps in a so-called dense-reader-mode which uses Miller-4 encoding of the tag data (see ISO 18000-63 (2013)) for increased robustness against interference. Since we also use the robust Miller-4 encoding, but at a faster data rate of 62.5 kbps, the achievable detection rates in our case should be higher than those reported therein.

Table 3.1: Parameters of the RFID reader link profile used in our measurements as defined in the ISO 18000-63 / GS1 standard (2013), corresponding to the default setting of both RFID readers, the MTI RU-824 and the MTI RU00-M03-X based prototype (Microelectronics Technology Inc., 2014, 2016).

Parameter	Value
Modulation Type	PR-ASK
Tari Duration [µs]	25
Data01 Difference	0.5

Parameter	Value
Pulse Width [µs]	12.5
R-T Calculation [µs]	62.5
T-R Calculation [µs]	85.33
Divide Ratio	21.33
Data Encoding	Miller-4
Pilot Tone	1
Link Frequency [kHz]	250
Data Rate [kbps]	62.5

One inherent drawback of our measurement system is the presence of metal parts of the 3D printer relatively close to the antenna under test (at distances which are comparable to the wavelengths). In our particular case this is not likely to have a significant influence, because our tags mainly couple to the magnetic field and require the magnetic coupling to the antenna to be quite strong (as they can only be detected very close to the antenna). Thus, any non-ferrous metal within the antenna near-field is unlikely to have a strong influence on our results. In the general case of measuring tags which also couple to the electric field however, this would have to be taken into account.

Furthermore, the scanning speed and movement range of the measurement system can be improved by utilising probes carrying more than one tag in a regular 1D, 2D or even 3D grid. First tests we performed using 1D and 2D arrays indicate that this method does work well and can yield speed gains linear in the number of probe tags used. However, calibration and alignment can be more difficult using this approach: for a probe with a single tag, the positioning precision and accuracy only depend on the alignment of the 3D printer, which for consumer grade printers is typically close to 0.1 mm (Zhang et al., 2013). This approach might also require taking into account mutual influences between the probe tags. However, we did not notice any obvious mutual influence using 5 probe tags located 3 to 6 mm from each other with two parallel pairs oriented perpendicular to each other pair and another single tag perpendicular to both pairs.

Finally, knowing the residual output power of the inactive antenna ports of the multi-port RFID reader (resulting from crosstalk with the active port) as well as the impedance of these inactive ports would be helpful for understanding the measurement results in terms of underlying field strengths. In the context of our application, this is however irrelevant, because we are ultimately interested in the actual tag detection performance as measured by this system.

4

IMPROVING DETECTION PERFORMANCE BY OPTIMISING A CONFIGURATION OF FOUR ANTENNAS BASED ON ELECTROMAGNETIC SIMULATIONS

4.1 INTRODUCTION

This chapter continues the analysis of the four-antenna configuration consisting of two opposing antenna pairs arranged side by side which was introduced in Chapter 3. There we showed that this antenna configuration exhibits a detection volume whose shape is well matched to detecting tagged bees walking through a hive or feeder entrance tunnel equipped with such an antenna configuration connected to a four-port RFID reader. However, the detection pattern measurement for such an antenna configuration with a separation of 89 mm between the antenna pairs also revealed that there was non-negligible cross-talk between the two antenna pairs, limiting our ability to detect the direction of motion of tagged bees passing through the tunnel (Figures 3.24 – 3.27). One way to mitigate this coupling issue while using the same interrogation signal power level to maintain the maximum possible detection volume would be to increase the separation between the antenna pairs. Due to the limited motion range of the 3D printer based detection volume measurement system used in Chapter 3, larger separations than 89 mm become difficult to measure.

Therefore, electromagnetic simulations were used to analyse the effects of larger pair separation distances.

4.2 METHODS AND MATERIALS

4.2.1 *Antenna modeling*

The coupling between the four antennas of the antenna configuration introduced in section 3.3.2 was analysed via electromagnetic simulations performed using the open-source software OpenEMS (Liebig et al., 2013), an equivalent circuit finite differences time domain (EC-FDTD) solver (Rennings et al., 2008). The proposed antenna configuration consists of four identical commercial ceramic patch UHF RFID antennas arranged in two opposing pairs located side by side.

The geometry of the individual antennas was modeled after the specification of the ABRACON ARRSN5-915.000MHz (Abracon Corporation, 2014a) antenna used in the laboratory experiments described in Chapter 3 as well as in associated field experiments (Warren, 2017).

The modeled geometry was slightly modified and simplified to generate a manageable FDTD discretisation:

- The antenna feed was modeled as a lumped element, because modeling a small-diameter co-axial feed would result in many small Yee cells (Taflove and Hagness, 2005), increasing the required simulation time which depends on the size of the smallest Yee cell (Rennings et al., 2008). The feed impedance was set to $50\,\Omega$.
- The FR-4 substrate underneath the ground plane was left out, since it would also result in small cell sizes.

The conducting elements of the antenna (ground plane and patch) were modeled as infinitely thin perfect conductors.

The antenna data sheet does not specify the dielectric properties of the ceramic substrate. However, supplementary documentation from the manufacturer lists the dielectric constant for the ARRUN5 antennas as $\varepsilon_r = 20$, but there is no information whether this applies to the 868 MHz or the 915 MHz version of the antenna or to both versions (Abracon Corporation, 2017). There is also no information available regarding the loss tangent of the material. We therefore estimated the dielectric properties ε_r and $\tan\delta$ of the ceramic substrate via gradient-free nonlinear numerical optimisation by iteratively simulating the antenna model with varying ε_r and $\tan\delta$. The otimisiation targeted a resonant frequency of $f_0 = 915\,\text{MHz}$ and an impedance of $Z_0 = 50\,\Omega$ at that frequency, consistent with the nominal values specified for the

antenna. This optimisation was performed using the Nelder-Mead method (Nelder and Mead, 1965) minimising the following cost function:

$$f_{\text{cost}}(\varepsilon_r, \tan\delta) = \left(\frac{f_{\text{res}} - f_0}{1\,\text{MHz}}\right)^2 + \left(\frac{Z|_{f_0} - Z_0}{1\,\Omega}\right)^2$$

where f_{res} is the resonant frequency (at which S_{11} is minimal), and $Z|_{f_0}$ is the simulated feed impedance of antenna 1 at the frequency f_0. The optimisation process was controlled by the generic command-line parameter optimisation program ParOpt (Seemayer, 2016), essentially a command-line interface to the `mimimize()` method of SciPy (Jones et al., 2001/), a package of scientific tools for Python (Rossum, 1995).

4.2.2 *Simulation of antenna configurations*

The single antenna model resulting from the optimisation described in 4.2.1 was then used to simulate the four-antenna configuration using a parametric model. This model consists of four copies of the single antenna model placed at the given distances between the opposing antennas of one pair and between the two pairs (see Figure 4.1).

The model was then simulated for combinations of within-pair distances between 20 mm and 50 mm in steps of 5 mm and between-pair distances ranging from 80 mm – 200 mm, covering feasible distances for use in bee hives.

4.2.3 *Pilot field trial*

Detection success ratio

The proposed antenna configuration consisting of two opposing pairs developed in section 3 was evaluated in a field trial conducted for three days in April 2017 at the University of Tasmania's Horticultural Research Centre in Sandy Bay, Tasmania (S 42°54′33″, W 147°19′27″) in the course of an honours thesis (Warren, 2017).

An RFID reader system as described in section 3.2.1 was installed at an artificial feeding station (Figure 4.2) close to an apiary consisting of 18 Langstroth hives located on site.

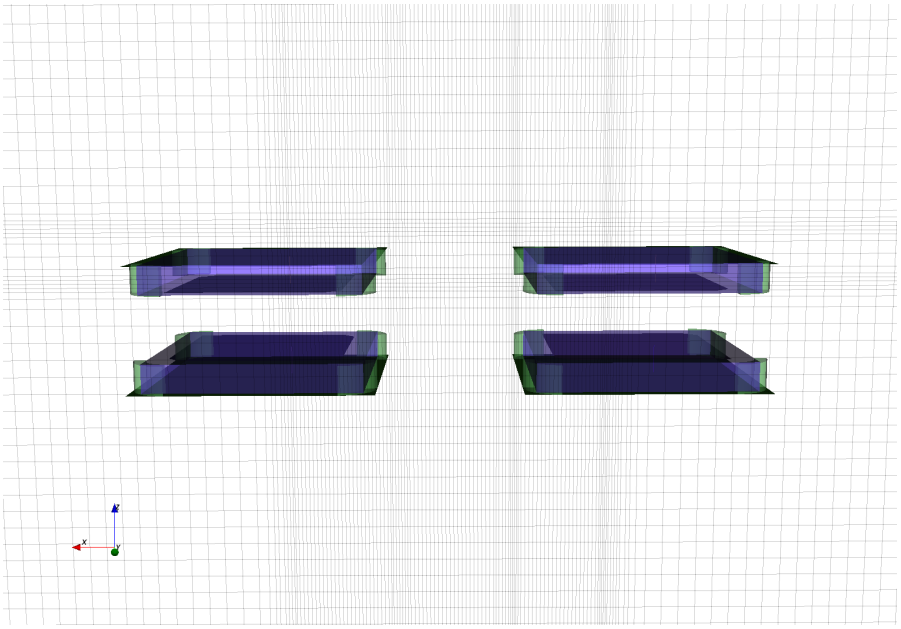

Figure 4.1: 3D model of four-antenna configuration used in electromagnetic simulation. Shown here is the model for a within-pair distance of 20 mm (measured between the antenna patch surfaces) and a between-pair distance of 80 mm (measured from center to center). The green arc shapes represent air. At a higher priority than the ceramic substrate (shown as purple), their effect is to round off the corners of the substrate. The (hardly visible) small vertical bars within the antenna structures represent the feed locations. The background shows part of the rectilinear grid projected onto the edge of the simulation volume. Smaller grid cells are used in regions of higher relative permittivity (ε_r) and along non-rectangular features of the structure. Connectors, cables and the printec circuit board substrate underneath the ground plane were left out of the model to reduce computation time.

A wooden experimental entrance tunnel was constructed to which the four antennas were attached using sticky tape to achieve an intra-pair distance of ca. 40 mm and an inter-pair distance of 170 mm.

The feeding station was situated on top of a 1.5 m wooden post. A modified Boardman beehive feeder containing microbe-free (autoclaved) 55% sugar water solution was used. To ensure constant sugar water supply, the feeder was checked daily and refilled if necessary.

Each day, 20 additional bees were tagged with Hitachi IM-PK2525 RFID tags (see section 2.2.1) at the feeder.

The data was analysed in the same way as described in section 2.4.1. To select representative data, only data from individuals detected at least once by all four antennas and at least 10 times were included in the analysis.

Figure 4.2: Experimental entrance tunnel equipped with four ceramic patch UHF RFID antennas in a dual opposing pair configuration (left, opened); Operational experimental feeding station (right). Source: Warren (2017)

Influence of antenna pair separation distance

We also examined the influence of the inter-pair separation distance in four further short-term field trials in August and September 2017 with separation distances of 0 cm (antennas placed right next to each other), 8.5 cm, 10.0 cm, and 12.8 cm, each running for 3 days, with 20 bees freshly tagged at the feeder each day. For consistency with the 17 cm separation distance data set, only data from individuals detected at least once by all four antennas and at least 10 times in total were included in the analysis of this data. In addition, data for one particular bee exhibiting a highly unusual detection pattern was excluded from the analysis as well. The selected data were explored graphically.

4.3 RESULTS AND DISCUSSION

Dielectric properties of the antenna

The product data sheet of the ABRACON ARRSN5-915.000MHz antenna (Abracon Corporation, 2014a) does not specify the dielectric properties of the ceramic substrate used. Therefore, the dielectric constant ε_r and loss tangent $\tan\delta$ were estimated via numerically optimising a single-antenna model dimensioned according to the data sheet

to match the resonance frequency and the S_{11} reflection coefficent given in the data sheet.

This optimisation resulted in an estimate of

$$\varepsilon_r \approx 18.8$$

for the dielectric constant of the ABRACON ARRSN5-915.000MHz antenna. This seems plausible given the value of $\varepsilon_r = 20$ stated in the manufacturer's on-line supplementary documentation (Abracon Corporation, 2017).

The result for the loss tangent was $\tan\delta \approx 144 \cdot 10^{-4}$. The radiation efficiency of the optimal model was quite low at$\approx$ 20%. The efficiency is also not specified in the data sheet (Abracon Corporation, 2014a). However, some commercially available UHF RFID ceramic patch antennas are assumed to have efficiencies around 40%.

These estimated values were used in the subsequent simulations of the four-antenna set-up.

4.3.1 *Four-antenna configuration simulation results*

Figure 4.4 shows how the simulated reflection coefficient S_{11} and coupling coefficients S_{21}, S_{31}, and S_{41} of the antenna configuration at the center frequency $f_0 = 915\,\text{MHz}$ depend on the distances within and between the antenna pairs. In this simulation, antenna 1 is actively driven and antennas 2–4 are parasitically coupled to antenna 1. All S-parameters vary smoothly with both, intra- and inter-pair distance. Within the shown parameter range, S_{11} varies between $-12.7\,\text{dB}$ and $-9.75\,\text{dB}$. It is nearly independent of the distance between the pairs and increases with increasing within-pair distance. The coupling to the second antenna of the first pair (S_{21}) varies mainly with the within-pair distance, with increasing separation leading to decreased coupling. Overall, S_{21} is higher than the coupling to the antennas of the other pair (S_{31} and S_{41}). While S_{31} is positively correlated with within-pair distance, S_{41} shows a weaker negative correlation. With increasing between-pair distance, the influence of the within-pair distance on S_{31} and S_{41} decreases. S_{31} and S_{41} both decrease monotonically with increasing between-pair distance.

The simulation results presented above suggest that the detection performance of the proposed dual opposing antenna configuration can be optimised according to the following rules:

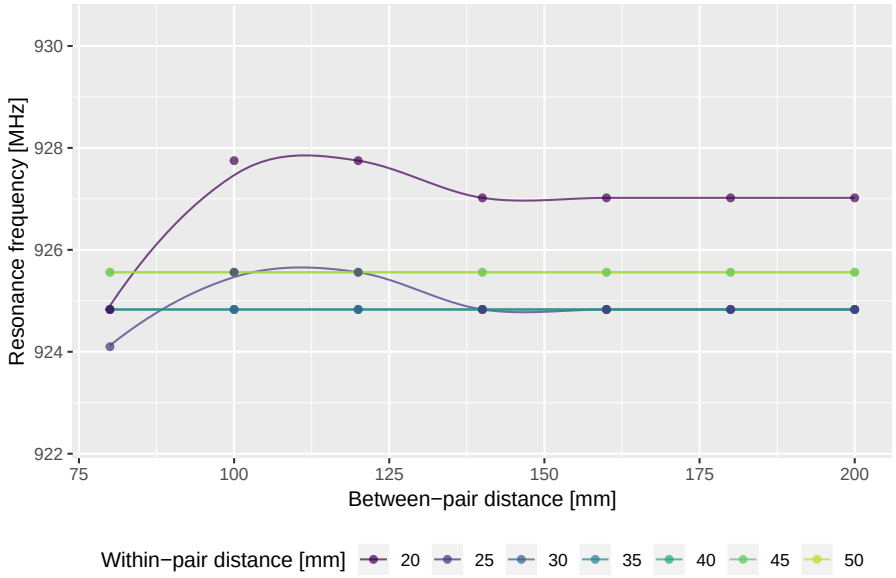

Figure 4.3: Simulated resonance frequency (at which S_{11} is minimal) of four antenna configuration consisting of two opposing pairs placed side by side depending on the separation of the antennas within and between the two pairs. Compared to the resonance frequency of $f_0 = 915\,MHz$ of a single constituent antenna, the four-antenna configuration is de-tuned towards higher frequencies. For all separations between the antenna pairs, the simulated resonance frequency varies consistently with the distance between two opposing antennas (within-pair distance). It is lowest for a within-pair distance of 30 mm – 40 mm. The resonance frequency only varies with the pair distance at distances below 120 mm and for within-pair distances below 30 mm. Note that the limited frequency resolution of the simulation leads to identical results for some within-pair distances, resulting in overplotting: the resonance frequencies for 45 mm and 50 mm are identical (upper straight line), as are those for 30 mm, 35 mm, and 40 mm (lower straight line). The continuous lines represent LOESS smoothing interpolations (Cleveland and Devlin, 1988) which have been added to aid visual interpretation.

- It is advisable to keep the within-pair antenna distance small to increase the reader sensitivity by reducing the amount of power reflected back into the transmitter (S_{11}), despite the antennas being more strongly de-tuned (Figure 4.3).
- To reduce unwanted coupling between the two pairs and thus minimize ambiguities in detecting in- or outward motions of tagged bees, the distance between the antenna pairs can be increased as required.

It should be noted that the presence of any metal elements in the vicinity of the antenna configuration will influence the reso-

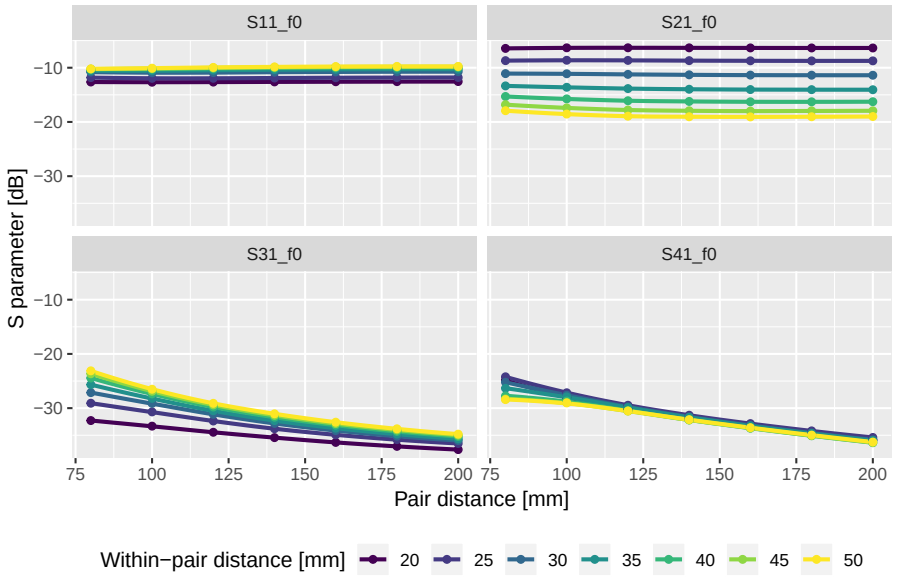

Figure 4.4: Simulated coupling coefficients of four antennas arranged in a dual opposing pair configuration (Fig. 4.1) at $f_0 = 915\,\mathrm{MHz}$ depending on intra- and inter-pair distances (shown on x-Axis and represented as different colours). Antenna 1 is actively driven, antennas 2–4 are parasitically coupled. S_{11} corresponds to the power reflected back into the transmitter port, S_{21} corresponds to the power transmitted from antenna 1 to antenna 2, etc. Over the analysed parameter range, the coupling from antenna 1 to antenna 2 (the opposing antenna of the same pair) is consistently higher than the coupling to antennas 3 and 4, which form the other antenna pair. As expected, the coupling to the second antenna pair decreases with increasing distance between the two pairs. The reflection coefficient S_{11} and the coupling within the first pair (S_{21}) depend only weakly on the distance between the pairs. At just below -10 dB, the reflection coefficient S_{11} approaches the specified limit of the RS2000/RU00-M03-X RFID reader module, which requires S_{11} to be -10 dB or less.

nance structure and coupling coefficients and should therefore be avoided.

The simulation results presented in this chapter should be taken as indicative only – partly because of the simplified model geometry, but also due to inevitable discrepancies resulting from imperfect modeling, as demonstrated for example by Vandenbosch et al. (2016).

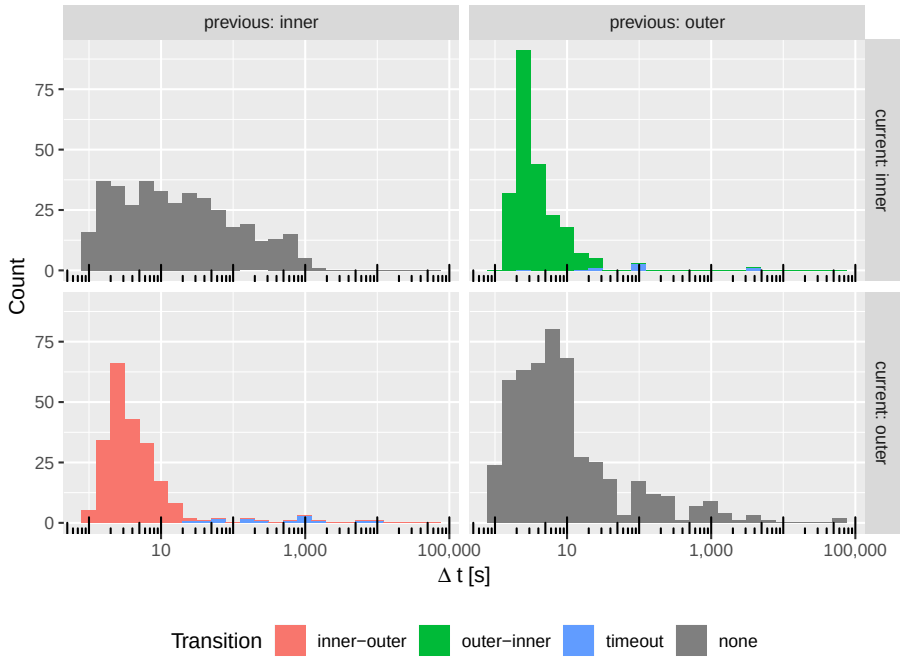

Figure 4.5: Histograms of inter-detection intervals for pairs of successive detections of the same tag, summed up for all tags. The panels correspond to the combination of the detection locations for the two detections of each pair (which can either be *inner* or *outer*, where *inner* corresponds to the antenna pair located closer to the feeder jar). Thus, the panels on the diagonal show subsequent detections which both occurred at the same end of the entrance tunnel, while the off-diagonal panels show *inner/outer* or *outer/inner* detection pairs. Colour represents the classification of the detection events into successfully detected inbound or outbound transitions, timeouts suggesting missed intermediate events, and successive detections by the same reader according to the heuristic described in section 2.4.1. Note the logarithmic scale of the time axis. Detection intervals of less than 1 s were excluded for this figure and from the analysis, because they do not represent actual bee movements, as they are most likely artefacts caused by antenna crosstalk (see Figure 4.6). Compared to Figure 2.9 showing corresponding results obtained using the previous prototype system based on MTI RU-824 USB RFID readers, the optimised four-antenna RFID system exhibits a much higher ratio of successfully detected transitions to timeouts.

4.3.2 *Field trial results*

Detection success ratio

The field trial resulted in 17557 detections from 13 bees which were detected at least once. To obtain results which are more representative of regularly active worker bees frequently moving into and out of the hive, we discarded all detections of bees which were detected less than 10 times over the 3 day duration of the experiment or which were not detected at least once by each of the four antennas. This left us with 17526 detections from the 7 most active tagged bees.

An upper bound on the probability to register a transition of a bee as a pair of detections at both sides given that we observed $n_{\text{success}} = 740$ successfuly detected transitions and $n_{\text{timeout}} = 19$ timeouts can be estimated (see Figure 4.5):

$$p_{\text{trip}} = \frac{n_{\text{success}}}{n_{\text{success}} + n_{\text{timeout}}} = \frac{740}{759} = 0.975$$

Assuming that both sides have identical detection probabilities, this results in:

$$p_{\text{i}} = p_{\text{o}} = \sqrt{p_{\text{t}}} = 0.987$$

Conversely, the probability to successfully detect all 4 events corresponding to a single foraging trip *(inner, outer, outer, inner)*, is:

$$p_{\text{trip}} = {p_{\text{trip}}}^2 = 0.951$$

The results of this preliminary pilot study represent a promising marked improvement in the detection success ratio over the MTI RU-824 USB RFID reader based system described in Chapter 2, corresponding to better data quality and hence improved power to analyse bee behaviour.

Influence of separation distance

Preliminary field tests of different separation distances between the *inner* and *outer* antenna pairs within the entrance tunnel were con-

Table 4.1: Overview of field test results for different antenna separation distances. Note that detections from bees which have not been detected at least 10 times in total and have not been detected by all four antennas have been excluded as well as those of one identified outlier individual. The particularly low number of detections for the 10 cm run was likely caused by a reader system malfunction.

Distance	Detections	Individuals
0.0	2753	5
8.5	3492	6
10.0	257	2
12.8	3493	5
17.0	17526	7

ducted for distances of 0 cm, 8.5 cm, 10 cm, and 12.75 cm. Each of these trials was conducted for 3 consecutive days, with 20 additional bees being tagged at the feeder each day.

Table 4.1 and Figure 4.6 summarise the results of these tests together with the 17 cm separation data discussed in the previous section.

Figure 4.6 clearly shows that the detection intervals corresponding to bees transitioning between the two antenna pairs increase with increasing separation distance, while spurious detections resulting from antenna crosstalk (which occur within ca. 0.5 s) remain constant. Even at the largest tested antenna separation of 17 cm, there are still spurious detections resulting from antenna crosstalk, but the two distributions of detection pairs representing actual bee movements and spurious detections (artefacts) appear clearly separated, confirming that this antenna separation is a suitable operating point for the tested experimental conditions.

The obvious difference between the detection intervals of the spurious detections for inbound versus outbound detection pairs is an artefact caused by the activation sequence of the antennas and the measurement and reporting algorithm used for this data set. The spurious detections tend to occur in short bursts, each containing a high number of detection events; this could explain why they are absent for the three medium-distance measurements.

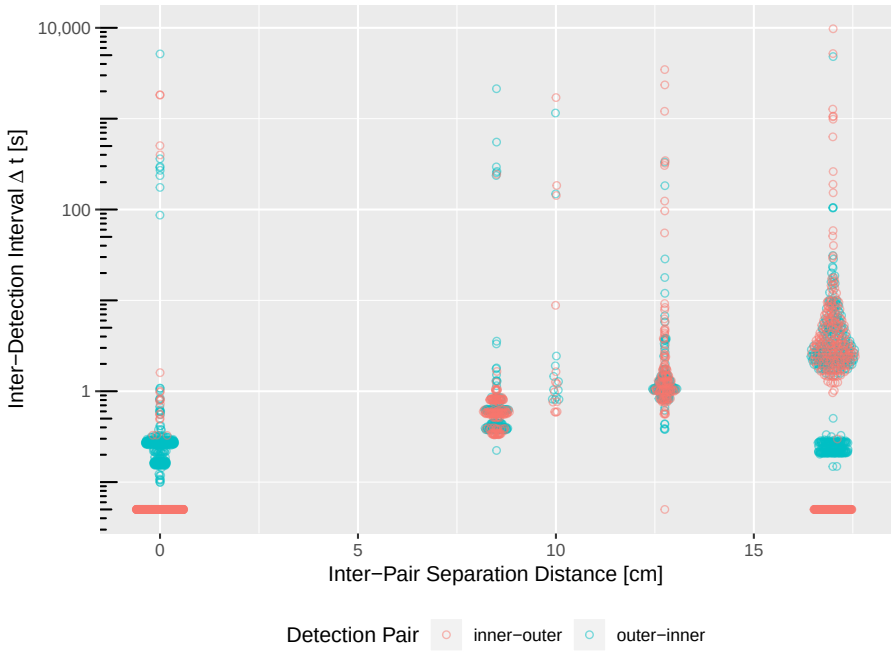

Figure 4.6: Distribution of time intervals between pairs of detections for the same bee at opposite ends of the entrance tunnel (corresponding to *inner* or *outer* antenna pair) for various inter-antenna-pair separation distances, pooled for all bees. Each recorded detection pair is represented as a point whose color indicates its combination of detecting antenna pairs. The points have been offset along the abscissa from their actual distance value to convey a sense of the data distribution along the ordinate according to a kernel density estimate. The maximum width of each point cloud is proportional to the square root of the number of observations at its separation distance value. Time differences reported as zero by the reader software were set to 50 ms in this graph, corresponding to the antenna switching frequency of 20 Hz (since only one antenna can be active at a time). Note the logarithmic scale on the ordinate.

4.4 CONCLUSIONS AND IDEAS FOR FURTHER RESEARCH

In this chapter we further analysed the antenna configuration consisting of two opposing antenna pairs arranged side by side which was introduced in Chapter 3.

Electromagnetic simulations were used to determine the influence of the geometric parameters of the antenna configuration (within-pair and between-pair distances) on the reflection coefficient and the coupling between the antennas. We examined a range of distances feasible for the intended application of using the antenna configuration to detect RFID tagged bees passing through an entrance tunnel of a bee hive or artificial feeding station: the separation between two

opposing antennas varied between 20 mm and 50 mm, and the distance between the antenna pairs ranged from 80 mm to 200 mm. We found that the reflection coefficient and the coupling between the antennas vary smoothly and predictably with both distance parameters over the analysed parameter range. As expected, a smaller separation between the two opposing antennas forming a pair increases the coupling between them and therefore leads to an increased detection volume close to the second antenna (as shown in Chapter 3). A smaller intra-pair gap also leads to reduced reflected input power, resulting in increased detector sensitivity. The coupling between the two antenna pairs decreases as the distance between them increases, allowing crosstalk between the antenna pairs to be reduced as desired by increasing the separation between them.

The detection pattern measurements presented in Chapter 3 showed that the proposed dual opposing pair antenna configuration exhibits a detection volume whose size and shape is well suited to detecting RFID tagged bees passing through it. However, crosstalk between the antenna pairs caused ambiguities in detecting the direction of motion of the passing bees. The simulation results presented in this chapter suggest that the coupling between the antenna pairs can be reduced and thus these errors can be minimised by increasing the distance between the antenna pairs.

A first field trial with a separation of 17 cm between the two antenna pairs (chosen as the maximum practicable distance) was conducted over three days in April 2017. Although this only yielded representative data for 7 individual bees, the results showed a promising marked improvement of the detection success rate over the first tested dual-reader prototype system of section 2.4.1, reaching a probability over 95% to detect all four antenna passes comprising a foraging trip. Similar tests with other antenna separation distances showed that a distance of 17 cm leads to a clear separation between detections resulting from actual bee movements and spurious detections resulting from antenna crosstalk.

Further research would be required to find optimal settings for system parameters like interrogation signal power level and antenna switching timing and sequence. Another idea for future research would be an analysis of the impact of the adjustable parameters of the ISO 18000-63 protocol on the detection performance of an RFID system used to detect tagged bees similar to the one conducted by Buettner and Wetherall (2008) on stationary tags.

Part II

TOWARDS LONG-RANGE IDENTIFICATION AND TRACKING OF A LARGE NUMBER OF INDIVIDUALS USING PASSIVE TRANSPONDERS

5

INTRODUCTION

In the first part of this thesis we demonstrated a UHF RFID monitoring system prototype for honey bees *(Apis mellifera)* tagged with small (2.5 mm × 2.5 mm × 0.4 mm) off-the-shelf RFID tags which only requires moderate changes to a beehive entrance and yet achieves a hit/miss ratio of > 97% in field tests, surpassing that of previous studies found in the literature (Warren, 2017).

A severe limitation of this system is a low detection range of just a few cm which is due to the currently available UHF RFID technology in combination with the small antenna size of the tags.

This second part of the thesis proposes the development of a new class of passive transponders combining concepts of RFID and harmonic radar to achieve increased detection range. It starts with an overview of the methods and current developments of classical and harmonic radar for tracking insects. This is followed by an introduction of basic ideas of the proposed new development and by an outline of a development roadmap towards this new class of harmonic RFID tag. We conclude this part with a detailed presentation of the development and prototype implementation of a compact dual band dipole antenna suitable for use in such harmonic transponders (Chapter 6) which was presented at the International Symposium on Antennas and Propagation (ISAP) 2015 (*ISAP2015 - International Symposium on Antennas and Propagation - Technical Program* 2015) and published as a summarised version in the conference proceedings (Hirsch et al., 2015).

5.1 CLASSICAL RADAR

Radar allows to monitor insect movements without attaching anything at all to the animal (Bridge et al., 2011; Chilson et al., 2012). One

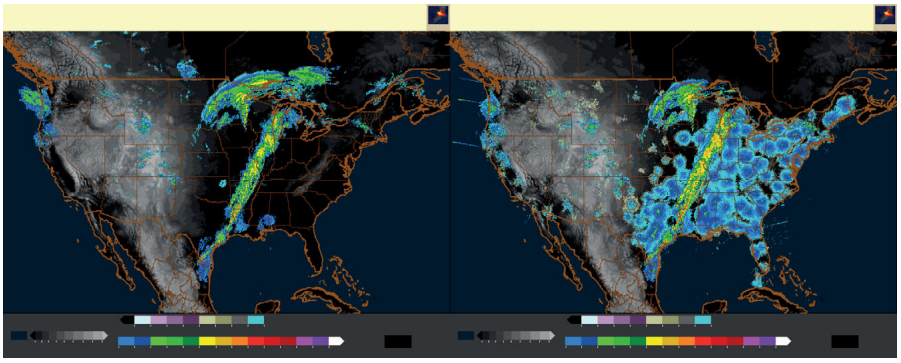

Figure 5.1: Radar reflectivity images showing the same weather situation. The right pane shows the uncorrected radar reflections – most of which are caused by animals in this case. Only after these 'nuisance' signals have been removed, the meteorologically relevant reflections from rain drops can be clearly seen (left pane). Source: Chilson et al. (2012).

way to do this is to point the radar beam straight up into the sky, a technique known as 'vertical-looking-entomological radar' (Kissling et al., 2014). During the middle of the 20th century, radar's potential for insect monitoring was discovered using radar equipment like that used for weather observations (Chapman, Drake et al., 2011; Drake and Reynolds, 2012). In fact, reflections from animals present a nuisance to meteorologists as can be seen in Figure 5.1. With this type of radar (today known as 'classical radar'), it is however only possible to monitor rather large low-flying insects like locusts over flat and featureless terrain (Riley and Smith, 2002; Chapman, Reynolds and Wilson, 2015) and not honey bees (Chapman, Reynolds and Smith, 2003; Chapman, Drake et al., 2011; Drake and Reynolds, 2012; Chapman, Nilsson et al., 2016).

5.2 VERTICAL LOOKING RADAR (VLR)

In a clutter-free environment, where the target insects are the only objects which reflect radar radiation, it is possible to detect single insects at distances of multiple hundred meters, as several authors have shown using a vertical looking radar (VLR) to detect migrating insects against the sky as a background (Chapman, Drake et al., 2011; Chapman, Reynolds, Smith et al., 2002; Chapman, Reynolds and Smith, 2003; Chapman, Reynolds and Smith, 2004; Kissling et al., 2014; Reynolds et al., 2005; Smith et al., 1993; Wood et al., 2009). The radar detectability of small objects like insects can be increased somewhat by attaching small metallic tags to them that reflect radar radiation better than the insects themselves, but all this can do is in-

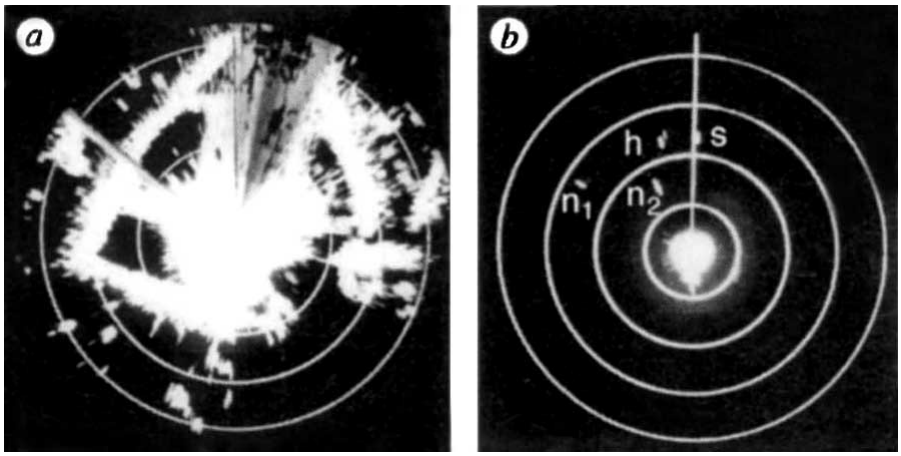

Figure 5.2: a) Conventional radar mode display showing clutter from avenues of trees and ground features, b) harmonic mode display of the same scene, showing only the harmonic tags (indicated as h, s, n1 and n2). Source: Riley, Smith et al. (1996). Copyright © 1996, Springer Nature.

crease the contrast between the insects' reflections and those from the background – there is no fundamental way to differentiate between those signals.

5.3 HARMONIC RADAR

Recent advances in processing power and algorithms allow insects in motion to be discriminated against other (background clutter) signals (Chilson et al., 2012; Shamoun-Baranes et al., 2014). However, these motion-based methods cannot cope with (temporarily) stationary animals in highly cluttered environments (Figure 5.2). Harmonic radar solves this problem by having the tags emit a different frequency than they receive – and thus stand out against the background ('clutter') which simply reflects the incident radar wave (Riley, Smith et al., 1996; Riley and Smith, 2002). This is achieved by feeding the signal received by the antenna of the tag through a non-linear element, which causes harmonics of the fundamental frequency to appear (hence the name 'harmonic radar') (Katib, 1976; Mascanzoni and Wallin, 1986; Tahir and Brooker, 2015).

This process of generating harmonic frequencies can be illustrated using a simple example: consider a pure sine wave signal of radial frequency ω:

$$y_0(t) = \sin \omega t$$

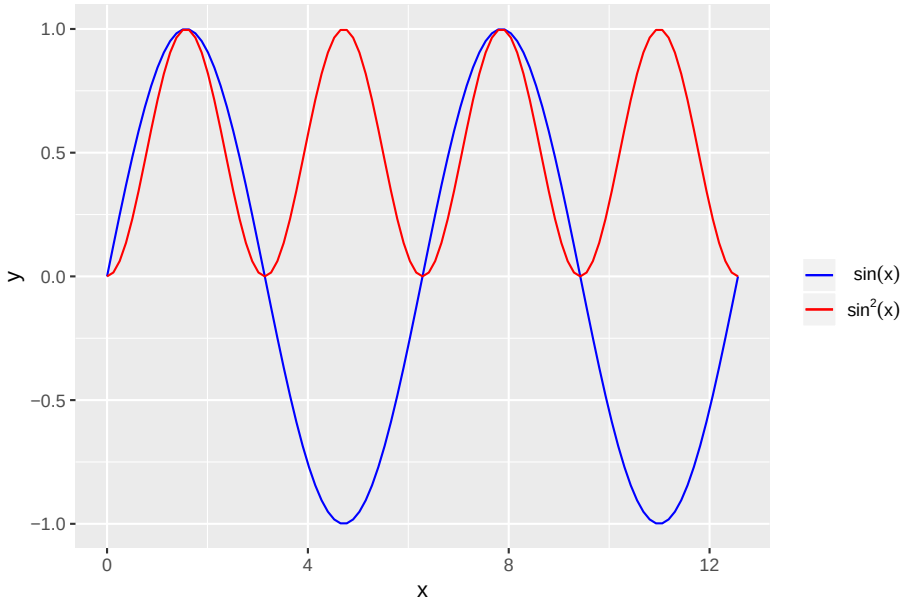

Figure 5.3: Illustration of harmonic frequency generation by passing a signal through a non-linear function, in this example by applying the function $f(y) = y^2$ to the input signal $y(x) = \sin x$.

If this signal passes through a quadratic non-linearity, i.e. is transformed by a function $f(y) = y^2$, the resulting signal is a sine wave with twice the original frequency that is scaled, phase shifted and has a DC offset (Figure 5.3):

$$y_1(t) = y_0^2(t) = \sin^2 \omega t = \frac{1 - \cos 2\omega t}{2} = \frac{1}{2} + \frac{1}{2}\sin(2\omega t - \frac{\pi}{2})$$

Harmonic radars often use diodes as non-linear elements to generate the harmonic signals (Tahir and Brooker, 2015; Mascanzoni and Wallin, 1986). At low frequencies, their non-linear response can be characterised by the Schottky diode equation (Zeljami et al., 2012):

$$I(V_d) = I_s \left(e^{\frac{q(V_d - I_d R_S)}{\eta k T}} - 1 \right)$$

where I_s is the saturation current, V_d the voltage across the semiconductor junction (which is proportional to the input signal), η the ideality factor and R_S the series resistance of the diode. For this type of non-linearity, the resulting signal contains all possible harmonic frequencies and its spectrum can not be described in a closed analytical form, but only as a series expansion (Katib, 1976). At high frequencies, the capacitive and inductive properties of real diodes become important; to make accurate predictions about the resulting signals usually requires physical model based electromagnetic simulations or models based upon those (Zeljami et al., 2012).

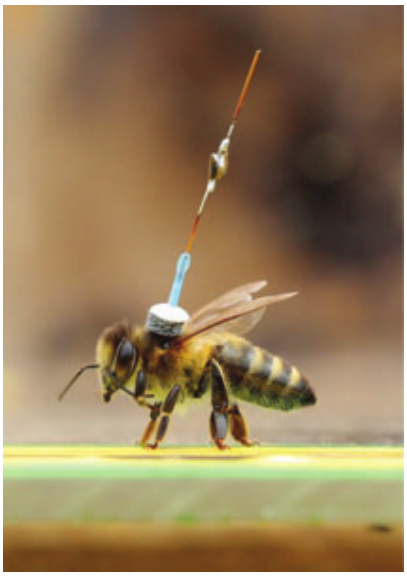

Figure 5.4: Honey bee with harmonic radar tag attached. Adapted from: Chapman, Drake et al. (2011)

Harmonic radar has first been used in the 1980s (Mascanzoni and Wallin, 1986; Riley, Smith et al., 1996; Tahir and Brooker, 2011; Kissling et al., 2014). It can basically be used at any radar frequency, depending on the application. For example, at 9.4 GHz (a wavelength of 3.2 cm) at 25 kW peak power, it is possible to detect a single tagged insect from a distance of up to about 1 km (Riley and Smith, 2002). For high frequencies, corresponding to short wavelengths, these tags can weigh between 1 mg and 20 mg and therefore are unlikely to strongly bias insect behaviour because of their weight, but still likely have a noticable impact as a result of the antenna length (Figure 5.4) (Kissling et al., 2014). To mitigate this disadvantage caused by the length of simple monopole or dipole wire antennas, alternative antenna designs have been evaluated for harmonic radar based insect tracking: using a small planar 9.63 mm × 9.63 mm modified Minkowski loop antenna and a Schottky diode (Figure 5.5, Zhu et al. (2011)) have demonstrated a harmonic radar working at 5.882/11.764 GHz which achieved a tracking range of more than 60 m in open terrain using a base station transmitter power of just 1 W.

Tsai et al. (2013) have recently been able to improve another aspect of harmonic radar tracking systems: They have been able to improve the signal-to-noise ratio (SNR) and localisation precision using spread spectrum techniques in their system. To this end, they modulated the signal emitted by the radar antenna using a pseudo-random noise (PNR) code. In that work, they also developed and tested a small custom harmonic radar tag that they have been fitting to honey bees. Modulating the signal transmitted by the base station using a Gold code (Gold, 1967), they have realised a processing gain of 30 dB, lead-

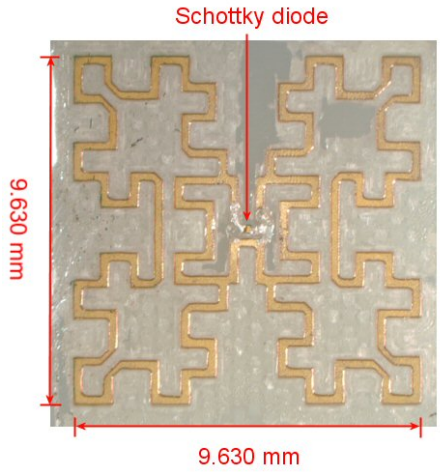

Figure 5.5: Harmonic transponder based on a modified Minkowski loop. Adapted from: Zhu et al. (2011). Copyright © 2011, IEEE.

ing to a 61 m detection range in open space using a small metamaterial inspired antenna of 2.8 mm × 3.8 mm at 9.4/18.8 GHz with a gain of -5 dBi.

While slightly differently tuned antennas have been used to achieve some degree of differentiation between a small number of tags (Woodgate et al., 2016, 2017), harmonic radar does not allow to distinguish between a large number of individual tags (> 5-10), because it does not generally yield identification information.

5.4 WORKING PRINCIPLE OF HARMONIC RFID

The basic idea is to modulate the harmonic signal which is generated from the incident radar signal and re-radiated. The passive harmonic UHF tag design by Lazaro et al. (2014), shown in Figure 5.6, could serve as a starting point for the development of a harmonic RFID transponder. They utilised some of the power of the incident signal to power a low-frequency oscillator which then modulates the harmonic output signal also derived from the input signal. They used a dual polarised reception antenna to collect the interrogation signal from an RFID reader at a frequency of f_0 (865–868 MHz) which was connected to a transmission patch antenna via a frequency doubler. The frequency doubler of their design was based on a zero-bias Schottky diode (Avago Technologies, model HSMS-2850). They modulated the generated harmonic signal according to the output of a simple low-frequency oscillator based on two NAND logic gates (74AUP1G00) by controlling the bias point of the frequency doubler. They powered this oscillator from the second port of the reception antenna via an

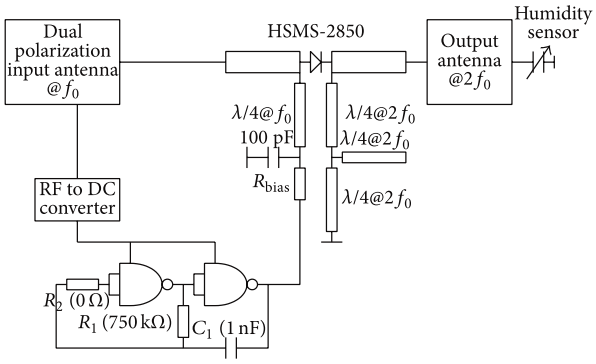

Figure 5.6: Passive Harmonic Tag for Humidity Sensing. Source: Lazaro et al. (2014).

RF to DC converter based on a diode voltage multiplier using series-connected zero-bias diodes (Avago Technologies, model HSMS-2852) (Figure 5.10).

The development of the harmonic radio frequency identification (HRFID) transponder proposed in this thesis could proceed along the steps outlined below.

5.5 REQUIREMENTS ANALYSIS

The following paragraphs outline the constraints for the proposed harmonic transponder regarding weight, size, frequency and bandwidth.

5.5.1 *Frequency Selection*

The ideal operating frequency pair for a harmonic radar system depends on a number of factors:

- Size, weight and volume of the transmitter (Kissling et al., 2014)
- Atmospheric transmissivity (Figure 5.7)
- Transmissivity of vegetation (Figure 5.8)
- Regulatory constraints
- Availability of components

For insect tracking applications, the size (and thus the weight) of the required antennas is a crucial factor (ibid.) which is directly linked to the operating wavelength (Hansen, 2006; Shahpari, 2015).

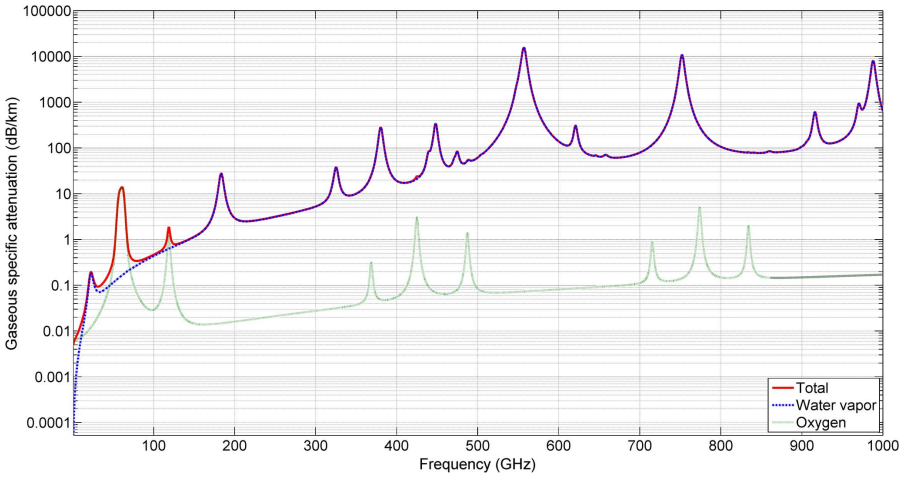

Figure 5.7: Specific attenuation of electromagnetic radiation caused by atmospheric gases, including the individual contributions of water vapour and oxygen (Siles et al., 2015). Copyright © 2015, IEEE.

Antennas that are small compared to the wavelength have a number of practical limitations that include the achievable bandwidth being narrow, and having low radiation efficiency because of increased losses in the matching network and a low radiation resistance (Hansen, 2006). For example, the radiation resistance R_{rad} of a short dipole antenna at a given wavelength λ is proportional to the square of its length l (Condon and Ransom, 2007):

$$R_{\text{rad}} = \frac{2\pi^2}{3c}\left(\frac{l^2}{\lambda^2}\right)$$

(where c denotes the speed of light in vacuum).

When electromagnetic radiation propagates through the earth's atmosphere, it is attenuated as a result of its interactions with atmospheric gas particles (Siles et al., 2015). Per unit length travelled, these processes cause the signal to lose a constant fraction of its remaining power; thus, the attenuation can be measured in dB / km. The losses vary with frequency and are dominated by the effects of water vapour and oxygen, as illustrated in Figure 5.7, which shows the attenuation spectrum for clean air under standard atmospheric conditions: ($T = 15°\text{C}$, $P = 1013\,\text{hPa}$, and $\rho = 7.5\,\text{g/m}^3$). As this Figure suggests, more humid weather conditions or even the presence of precipitation along the path of the signal lead to increased attenuation (Appleby and Wallace, 2007).

Another important aspect to consider for an outdoor localisation and tracking system for insects are the effects of vegetation on radio waves passing through it. The International Telecommunications Union (ITU) proposes a general model for estimating the attenuation

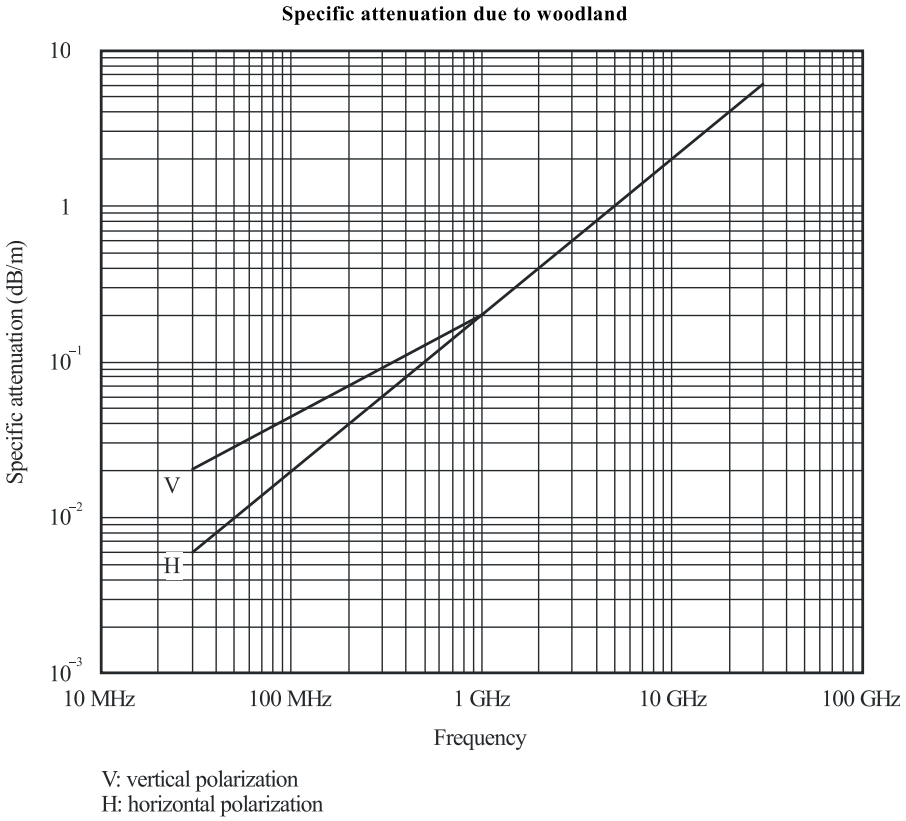

Figure 5.8: Specific attenuation of electromagnetic radiation in woodland (typical values). Original Fig. 2 of ITU (2012)

of radio waves between 30 MHz and 60 GHz in vegetation (ITU, 2012), as shown in Figure 5.8.

The authors stress that these values should be regarded only as typical, because the actual attenuation strongly depends on the type and density of the vegetation, and, in particular, on its water content. Rogers et al. (2002) developed an attenuation model for 1 GHz to 60 GHz based on a set of measurements. Cheffena and Ekman (2008) investigated the dynamic effects of swaying vegetation in windy conditions on radio-wave propagation and developed a model to simulate the resulting signal fading.

According to the Radiocommunications Act (Australian Government, 2015), the use of radio frequencies in Australia is regulated by the Australian Communications and Media Authority (ACMA) which develops the Australian Radio Frequency Spectrum Plan (ARSP) (ACMA, 2013). Except for devices operating within the frequency and power limits governing the unlicensed bands of the spectrum such as those allocated to industrial, scientific, and medical use ('ISM' bands), every radio transmitter has to be licensed according to these regulations.

5.5.2 *Power Budget*

In a passive tag, the modulator circuitry is powered by energy harvested from the environment (Finkenzeller, 2010) – in this case from the radar signal which the tag receives. Therefore, the returned signal is weaker than it could be by simply re-radiating the full power of the input signal. This can however be compensated for by applying spread-spectrum modulation techniques to increase the achievable SNR (Meel, 1999).

The total power available to the transponder circuit can be calculated starting from the power of the signal radiated by the base station using Friis' transmission equation (Shaw, 2013):

$$P_\mathrm{r} = P_\mathrm{t} G_\mathrm{t} G_\mathrm{r} \left(\frac{\lambda}{4\pi R} \right)^2$$

where P_r is the received power, P_t is the transmitted power, G_r and G_t are the gains of the receiving and transmitting antennas, R is the distance between the receiving and transmitting antennas, and λ is the wavelength of the signal.

In a harmonic transponder system, the power which the base station receives back from the transponder can thus be written (Tsai et al., 2013):

$$P_\mathrm{r} = P_\mathrm{t} G_\mathrm{bf} G_\mathrm{bh} \left(\frac{\lambda_\mathrm{f}}{4\pi R} \right)^2 G_\mathrm{tf} E_\mathrm{d} G_\mathrm{th} \left(\frac{\lambda_\mathrm{h}}{4\pi R} \right)^2$$

where λ_f is the wavelength of the fundamental frequency transmitted by the base station, λ_h is the wavelength of the harmonic frequency re-radiated by the tag, G_bf and G_bh are the gains of the base station antennas and G_tf and G_th are the gains of the transponder antennas at the fundamental and harmonic frequencies respectively, and E_d is the conversion efficiency of the frequency doubler diode.

From this follows the maximum detection distance R_max for the system:

$$R_\mathrm{max} = \frac{1}{4\pi} \left(\frac{P_\mathrm{t} G_\mathrm{bf} G_\mathrm{bh} G_\mathrm{tf} E_d G_\mathrm{th} \lambda_\mathrm{f}^2 \lambda_\mathrm{h}^2}{P_\mathrm{min}} \right)^{\frac{1}{4}}$$

where P_min is the sensitivity of the base station receiver (i.e. the minimum power required for successful detection).

The receiver's effective sensitivity can be increased using spread-spectrum techniques, which are based on Shannon's insight (2001)

that the upper limit C to the rate at which information can be transmitted using a signal of bandwidth B and average power S through a channel subject to additive white Gaussian noise of power N is

$$C = B \log_2 \left(1 + \frac{S}{N}\right).$$

Therefore, spreading a signal of bandwidth B_{D} out over a target bandwidth of B_{SS} by modulating it with a suitable pseudo-random spreading code results in a processing gain of

$$G_p = \frac{B_{\mathrm{SS}}}{B_D}$$

(Pickholtz et al., 1982). This spreading is usually achieved by multiplying the original signal by a pseudo-random binary code before it is transmitted (Ström et al., 2002). Because of the autocorrelation structure of the code, which is similar to the autocorrelation of true random noise, i.e. it has a strong peak at a displacement of zero and is very small everywhere else (Figure 5.9), the receiver can detect the signal even in the presence of noise by computing the correlation with the identical code sequence (ibid.).

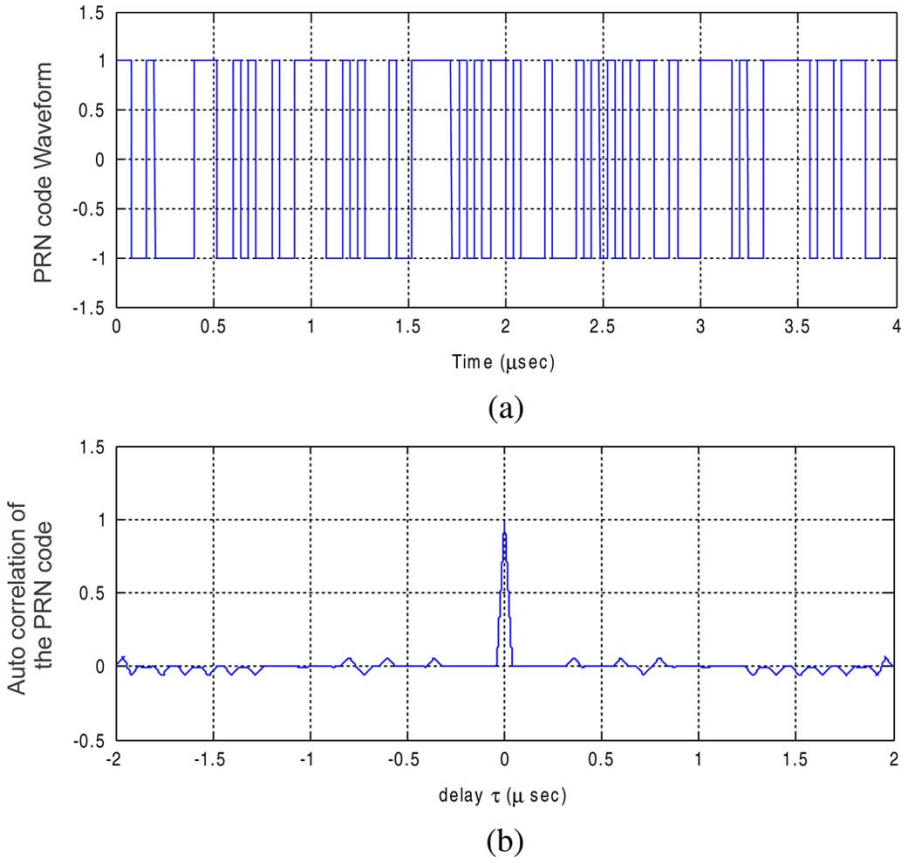

Figure 5.9: A pseudo-random noise (PRN) code (a) and its autocorrelation function (b) (Source: Tsai et al., 2013). Copyright © 2013, IEEE.

5.6 DESIGN RF ENERGY HARVESTER (RF-DC CONVERTER)

Lazaro et al. (2014) used a diode voltage multiplier based RF-to-DC converter to harvest energy from the incident radar signal to modulate the output of a passive harmonic tag (Figure 5.10). The suitability of this design for the application in our HRFID tag will first be assessed using circuit simulations using the COMSOL Multiphysics and CST Microwave Studio software available at CSIRO.

Figure 5.11 shows how the output voltage of their RF-DC converter depends on the input power measured at 868 MHz.

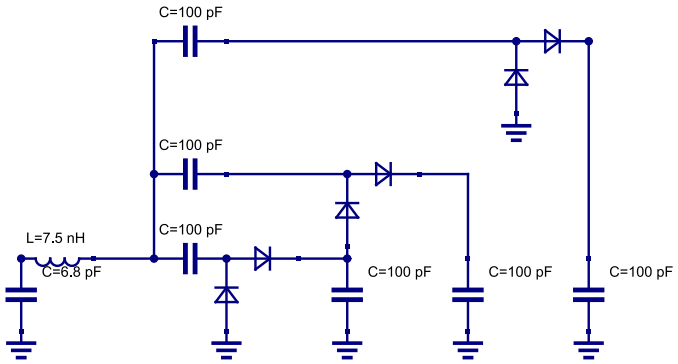

Figure 5.10: RF-DC Converter (after Lazaro et al., 2014).

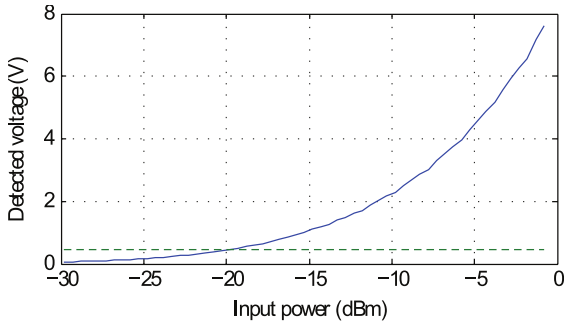

Figure 5.11: DC output voltage of RF-DC converter at 868 MHz for different input power levels from Lazaro et al. (2014).

5.7 MODULATING FREQUENCY DOUBLER CIRCUIT

The circuit modulating the bias of the non-linear element of an HRFID tag has to be designed according to the power budget derived above (see 5.5.2). This circuit will be evaluated using the COMSOL Multiphysics and/or CST Studio simulation software mentioned above.

The output signal is modulated by altering the bias voltage of the frequency doubling Schottky diode. Figure 5.12 shows the difference in the conversion loss for bias voltages of 0 V and 0.5 V as measured by Lazaro et al. (ibid.). According to this, a modulation depth of about 15 dB can be expected for input powers less than ca. -15 dBm.

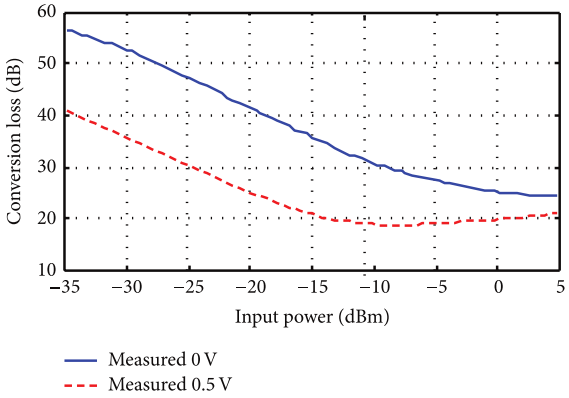

Figure 5.12: Conversion loss measurement from Lazaro et al. (2014).

5.8 ANTENNAS

An ideal antenna for insect tracking applications would have a number of desirable characteristics: It would be unobtrusive – i.e. small in size, lightweight and shaped to conform to the animal's body, such that it would impede the animal in the least possible way – and at the same time it would exhibit high radiation efficiency at the fundamental as well as the second harmonic frequency, it would be robust and durable, cheap and easy to manufacture.

As mentioned in 5.3, there have been a number of developments aiming to design small, efficient dual-band antennas for use in harmonic radar animal tracking applications that come close to this ideal: Tsai et al. (2013) presented a small harmonic radar transponder for 9.4 GHz/18.8 GHz measuring 2.8 mm by 3.8 mm, weighing 20 mg. In their design, they used a composite right-/left-handed meta-material transmission-line (CRLH TL) antenna (Lai et al., 2007) with a gain of -5 dBi. Earlier, Zhu et al. (2011) designed a modified Minkowski loop antenna (Figure 5.5) sized 9.63 mm × 9.63 mm at 5.9/11.8 GHz with a gain of 1.5 dBi.

5.9 BUILD PROTOTYPE HARMONIC TRANSPONDER

After successful simulation, a prototype of a non-modulating harmonic transponder based on the dual-band antenna developed and presented in this thesis was built and tested in the RF laboratories at CSIRO (Chapter 6).

Figure 5.13: Bee with attached RFID tag. Photo: CSIRO

5.10 DESIGN AND BUILD HRFID TAG

The developed circuit will be integrated into a small tag based on the design recently developed by Tsai et al. (2013) that can be attached to the dorsal thorax of a honeybee as shown in Figures 1.2 and 5.13.

The technological advances described below will give us the opportunity to combine the large detection range and battery-free operation of harmonic radar with identification features similar to RFID. The idea is to combine aspects of harmonic radar and RFID into one system: Altering the bias of the non-linear element of a harmonic tag allows modulating the generated harmonic signal with a uniquely identifying individual code for each tag that can be detected by the receiver.

Due to time and logistic constraints associated with intended collaborative work, this part could not be addressed during my thesis but will hopefully be addressed in future work.

Chapter 6 has been removed for copyright or proprietary reasons.

Similar research been published as: Hirsch, P., Weily, A. R., de Souza, P., 2015. Compact dual-band parasitic dipole antenna for harmonic transponders, in 2015 International Symposium on Ante nnas and Propagation (ISAP), Hobart, Australia, 2015, pp. 1–3. https://ieeexplore.ieee.org/document/7447481

7

CONCLUSION AND OUTLOOK

Radio technology has been an invaluable tool to gain insights into animal behaviour since it has first been used to monitor animal locations using animal-mounted transmitters in the 1960s (Kissling et al., 2014). Despite many developments in this area, it is still impossible to track a large number of individually tagged small animals over large ranges. Yet exactly this combination would be required to gain more insight into the behaviour of honey bees *(Apis mellifera)*, which are crucial for human food production but whose populations have seen steep declines in many areas of the world (Goulson, Nicholls et al., 2015).

While it is possible to monitor a large number of individually tagged bees using RFID technology, the achievable detection ranges are very small (up to a few cm). Furthermore, special RFID equipment used for monitoring honey bees has been expensive and its usefulness has been limited by relatively low detection success rates. These issues are addressed in the first part of this thesis.

Synthesising concepts from RFID and harmonic radar, which in contrast to RFID allows long detection ranges, albeit with only a small number of individual tags, the second part proposes the development of a new type of transponder, aiming to enable monitoring of a large number of individual tags at increased ranges compared to traditional RFID.

A summary of these two parts followed by suggestions for future research is given below.

In the first part, we aimed to advance the state of the art in automatically monitoring a large number of individually tagged honey bees using UHF RFID technology while simultaneously striving to reduce monitoring system cost by utilising commercial off-the-shelf components. We presented three increasingly complex monitoring system

prototypes based on commercially available RFID modules which we used in conjunction with off-the-shelf ultra-small package RFID tags glued to the dorsal thorax of a honey bee. The suitability of these systems for monitoring honeybees at their hives and at artificial feeding stations (which could e.g. be used for controlled exposure to chemicals) was investigated through field trials (Chapter 2). The first two prototypes employed palm-sized USB RFID readers with integrated antennas which are available off-the-shelf as PC or Notebook peripherals. The first prototype used a single such RFID reader module and could detect the presence of tagged bees in close proximity to the integrated antenna. The second prototype combining two of these RFID reader modules added the ability to detect not only the presence of tagged bees at the location of the reader but also the direction (into or out of the hive / feeding station) of their movements (Susanto et al., 2018). We quantified the detection success rate of this second prototype using data from a field trial of this system and found that the average probability of detecting all four reader passages corresponding to a round-trip of a tagged bee was quite low (less than 15%). We also found that the maximum detection distance was less than 1 cm over an area of only a few cm^2 on the surface of the reader modules. Given this low detection rate, we decided to use a more capable industrial RFID reader module with a higher maximum output power, increased sensitivity and the ability to connect up to four antennas. Chapter 3 introduced the third and final prototype system and described the development of a measurement system to determine the spatial detection probability pattern of our RFID tags in the vicinity of the reader antennas. Further, we present measurement results for the RFID reader modules used in the first two prototypes and for a range of candidate antenna configurations considered for use with the final prototype system. Based on these measurement results, we identified an antenna configuration consisting of four ceramic patch antennas arranged in two opposing pairs placed side by side as the most promising structure (de Souza et al., 2018) even though it exhibited some crosstalk between the antenna pairs. We expected that the crosstalk could be reduced by increasing the distance between the antenna pairs, which we could not test using the measurement system because of the limited movement range of the probe tag. Therefore, we addressed this issue by analysing the selected antenna configuration in more detail using electromagnetic simulations in a separate chapter (Chapter 4). A preliminary field trial of the third prototype system in the context of an honours thesis in our group confirmed that this new prototype system exhibits drastically improved detection rates of 97.3%, surpassing those previously published for RFID systems used for monitoring bees which do not require the bees to pass through a narrow tube (Warren, 2017).

The second part presented a road map for the development of a new kind of digital radio transponder for animal tagging combining concepts of traditional RFID technology with those of harmonic radar aiming to overcome range limitations of UHF RFID technology evident in the first part. Chapter 5 gives some theoretical background on different types of radar (classical, vertical-looking, harmonic) and the working principle of the proposed harmonic RFID transponder. Chapter 6 is a detailed description of the development and prototype implementation of a compact dual band dipole antenna suitable for use in harmonic transponders. This development was presented at the International Symposium on Antennas and Propagation (ISAP) 2015 (*ISAP2015 - International Symposium on Antennas and Propagation - Technical Program* 2015) and published as a summarised version in the conference proceedings (Hirsch et al., 2015).

In this thesis, I was able to demonstrate that the final prototype system advances the state of the art in monitoring bees using UHF RFID by achieving a higher ratio of successful to missed detections than previously reported in the literature. As a first step towards developing harmonic RFID transponders outlined in the second part, a dual-band dipole antenna with two additional parasitically coupled dipole elements for use in harmonic radar applications was developed which showed high radiation efficiency at both the fundamental frequency and the second harmonic. The design has the advantages of being compact and allowing independent control of the fundamental and second harmonic resonant frequencies.

SUGGESTIONS FOR FUTURE RESEARCH AND DEVELOPMENT

Recently, even smaller UHF RFID tags measuring just 1.25 mm × 1.25 mm × 0.55 mm have become available (Murata Manufacturing Co., Ltd., 2017). These tags are based on a newer generation of the Impinj Monza RFID IC line (Monza R6) with a slightly decreased minimum power requirement of -22.1 dBm instead of -20 dBm for the Monza 5 chip inside the Hitachi IM-PK2525 tags used in this thesis (Impinj, Inc., 2016a, 2017c). It would be interesting to characterise their performance resulting from smaller antenna and increased sensitivity relative to the IM-PK2525 tags.

One promising area for future research would be exploring other antenna configurations for RFID based insect monitoring systems, possibly based on segmented magnetic antennas for near-field UHF RFID as described by Dobkin et al. (2007), microstrip line antennas which could be designed to fit the dimensions of the bee hive entrance sim-

ilar to those intended for inclusion in smart shelves described by Medeiros et al. (2011), or metamaterial based antennas designed for spatially confined detection (Morgado et al., 2014). This could lead to detection range improvements and/or reduction of required RF power and thus further increased detection success rates, increased battery run times, and reduced RF exposure for the bees.

The latter point touches on another interesting research topic: investigating potential effects of RF radiation on bee/insect health and behaviour. This would be of particular interest in the case of the RFID monitoring system described in this thesis, because guard bees do not just cross the entrance area for entering or leaving the hive but stay there — and thus very close to the antennas and therefore in areas of high electromagnetic field strengh — for extended periods (personal observation). While many studies investigate the effect of RF radiation on insects in the context of pest control (e.g. Gaikwad, Gaikwad et al., 2015; Gaikwad, Harsh et al., 2014; Nelson et al., 1998), some deal with unintentional radiation effects on insects (e.g. Lázaro et al., 2016; Panagopoulos et al., 2004; Weisbrot et al., 2003; Balmori, 2016). Darney et al. (2016) specifically looked at the effect of RFID monitoring on honey bees and recommend limiting RFID exposure of bees to 2 h per day in the case of HF RFID.

Although we were able to improve the detection success ratio, the detection range achievable with UHF RFID technology in its current form used with such small tags remains limited to within a few cm. Current developments outside the area of standardised UHF RFID could lead to interesting alternative radio tags. Recently, experimental non-standard semi-passive long range microwave (5.8 GHz) RFID tags using tunnel diodes have been demonstrated to achieve increased reading ranges compared to ideal semi-passive tags by up to 10 times when used with a highly sensitive (-110 dBm) bistatic reader (Amato et al., 2018).

Ongoing trends such as increasing adoption of UHF RFID, e.g. in the retail sector, and increasing performance and capabilities of small, low-power embedded computing devices will likely lead to the availability of improved and cheaper hardware components which would allow to develop even more affordable RFID insect monitoring systems, bringing this research tool within range of more researchers, and ultimately leading to more available data on bee activity/behaviour. Once system cost has been substantially reduced, such systems could even become attractive for hobby bee keepers.

Another promising line of research could make use of the automatic detection of individual insects to selectively apply different treat-

ments: selected individuals could be presented with different stimuli, exposed to different substances or dosages, or even selectively captured, e.g. for lab tests. This would allow a wide range of possible selection criteria, including for example a priori or retrospective group assignments, or age cohorts.

When longer range passive RFID tags such as those proposed in the second part of this thesis or based on other technologies become available (possibly working at mm wave frequencies allowing for narrowly focused interrogation beams), it will be interesting to apply localisation techniques to gather information about individual insect movements both inside and – depending on reading range – also outside of the hive. Once reading range is sufficient for monitoring outside of the hive, the effective reading range, it could make sense to deploy an array of localising readers around the hive location to further extend the effective read range to cover an even larger area.

The affordable and easily replicable 3D printer based robotic detection pattern measurement system developed in Chapter 3 brings detailed detection pattern measurements with high spatial resolution within reach of research groups without access to specialised RF measurement equipment. Its spatial scanning range as well as its scanning speed could be increased by using one, two or three-dimensional arrays of identical probe tags to simultaneously probe multiple locations. This would require taking detailed calibration measurements to determine whether individual sensitivity variations of and mutual influences between multiple probe tags can be neglected or how they could be compensated for.

A

COMPUTING ENVIRONMENT

Data analysis within this thesis was performed using the following computing environment based on GNU/Linux (Stallman, 2007):

```
## R version 3.5.2 (2018-12-20)
## Platform: x86_64-pc-linux-gnu (64-bit)
## Running under: Ubuntu 14.04.6 LTS
##
## Matrix products: default
## BLAS: /usr/lib/openblas-base/libblas.so.3
## LAPACK: /usr/lib/lapack/liblapack.so.3.0
##
## locale:
##  [1] LC_CTYPE=en_AU.UTF-8       LC_NUMERIC=C
##  [3] LC_TIME=en_AU.UTF-8        LC_COLLATE=en_AU.UTF-8
##  [5] LC_MONETARY=en_AU.UTF-8    LC_MESSAGES=en_AU.UTF-8
##  [7] LC_PAPER=en_AU.UTF-8       LC_NAME=C
##  [9] LC_ADDRESS=C               LC_TELEPHONE=C
## [11] LC_MEASUREMENT=en_AU.UTF-8 LC_IDENTIFICATION=C
##
## attached base packages:
## [1] stats     graphics  grDevices utils     datasets  methods   base
##
## other attached packages:
##  [1] bindrcpp_0.2.2       Rcpp_1.0.1           viridis_0.5.1
##  [4] viridisLite_0.3.0    stargazer_5.2.2      cowplot_0.9.4
##  [7] units_0.6-2          ggpmisc_0.3.0        ggforce_0.1.3
## [10] ggbeeswarm_0.6.0     fst_0.8.10           latex2exp_0.4.0
## [13] kableExtra_1.0.1     magick_2.0           DiagrammeRsvg_0.1
## [16] DiagrammeR_1.0.0     ggfortify_0.4.5      broom_0.5.1
## [19] scales_1.0.0         printr_0.1           lubridate_1.7.4.9000
## [22] glue_1.3.1           magrittr_1.5         forcats_0.4.0
## [25] stringr_1.4.0        dplyr_0.7.8          purrr_0.3.2
## [28] readr_1.3.1          tidyr_0.8.3          tibble_2.1.1
## [31] ggplot2_3.1.0        tidyverse_1.2.1      knitr_1.22
## [34] pacman_0.5.0
##
## loaded via a namespace (and not attached):
##  [1] nlme_3.1-137       webshot_0.5.1      RColorBrewer_1.1-2
##  [4] httr_1.4.0         tools_3.5.2        backports_1.1.3
##  [7] R6_2.4.0           vipor_0.4.5        lazyeval_0.2.2
```

```
## [10] colorspace_1.4-1   withr_2.1.2        processx_3.3.0
## [13] tidyselect_0.2.5   gridExtra_2.3      curl_3.3
## [16] compiler_3.5.2     cli_1.1.0          rvest_0.3.2
## [19] xml2_1.2.0         influenceR_0.1.0   labeling_0.3
## [22] bookdown_0.9       callr_3.2.0        digest_0.6.18
## [25] rmarkdown_1.12     pkgconfig_2.0.2    htmltools_0.3.6
## [28] htmlwidgets_1.3    rlang_0.3.3        readxl_1.3.0
## [31] rstudioapi_0.9.0   bindr_0.1.1        visNetwork_2.0.5
## [34] generics_0.0.2     farver_1.1.0       jsonlite_1.6
## [37] rgexf_0.15.3       munsell_0.5.0      mallinfo_0.1-0
## [40] stringi_1.4.3      yaml_2.2.0         MASS_7.3-51.1
## [43] plyr_1.8.4         grid_3.5.2         parallel_3.5.2
## [46] crayon_1.3.4       lattice_0.20-38    haven_2.1.0
## [49] hms_0.4.2          ps_1.3.0           pillar_1.3.1
## [52] igraph_1.2.4       reshape2_1.4.3     XML_3.98-1.17
## [55] evaluate_0.13      V8_2.0             downloader_0.4
## [58] data.table_1.12.0  modelr_0.1.4       tweenr_1.0.1
## [61] cellranger_1.1.0   gtable_0.3.0       assertthat_0.2.1
## [64] xfun_0.6           beeswarm_0.2.3     Rook_1.1-1
## [67] brew_1.0-6
```

In addition, GNU parallel (Tange, 2015) was used in data preparation, and ParaView (Ayachit, 2017) in analysis and visualisation.

R PACKAGES USED IN DATA ANALYSIS

Aphalo, P. J. (2018). *ggpmisc: Miscellaneous Extensions to 'ggplot2'*. R package version 0.3.0.

Bache, S. M. and H. Wickham (2014). *magrittr: A Forward-Pipe Operator for R*. R package version 1.5.

Clarke, E. and S. Sherrill-Mix (2017). *ggbeeswarm: Categorical Scatter (Violin Point) Plots*. R package version 0.6.0.

Eddelbuettel, D. et al. (2019). *Rcpp: Seamless R and C++ Integration*. R package version 1.0.1.

Garnier, S. (2018a). *viridis: Default Color Maps from 'matplotlib'*. R package version 0.5.1.

Garnier, S. (2018b). *viridisLite: Default Color Maps from 'matplotlib' (Lite Version)*. R package version 0.3.0.

Henry, L. and H. Wickham (2019). *purrr: Functional Programming Tools*. R package version 0.3.2.

Hester, J. (2019). *glue: Interpreted String Literals*. R package version 1.3.1.

Hlavac, M. (2018). *stargazer: Well-Formatted Regression and Summary Statistics Tables*. R package version 5.2.2.

Horikoshi, M. and Y. Tang (2018). *ggfortify: Data Visualization Tools for Statistical Analysis Results*. R package version 0.4.5.

Iannone, R. (2016). *DiagrammeRsvg: Export DiagrammeR Graphviz Graphs as SVG*. R package version 0.1.

Iannone, R. (2018). *DiagrammeR: Graph/Network Visualization*. R package version 1.0.0.

Klik, M. (2018). *fst: Lightning Fast Serialization of Data Frames for R*. R package version 0.8.10.

Meschiari, S. (2015). *latex2exp: Use LaTeX Expressions in Plots*. R package version 0.4.0.

Müller, K. (2018). *bindrcpp: An 'Rcpp' Interface to Active Bindings*. R package version 0.2.2.

Müller, K. and H. Wickham (2019). *tibble: Simple Data Frames*. R package version 2.1.1.

Ooms, J. (2018). *magick: Advanced Graphics and Image-Processing in R*. R package version 2.0.

Pebesma, E., T. Mailund and T. Kalinowski (2018). *units: Measurement Units for R Vectors*. R package version 0.6-2.

Pedersen, T. L. (2018). *ggforce: Accelerating 'ggplot2'*. R package version 0.1.3.

R Core Team (2018). *R: A Language and Environment for Statistical Computing*. R Foundation for Statistical Computing. Vienna, Austria.

Rinker, T. and D. Kurkiewicz (2018). *pacman: Package Management Tool*. R package version 0.5.0.

Robinson, D. and A. Hayes (2018). *broom: Convert Statistical Analysis Objects into Tidy Tibbles*. R package version 0.5.1.

Spinu, V., G. Grolemund and H. Wickham (2019). *lubridate: Make Dealing with Dates a Little Easier*. http://lubridate.tidyverse.org, https://github.com/tidyverse/lubridate.

Wickham, H. (2017). *tidyverse: Easily Install and Load the 'Tidyverse'*. R package version 1.2.1.

Wickham, H. (2018). *scales: Scale Functions for Visualization*. R package version 1.0.0.

Wickham, H. (2019a). *forcats: Tools for Working with Categorical Variables (Factors)*. R package version 0.4.0.

Wickham, H. (2019b). *stringr: Simple, Consistent Wrappers for Common String Operations*. R package version 1.4.0.

Wickham, H., W. Chang et al. (2018). *ggplot2: Create Elegant Data Visualisations Using the Grammar of Graphics*. R package version 3.1.0.

Wickham, H., R. François et al. (2019). *dplyr: A Grammar of Data Manipulation*. http://dplyr.tidyverse.org, https://github.com/tidyverse/dplyr.

Wickham, H. and L. Henry (2019). *tidyr: Easily Tidy Data with 'spread()' and 'gather()' Functions*. R package version 0.8.3.

Wickham, H., J. Hester and R. Francois (2018). *readr: Read Rectangular Text Data*. R package version 1.3.1.

Wilke, C. O. (2019). *cowplot: Streamlined Plot Theme and Plot Annotations for 'ggplot2'*. R package version 0.9.4.

Xie, Y. (2017). *printr: Automatically Print R Objects to Appropriate Formats According to the 'knitr' Output Format*. R package version 0.1.

Xie, Y. (2019). *knitr: A General-Purpose Package for Dynamic Report Generation in R*. R package version 1.22.

Zhu, H. (2019). *kableExtra: Construct Complex Table with 'kable' and Pipe Syntax*. R package version 1.0.1.

BIBLIOGRAPHY

Abracon Corporation (2014a). *ARRSN5-915.000MHz Data Sheet*. URL: http://www.abracon.com/RFID-Readers/ARRSN5-915.000MHz.pdf (visited on 2018-03-02).

Abracon Corporation (2014b). *ARRUN5-915.000MHz Data Sheet*. URL: http://www.abracon.com/RFID-Readers/ARRUN5-915.000MHz.pdf (visited on 2018-03-02).

Abracon Corporation (2017). *RFID Product Training Module*. URL: https://abracon.com/uploads/resources/RFID_Tags_and_Readers_PTM.pdf (visited on 2018-04-27).

ACMA (2013). *Australian Radiofrequency Spectrum Plan 2013*. URL: http://www.acma.gov.au/~/media/Spectrum%20Transformation%20and%20Government/Information/pdf/Australian%20Radiofrequency%20Spectrum%20Plan%202013.pdf.

Amato, F., H. M. Torun and G. D. Durgin (2018). 'RFID Backscattering in Long-Range Scenarios'. In: *IEEE Transactions on Wireless Communications* 17.4, pp. 2718–2725. DOI: 10.1109/TWC.2018.2801803.

Appleby, R. and H. Wallace (2007). 'Standoff Detection of Weapons and Contraband in the 100 GHz to 1 THz Region'. In: *IEEE Transactions on Antennas and Propagation* 55.11, pp. 2944–2956. DOI: 10.1109/TAP.2007.908543.

Arruda, H. M. (2016). 'Arquitetura Computacional Para Manuseio de Dados de Clima e Movimentação de Abelhas Com Etiquetas Eletrônicas'. Mestrado Profissional em Uso Sustentável de Recursos Naturais em Regiões Tropicais. Belém, Pará, Brasil.

Australian Government (2015). *Radiocommunications Act 1992*. URL: http://www.comlaw.gov.au/Details/C2015C00143/Download (visited on 2015-06-14).

Ayachit, U. (2017). *The ParaView Guide: Updated for ParaView Version 5.4.0*. Ed. by L. Avila. In collab. with B. Geveci. Community Edition. Los Alamos: Kitware. ISBN: 978-1-930934-30-6.

Balmori, A. (2016). 'Radiotelemetry and Wildlife: Highlighting a Gap in the Knowledge on Radiofrequency Radiation Effects'. In: *Science of The Total Environment* 543, pp. 662–669. DOI: 10.1016/j.scitotenv.2015.11.073.

Bazazi, S. et al. (2016). 'Responses to Nutritional Challenges in Ant Colonies'. In: *Animal Behaviour* 111, pp. 235–249. DOI: 10.1016/j.anbehav.2015.10.021.

Beddeleem, G. et al. (2008). 'Dual-Frequency Circularly Polarized Antenna'. In: *Microwave and Optical Technology Letters* 50.1, pp. 177–180. DOI: 10.1002/mop.23028.

Berenbaum, M. R. (2016). 'Does the Honey Bee "Risk Cup" Runneth Over? Estimating Aggregate Exposures for Assessing Pesticide Risks to Honey Bees in Agroecosystems'. In: *Journal of Agricultural and Food Chemistry* 64.1, pp. 13–20. DOI: 10.1021/acs.jafc.5b01067.

Beyaert, L., U. Greggers and R. Menzel (2012). 'Honeybees Consolidate Navigation Memory during Sleep'. In: *The Journal of Experimental Biology* 215.22, pp. 3981–3988. DOI: 10.1242/jeb.075499. pmid: 23100488.

Bridge, E. S. et al. (2011). 'Technology on the Move: Recent and Forthcoming Innovations for Tracking Migratory Birds'. In: *BioScience* 61.9, pp. 689–698. DOI: 10.1525/bio.2011.61.9.7.

British Columbia Ministry of Agriculture (2015). *Bee Behaviour During Foraging*. Apiculture Bulletin 111. Abbotsford, British Columbia, Canada: Ministry of Agriculture, British Columbia. URL: https://www2.gov.bc.ca/assets/gov/farming-natural-resources-and-industry/agriculture-and-seafood/animal-and-crops/animal-production/bee-assets/api_fs111.pdf (visited on 2018-07-31).

Buettner, M. and D. Wetherall (2008). 'An Empirical Study of UHF RFID Performance'. In: *Proceedings of the 14th ACM International Conference on Mobile Computing and Networking*. ACM, pp. 223–234. ISBN: 1-60558-096-1.

Chapman, J. W., V. A. Drake and D. R. Reynolds (2011). 'Recent Insights from Radar Studies of Insect Flight'. In: *Annual Review of Entomology* 56.1, pp. 337–356. DOI: 10.1146/annurev-ento-120709-144820. pmid: 21133761.

Chapman, J. W., C. Nilsson et al. (2016). 'Adaptive Strategies in Nocturnally Migrating Insects and Songbirds: Contrasting Responses to Wind'. In: *Journal of Animal Ecology* 85.1. Ed. by J. Gill, pp. 115–124. DOI: 10.1111/1365-2656.12420.

Chapman, J. W., D. R. Reynolds and A. D. Smith (2003). 'Vertical-Looking Radar: A New Tool for Monitoring High-Altitude Insect Migration'. In: *Bioscience* 53.5, pp. 503–511.

Chapman, J. W., D. R. Reynolds, A. D. Smith et al. (2002). 'High-Altitude Migration of the Diamondback Moth Plutella Xylostella to the UK: A Study Using Radar, Aerial Netting, and Ground Trapping'. In: *Ecological Entomology* 27.6, pp. 641–650.

Chapman, J. W., D. R. Reynolds and K. Wilson (2015). 'Long-Range Seasonal Migration in Insects: Mechanisms, Evolutionary Drivers and Ecological Consequences'. In: *Ecology Letters*.

Chapman, J., D. Reynolds and A. Smith (2004). 'Migratory and Foraging Movements in Beneficial Insects: A Review of Radar Mon-

itoring and Tracking Methods'. In: *International Journal of Pest Management* 50.3, pp. 225–232.

Cheffena, M. and T. Ekman (2008). 'Modeling the Dynamic Effects of Vegetation on Radiowave Propagation'. In: *IEEE International Conference on Communications, 2008 (ICC'08)*. IEEE, pp. 4466–4471.

Chen, Y.-C., S.-Y. Chen and P. Hsu (2011). 'Modification of Radiation Patterns of First Harmonic Mode of Slot Dipole for Dual-Frequency Operation'. In: *IEEE Transactions on Antennas and Propagation* 59.7, pp. 2707–2710. DOI: 10.1109/TAP.2011.2152351.

Chilson, P. B. et al. (2012). 'Radar Aeroecology: Exploring the Movements of Aerial Fauna through Radio-Wave Remote Sensing'. In: *Biology Letters* 8.5, pp. 698–701. DOI: 10.1098/rsbl.2012.0384.

Cleveland, W. S. and S. J. Devlin (1988). 'Locally Weighted Regression: An Approach to Regression Analysis by Local Fitting'. In: *Journal of the American statistical association* 83.403, pp. 596–610.

Cole, P. H., B. Jamali and D. C. Ranasinghe (2003). *Coupling Relations in RFID Systems*. Auto-ID Center white paper. Auto-ID Center, University of Adelaide.

Colpitts, B. and G. Boiteau (2004). 'Harmonic Radar Transceiver Design: Miniature Tags for Insect Tracking'. In: *IEEE Transactions on Antennas and Propagation* 52.11, pp. 2825–2832. DOI: 10.1109/TAP.2004.835166.

Condon, J. J. and S. M. Ransom (2007). *NRAO Essential Radio Astronomy Course*. URL: https://www.cv.nrao.edu/course/astr534/ERA.shtml (visited on 2015-06-15).

CSIRO (2015). *The GIHH*. URL: https://research.csiro.au/gihh/about/ (visited on 2017-06-08).

CSIRO (2018-02-26). *CSIRO Wireless Group*. URL: https://research.csiro.au/wireless/ (visited on 2018-02-26).

CST - Computer Simulation Technology AG (2015). *CST Studio Suite 2015*. URL: https://www.cst.com/Content/Articles/article909/CST-STUDIO-SUITE-2015.pdf.

Darney, K. et al. (2016). 'Effect of High-Frequency Radiations on Survival of the Honeybee (Apis Mellifera L.)' In: *Apidologie* 47.5, pp. 703–710.

De Souza, P. et al. (2018). 'Low-Cost Electronic Tagging System for Bee Monitoring'. In: *Sensors* 18.7, p. 2124. DOI: 10.3390/s18072124.

Decourtye, A. et al. (2011). 'Honeybee Tracking with Microchips: A New Methodology to Measure the Effects of Pesticides'. In: *Ecotoxicology* 20.2, pp. 429–437. DOI: 10.1007/s10646-011-0594-4.

Doan, C. et al. (2005). 'Millimeter-Wave CMOS Design'. In: *IEEE Journal of Solid-State Circuits* 40.1, pp. 144–155. DOI: 10.1109/JSSC.2004.837251.

Dobkin, D. M., S. M. Weigand and N. Iyer (2007). 'Segmented Magnetic Antennas for Near-Field UHF RFID.' In: *Microwave Journal* 50.6.

Dobkin, D. M. (2013). *The RF in RFID: UHF RFID in Practice*. Second edition. Amsterdam: Elsevier/Newnes. 529 pp. ISBN: 978-0-12-394583-9.

Drake, V. A. and D. R. Reynolds (2012). *Radar Entomology: Observing Insect Flight and Migration*. CABI. 515 pp. ISBN: 978-1-84593-556-6.

Duroc, Y. and S. Tedjini (2018). 'RFID: A Key Technology for Humanity'. In: *Comptes Rendus Physique*. Radio Science for Humanity / Radiosciences Au Service de l'humanité Journées Scientifiques URSI-France 2017 – SophiaTech, Sophia Antipolis, France, 1–3 February 2017 / 1er–3 Mars 2017 19.1, pp. 64–71. DOI: 10.1016/j.crhy.2018.01.003.

Endou, T. et al. (2015). 'RFID Tag'. U.S. pat. 9171244 B2. Hitachi Chemical Company, Ltd. URL: http://www.google.com/patents/US9171244 (visited on 2017-02-27).

Engelke, U., P. Marendy et al. (2016). 'A Visual Analytics Framework to Study Honey Bee Behaviour'. In: *2016 IEEE 18th International Conference on High Performance Computing and Communications; IEEE 14th International Conference on Smart City; IEEE 2nd International Conference on Data Science and Systems (HPCC/SmartCity/DSS)*. 2016 IEEE 18th International Conference on High Performance Computing and Communications; IEEE 14th International Conference on Smart City; IEEE 2nd International Conference on Data Science and Systems (HPCC/SmartCity/DSS), pp. 1504–1511. DOI: 10.1109/HPCC-SmartCity-DSS.2016.0214.

Engelke, U., H. Hutson et al. (2016). 'MelissAR: Towards Augmented Visual Analytics of Honey Bee Behaviour'. In: *Proceedings of the 2016 CHI Conference Extended Abstracts on Human Factors in Computing Systems*. ACM Press, pp. 2057–2063. ISBN: 978-1-4503-4082-3. DOI: 10.1145/2851581.2892367.

Finkenzeller, K. (2010). *RFID Handbook - Fundamentals and Applications in Contactless Smart Cards, Radio Frequency Identification and near-Field Communication*. 3rd ed. Chichester, West Sussex ; Hoboken, NJ: Wiley. 462 pp. ISBN: 978-0-470-69506-7.

Gaikwad, S. V., A. N. Gaikwad et al. (2015). 'Simulation Modeling and Implementation of RF and MW System to Control the Insect Pests in Agriculture'. In: *2015 Annual IEEE India Conference (INDICON)*. 2015 Annual IEEE India Conference (INDICON), pp. 1–4. DOI: 10.1109/INDICON.2015.7443504.

Gaikwad, S. V., R. Harsh et al. (2014). 'Low Power Microwave Heating to Control Insect Pests on Tomato Plants.' In: *IMPI's*.

Gama, F. et al. (2017). 'Improving Our Understanding of the Behavior of Bees Through Anomaly Detection Techniques'. In: *Artifi-*

cial Neural Networks and Machine Learning – ICANN 2017. International Conference on Artificial Neural Networks. Lecture Notes in Computer Science. Springer, Cham, pp. 520–527. ISBN: 978-3-319-68611-0 978-3-319-68612-7. DOI: 10.1007/978-3-319-68612-7_59.

Gill, R. J., O. Ramos-Rodriguez and N. E. Raine (2012). 'Combined Pesticide Exposure Severely Affects Individual- and Colony-Level Traits in Bees'. In: *Nature* 491.7422, pp. 105–108. DOI: 10.1038/nature11585.

Gold, R. (1967). 'Optimal Binary Sequences for Spread Spectrum Multiplexing (Corresp.)' In: *IEEE Transactions on Information Theory* 13.4, pp. 619–621. DOI: 10.1109/TIT.1967.1054048.

Gomes, P. A. B. et al. (2017). 'Exploiting Recurrent Neural Networks in the Forecasting of Bees' Level of Activity'. In: *Artificial Neural Networks and Machine Learning – ICANN 2017*. International Conference on Artificial Neural Networks. Lecture Notes in Computer Science. Springer, Cham, pp. 254–261. ISBN: 978-3-319-68599-1 978-3-319-68600-4. DOI: 10.1007/978-3-319-68600-4_30.

Goulson, D., K. J. Park et al. (2013). 'Social Learning Drives Handedness in Nectar-Robbing Bumblebees'. In: *Behavioral Ecology and Sociobiology* 67.7, pp. 1141–1150. DOI: 10.1007/s00265-013-1539-0.

Goulson, D., E. Nicholls et al. (2015). 'Bee Declines Driven by Combined Stress from Parasites, Pesticides, and Lack of Flowers'. In: *Science* 347.6229, p. 1255957.

GS1 AISBL (2016). *UHF for RFID Regulations*. URL: http://www.gs1.org/docs/epcglobal/UHF_Regulations.pdf (visited on 2014-12-20).

Hajimiri, A. (2007). 'Mm-Wave Silicon ICs: Challenges and Opportunities'. In: *Custom Integrated Circuits Conference, 2007. CICC'07. IEEE*. IEEE, pp. 741–747.

Hansen, R. (1981). 'Fundamental Limitations in Antennas'. In: *Proceedings of the IEEE* 69.2, pp. 170–182. DOI: 10.1109/PROC.1981.11950.

Hansen, R. C. (2006). *Electrically Small, Superdirective, and Superconducting Antennas*. Hoboken, N.J: Wiley-Interscience. 168 pp. ISBN: 0-471-78255-6.

Harrington, R. F. (1960). 'Effect of Antenna Size on Gain, Bandwidth, and Efficiency'. In: *J. Res. Nat. Bur. Stand* 64.1, pp. 1–12.

Henry, M. et al. (2012). 'A Common Pesticide Decreases Foraging Success and Survival in Honey Bees'. In: *Science* 336.6079, pp. 348–350. DOI: 10.1126/science.1215039. pmid: 22461498.

Hirsch, P., A. R. Weily and P. de Souza (2015). 'Compact Dual-Band Parasitic Dipole Antenna for Harmonic Transponders'. In: *2015 International Symposium on Antennas and Propagation (ISAP)*. 2015

International Symposium on Antennas and Propagation (ISAP). Hobart, Australia: IEEE, pp. 1–3. ISBN: 978-4-88552-303-8.

Hitachi Chemical Co., Ltd. (2012a). *IM5-PK2525 - Ultra Small Package Tag*. URL: http://www.hitachi-chem.co.jp/english/products/ppcm/014.html (visited on 2013-05-26).

Hitachi Chemical Co., Ltd. (2012b). *IM5-PK2525 Specification - UHF RFID Ultra Small Package Tag*. URL: http://www.hitachi-chemical.com/PDF%20files/im5_pk2525.pdf (visited on 2018-01-26).

Hou, L., M. Verdirame and K. C. Welch (2015). 'Automated Tracking of Wild Hummingbird Mass and Energetics over Multiple Time Scales Using Radio Frequency Identification (RFID) Technology'. In: *Journal of Avian Biology* 46.1, pp. 1–8. DOI: 10.1111/jav.00478.

Impinj, Inc. (2016a). *Monza 5 Tag Chip Datasheet Version 3.0*. URL: https://support.impinj.com/hc/article_attachments/203268870/Monza%205%20Tag%20Chip%20Datasheet%20R3%2020160823.pdf (visited on 2018-02-09).

Impinj, Inc. (2017a). *Ao303 Mini-Guardrail Antenna Datasheet*. URL: http://support.impinj.com/hc/en-us/articles/202755678-Mini-Guardrail-Antenna-Datasheet (visited on 2018-03-22).

Impinj, Inc. (2017b). *Indy RS2000 Datasheet*. URL: https://support.impinj.com/hc/en-us/article_attachments/115002216144/Indy_RS2000_Datasheet.pdf (visited on 2018-02-10).

Impinj, Inc. (2017c). *Monza R6 Tag Chip Datasheet Version 5.0*. URL: https://support.impinj.com/hc/article_attachments/203268870/Monza%205%20Tag%20Chip%20Datasheet%20R3%2020160823.pdf (visited on 2018-02-09).

Impinj, Inc. (2016b-09-19). *Indy RS2000 Development Kit Files*. URL: http://support.impinj.com/hc/en-us/articles/206700898-Indy-RS2000-Development-Kit-Files (visited on 2016-09-19).

Intel Corporation (2017). *Documentation for the Intel® Edison Module | IoT | Intel® Software*. URL: https://software.intel.com/en-us/iot/hardware/edison/documentation (visited on 2018-03-21).

International Organization for Standardization (2006). *ISO/IEC 15693-2:2006 - Identification Cards – Contactless Integrated Circuit Cards – Vicinity Cards – Part 2: Air Interface and Initialization*. Standard. Geneva, CH: International Organization for Standardization.

International Organization for Standardization (2011). *ISO 14223-1:2011 - Radiofrequency Identification of Animals – Advanced Transponders – Part 1: Air Interface*. Standard. Geneva, CH: International Organization for Standardization.

International Organization for Standardization (2013). *ISO/IEC 18000-6:2013 - Information Technology – Radio Frequency Identifi-*

cation for Item Management – Part 6: Parameters for Air Interface Communications at 860 MHz to 960 MHz General. Standard. Geneva, CH: International Organization for Standardization.

ISAP2015 - International Symposium on Antennas and Propagation - Technical Program (2015-11-05). URL: http://isap2015.org/index.php/program/technical-program (visited on 2015-11-05).

ITU (2012). *Attenuation in Vegetation (ITU-T Recommendation P.833-7)*. ITU-T Recommendation. Geneva, Switzerland: International Telecommunications Union. URL: https://www.itu.int/dms_pubrec/itu-r/rec/p/R-REC-P.833-7-201202-S!!PDF-E.pdf (visited on 2016-05-15).

Jones, E., T. Oliphant, P. Peterson et al. (2001–). *SciPy: Open Source Scientific Tools for Python*. URL: http://www.scipy.org/.

Katib, M. K. (1976). 'Evaluation of Harmonic Generating Properties of Schottky Barrier Diodes'. Ph. D. dissertation. Durham University. 172p. URL: http://etheses.dur.ac.uk/8152/ (visited on 2015-04-08).

Kells, A. R. and D. Goulson (2000). 'Evidence for Handedness in Bumblebees'. In: *Journal of Insect Behavior*, p. 9.

King, H. E. and J. L. Wong (1972). 'An Experimental Study of a Balun-Fed Open-Sleeve Dipole in Front of a Metallic Reflector'. In: *IEEE Transactions on Antennas and Propagation* 20.2, pp. 201–204.

Kissling, D. W., D. E. Pattemore and M. Hagen (2014). 'Challenges and Prospects in the Telemetry of Insects'. In: *Biological Reviews* 89.3, pp. 511–530. DOI: 10.1111/brv.12065.

Klair, D. K., K.-W. Chin and R. Raad (2010). 'A Survey and Tutorial of RFID Anti-Collision Protocols'. In: *IEEE Communications Surveys & Tutorials* 12.3, pp. 400–421.

Klein, S. et al. (2017). 'Why Bees Are So Vulnerable to Environmental Stressors'. In: *Trends in Ecology & Evolution* 32.4, pp. 268–278. DOI: 10.1016/j.tree.2016.12.009.

Lai, A., K. M. K. H. Leong and T. Itoh (2007). 'Infinite Wavelength Resonant Antennas With Monopolar Radiation Pattern Based on Periodic Structures'. In: *IEEE Transactions on Antennas and Propagation* 55.3, pp. 868–876. DOI: 10.1109/TAP.2007.891845.

Landt, J. (2005). 'The History of RFID'. In: *Potentials, IEEE* 24.4, pp. 8–11.

Lázaro, A. et al. (2016). 'Electromagnetic Radiation of Mobile Telecommunication Antennas Affects the Abundance and Composition of Wild Pollinators'. In: *Journal of Insect Conservation* 20.2, pp. 315–324. DOI: 10.1007/s10841-016-9868-8.

Lazaro, A., R. Villarino and D. Girbau (2014). 'A Passive Harmonic Tag for Humidity Sensing'. In: *International Journal of Antennas and Propagation* 2014, pp. 1–11. DOI: 10.1155/2014/670345.

Lehpamer, H. (2012). *RFID Design Principles, Second Edition*. 2 edition. Boston: Artech House Publishers. 363 pp. ISBN: 978-1-60807-470-9.

Liebig, T. et al. (2013). 'openEMS - a Free and Open Source Equivalent-Circuit (EC) FDTD Simulation Platform Supporting Cylindrical Coordinates Suitable for the Analysis of Traveling Wave MRI Applications'. In: *International Journal of Numerical Modelling: Electronic Networks, Devices and Fields* 26.6, pp. 680–696. DOI: 10.1002/jnm.1875.

Mahbub, M. S., P. de Souza and R. Williams (2017). 'Describing Environmental Phenomena Variation Using Entropy Theory'. In: *International Journal of Data Science and Analytics* 3.1, pp. 49–60. DOI: 10.1007/s41060-016-0036-8.

Marques dos Santos, L. C. (2016). 'Otimização Do Consumo Energético Em Sistemas de Monitoramento de Colmeias Utilizando Etiquetas Eletrônicas'.

Marrocco, G. (2008). 'The Art of UHF RFID Antenna Design: Impedance-Matching and Size-Reduction Techniques'. In: *IEEE Antennas and Propagation Magazine* 50.1, pp. 66–79. DOI: 10.1109/MAP.2008.4494504.

Mascanzoni, D. and H. Wallin (1986). 'The Harmonic Radar: A New Method of Tracing Insects in the Field'. In: *Ecological entomology* 11.4, pp. 387–390.

McLean, J. (1996). 'A Re-Examination of the Fundamental Limits on the Radiation Q of Electrically Small Antennas'. In: *IEEE Transactions on Antennas and Propagation* 44.5, pp. 672–. DOI: 10.1109/8.496253.

Medeiros, C. R., J. R. Costa and C. A. Fernandes (2011). 'RFID Reader Antennas for Tag Detection in Self-Confined Volumes at UHF'. In: *IEEE Antennas and Propagation Magazine* 53.2, pp. 39–50.

Meel, J. (1999). 'Spread Spectrum (SS)'. In: *De Nayer Instituut, Hogeschool Voor Wetenschap & Kunst*.

Microelectronics Technology Inc. (2012). *MTI RU-824 UHF RFID USB Desktop Reader*. URL: http://www.mti.com.tw/upfiles/e_pro_tb01332504386.pdf (visited on 2015-02-23).

Microelectronics Technology Inc. (2014). *MTI RU-824 RFID Module Command Reference Manual v3.3*. URL: https://github.com/mti-rfid/RFID_Explorer/blob/master/MTI%20RU-824%20RFID%20Module%20Command%20Reference%20Manual%20v3.3.pdf.

Microelectronics Technology Inc. (2016). *MTI RUoo-Mo3-X RFID HP-SiP Module Command Reference Manual Version 1.1*. URL: https://raw.githubusercontent.com/mti-rfid/RFID_Explorer/master/MTI%20RU00-M03-X%20RFID%20Module%20Command%20Reference%20Manual%20v1.1.pdf (visited on 2018-03-15).

Molet, M. et al. (2008). 'Colony Nutritional Status Modulates Worker Responses to Foraging Recruitment Pheromone in the Bumblebee *Bombus Terrestris*'. In: *Behavioral Ecology and Sociobiology* 62.12, pp. 1919–1926. DOI: 10.1007/s00265-008-0623-3.

Moreau, M. et al. (2011). 'Use of Radio-Tagging to Map Spatial Organization and Social Interactions in Insects'. In: *The Journal of Experimental Biology* 214.1, pp. 17–21. DOI: 10.1242/jeb.050526. pmid: 21147964.

Morgado, T. A. et al. (2014). 'Spatially Confined UHF RFID Detection With a Metamaterial Grid'. In: *IEEE Transactions on Antennas and Propagation* 62.1, pp. 378–384. DOI: 10.1109/TAP.2013.2287027.

Mouly, M. and M.-B. Pautet (1992). *The GSM System for Mobile Communications*. Telecom publishing. ISBN: 0-945592-15-9.

Murata Manufacturing Co., Ltd. (2017). *UHF MAGICSTRAP LXMSJZNCMF-198 Datasheet Rev1.1*. URL: https://www.murata.com/~/media/webrenewal/products/rfid/rfid/uhf/uhf-smd/media-datasheets/uhf%20magicstrap%20lxmsjzncmf_198%20datasheet%20171012rev1_1.ashx?la=en-us (visited on 2018-07-16).

Nelder, J. A. and R. Mead (1965). 'A Simplex Method for Function Minimization'. In: *The computer journal* 7.4, pp. 308–313.

Nelson, S. O., P. G. Bartley and K. C. Lawrence (1998). 'RF and Microwave Dielectric Properties of Stored-Grain Insects and Their Implications for Potential Insect Control'. In: *Transactions of the ASAE* 41.3, p. 685.

Nguyen, H., S. Ketchell et al. (2017). 'Augmented Reality Based Bee Drift Analysis: A User Study'. In: *2017 International Symposium on Big Data Visual Analytics (BDVA)*. 2017 International Symposium on Big Data Visual Analytics (BDVA), pp. 1–8. DOI: 10/gfwdt6.

Nguyen, H., F. Wang et al. (2017). 'Immersive Visual Analysis of Insect Flight Behaviour'. In: Workshop on Immersive Analytics: Exploring Future Interaction and Visualization Technologies for Data Analytics at IEEE VIS 2017. Phoenix, AZ, USA.

Nikitin, P. V. and K. V. S. Rao (2008). 'Antennas and Propagation in UHF RFID Systems'. In: *2008 IEEE International Conference on RFID*. IEEE, pp. 277–288. ISBN: 1-4244-1711-2.

Nikitin, P. V. and K. V. S. Rao (2009). 'Effect of Gen2 Protocol Parameters on RFID Tag Performance'. In: *2009 IEEE International Conference on RFID*. IEEE, pp. 117–122.

Nikitin, P. V., K. V. S. Rao and S. Lazar (2007). 'An Overview of near Field UHF RFID'. In: *2007 IEEE International Conference on RFID*. Vol. 167. Citeseer.

Nikitin, P., K. V. S. Rao and S. Lam (2012). 'UHF RFID Tag Characterization: Overview and State-of-the-Art'. In: *Antenna Measurement Techniques Association Symposium (AMTA)*.

Occhiuzzi, C. and G. Marrocco (2016). 'Precision and Accuracy in UHF-RFID Power Measurements for Passive Sensing'. In: *IEEE Sensors Journal* 16.9, pp. 3091–3098. DOI: 10.1109/JSEN.2016.2526678.

Ong, A. O. and P. A. De Souza Junior (2016). 'An Electromechanical Transducer'. Pat. WO/2016/004476. Commonwealth Scientific and Industrial Research Organisation. URL: https://patentscope.wipo.int/search/en/detail.jsf?docId=WO2016004476 (visited on 2019-03-14).

Pachler, W. et al. (2013). 'A Novel Booster Antenna Design Coupled to a One Square Millimeter Coil-on-Chip RFID Tag Enabling New Medical Applications'. In: *2013 European Microwave Conference*. 2013 European Microwave Conference, pp. 1003–1006. DOI: 10.23919/EuMC.2013.6686829.

Pahl, M. et al. (2011). 'Large Scale Homing in Honeybees'. In: *PLoS ONE* 6.5, e19669. DOI: 10.1371/journal.pone.0019669.

Panagopoulos, D. J., A. Karabarbounis and L. H. Margaritis (2004). 'Effect of GSM 900-MHz Mobile Phone Radiation on the Reproductive Capacity of *Drosophila Melanogaster*'. In: *Electromagnetic Biology and Medicine* 23.1, pp. 29–43. DOI: 10/ftmvt5.

Perry, C. J. et al. (2015). 'Rapid Behavioral Maturation Accelerates Failure of Stressed Honey Bee Colonies'. In: *Proceedings of the National Academy of Sciences* 112.11, pp. 3427–3432. DOI: 10.1073/pnas.1422089112.

Pickholtz, R. L., D. L. Schilling and L. B. Milstein (1982). 'Theory of Spread-Spectrum Communications–a Tutorial'. In: *IEEE Transactions on Communications* 30.5, pp. 855–884.

Qing, X., C. K. Goh and Z. N. Chen (2009). 'Segmented Loop Antenna for UHF Near-Field RFID Applications'. In: *Electronics Letters* 45.17, pp. 872–873.

Rasilainen, K. et al. (2015). 'On Design and Evaluation of Harmonic Transponders'. In: *IEEE Transactions on Antennas and Propagation* 63.1, pp. 15–23. DOI: 10.1109/TAP.2014.2366193.

Rennings, A. et al. (2008). 'Equivalent Circuit (EC) FDTD Method for Dispersive Materials: Derivation, Stability Criteria and Application Examples'. In: *Time Domain Methods in Electrodynamics*. Springer, pp. 211–238.

Reynolds, D. R. et al. (2005). 'Radar Studies of the Vertical Distribution of Insects Migrating over Southern Britain: The Influence of Temperature Inversions on Nocturnal Layer Concentrations'. In: *Bulletin of entomological research* 95.03, pp. 259–274.

Riley, J. R., A. D. Smith et al. (1996). 'Tracking Bees with Harmonic Radar'. In: *Nature* 379.6560, pp. 29–30. DOI: 10.1038/379029b0.

Riley, J. R. and A. D. Smith (2002). 'Design Considerations for an Harmonic Radar to Investigate the Flight of Insects at Low Altitude'. In: *Computers and Electronics in Agriculture* 35.2–3, pp. 151–169. DOI: 10.1016/S0168-1699(02)00016-9.

Robinson, E. J. H. et al. (2009). 'Radio Tagging Reveals the Roles of Corpulence, Experience and Social Information in Ant Decision Making'. In: *Behavioral Ecology and Sociobiology* 63.5, pp. 627–636. DOI: 10.1007/s00265-008-0696-z.

Rogers, N. C. et al. (2002). *A Generic Model of 1-60 GHz Radio Propagation through Vegetation - Final Report*. Radio Agency, UK. URL: http://www.nashville.dyndns.org:800/WirelessDownloads/propagation/foliage%20effects/vegetation-finalreportv1_0.pdf (visited on 2015-03-09).

Rossum, G. van (1995). 'Python Reference Manual'. In: (CS-R9525), pp. ii + 54.

Schneider, C. W. et al. (2012). 'RFID Tracking of Sublethal Effects of Two Neonicotinoid Insecticides on the Foraging Behavior of Apis Mellifera'. In: *PLoS ONE* 7.1. Ed. by N. Chaline, e30023. DOI: 10.1371/journal.pone.0030023.

Seemayer, S. (2016). *ParOpt: Generic Command-Line Parameter Optimization*. URL: https://github.com/sseemayer/ParOpt (visited on 2018-04-15).

Shahpari, M. (2015). 'Fundamental Limitations of Small Antennas'. Ph. D. dissertation. Griffith University. 136 pp.

Shamoun-Baranes, J. et al. (2014). 'Continental-Scale Radar Monitoring of the Aerial Movements of Animals'. In: *Movement Ecology* 2.1, p. 9. DOI: 10.1186/2051-3933-2-9.

Shannon, C. E. (2001). 'A Mathematical Theory of Communication'. In: *ACM SIGMOBILE Mobile Computing and Communications Review* 5.1, pp. 3–55.

Shaw, J. A. (2013). 'Radiometry and the Friis Transmission Equation'. In: *American Journal of Physics* 81.1, pp. 33–37. DOI: 10.1119/1.4755780.

Siles, G., J. Riera and P. Garcia-del-Pino (2015). 'Atmospheric Attenuation in Wireless Communication Systems at Millimeter and THz Frequencies [Wireless Corner]'. In: *IEEE Antennas and Propagation Magazine* 57.1, pp. 48–61. DOI: 10.1109/MAP.2015.2401796.

Smith, A. D., J. R. Riley and R. D. Gregory (1993). 'A Method for Routine Monitoring of the Aerial Migration of Insects by Using a Vertical-Looking Radar'. In: *Philosophical Transactions: Biological Sciences* 340.1294, pp. 393–404. JSTOR: 3030172.

Stallman, R. (2007). 'Linux and the GNU System'. In:

Streit, S. et al. (2003). 'Automatic Life-Long Monitoring of Individual Insect Behaviour Now Possible'. In: *Zoology* 106.3, pp. 169–171.

Ström, E., T. Ottosson and A. Svensson (2002). *An Introduction to Spread Spectrum Systems*. Technical report R016/2002. Chalmers

University of Technology, Goteborg, Sweden. URL: http://www.mayigg.com/UploadFiles/TA_20130406161203R3Y2.pdf (visited on 2015-06-11).

Sumner, S. et al. (2007). 'Radio-Tagging Technology Reveals Extreme Nest-Drifting Behavior in a Eusocial Insect'. In: *Current Biology* 17.2, pp. 140–145. DOI: 10.1016/j.cub.2006.11.064.

Susanto, F. et al. (2018). 'Addressing RFID Misreadings to Better Infer Bee Hive Activity'. In: *IEEE Access* 6, pp. 31935–31949. DOI: 10.1109/ACCESS.2018.2844181.

Taflove, A. and S. C. Hagness (2005). *Computational Electrodynamics: The Finite-Difference Time-Domain Method, Third Edition*. 3 edition. Boston: Artech House. 1038 pp. ISBN: 978-1-58053-832-9.

Tahir (nee Mariam), N. (2013). 'Towards the Development of Millimetre Wave Harmonic Transponders for Tracking Small Insects'. Ph. D. dissertation. Sydney, Australia: University of Sydney. 249 pp. URL: http://db.acfr.usyd.edu.au/content.php/292.html?publicationid=1073&displaypage=1 (visited on 2015-02-10).

Tahir, N. and G. Brooker (2009). 'Efficient Design of Harmonic Transponder for UAV Based Harmonic Tracker'. In: *5th International Conference on Intelligent Sensors, Sensor Networks and Information Processing (ISSNIP 09)*. Melbourne, Australia.

Tahir, N. and G. Brooker (2011). 'Recent Developments and Recommendations for Improving Harmonic Radar Tracking Systems'. In: *Proceedings of the 5th European Conference on Antennas and Propagation (EUCAP)*. IEEE, pp. 1531–1535.

Tahir, N. and G. Brooker (2015). 'Toward the Development of Millimeter Wave Harmonic Sensors for Tracking Small Insects'. In: *IEEE Sensors Journal* 15.10, pp. 5669–5676. DOI: 10.1109/JSEN.2015.2445933.

Tange, O. (2015). *GNU Parallel 20150322 ('Hellwig')*. DOI: 10.5281/zenodo.16303. URL: https://zenodo.org/record/16303 (visited on 2018-03-08).

Tenczar, P. et al. (2014). 'Automated Monitoring Reveals Extreme Interindividual Variation and Plasticity in Honeybee Foraging Activity Levels'. In: *Animal Behaviour* 95, pp. 41–48. DOI: 10.1016/j.anbehav.2014.06.006.

Thomas, S. J. et al. (2013). 'Rich-Media Tags: Battery-Free Wireless Multichannel Digital Audio and Image Transmission with UHF RFID Techniques'. In: *2013 IEEE International Conference on RFID*. IEEE, pp. 231–236. ISBN: 1-4673-5750-2.

Thompson, H. et al. (2016). 'Thiamethoxam: Assessing Flight Activity of Honeybees Foraging on Treated Oilseed Rape Using Radio Frequency Identification Technology: Effects of Thiamethoxam on Honeybee Foraging'. In: *Environmental Toxicology and Chemistry* 35.2, pp. 385–393. DOI: 10.1002/etc.3183.

Tsai, Z.-M. et al. (2013). 'A High-Range-Accuracy and High-Sensitivity Harmonic Radar Using Pulse Pseudorandom Code for Bee Searching'. In: *IEEE Transactions on Microwave Theory and Techniques* 61.1, pp. 666–675. DOI: 10.1109/TMTT.2012.2230020.

Van Geystelen, A. et al. (2016). 'Track-a-Forager: A Program for the Automated Analysis of RFID Tracking Data to Reconstruct Foraging Behaviour'. In: *Insectes Sociaux* 63.1, pp. 175–183. DOI: 10.1007/s00040-015-0453-z.

Van Tuyl, R. L. (1996). 'Unlicensed Millimeter Wave Communications. a New Opportunity for MMIC Technology at 60 GHz'. In: *18th Annual Gallium Arsenide Integrated Circuit (GaAs IC) Symposium, 1996. Technical Digest 1996.* IEEE, pp. 3–5.

Vandenbosch, G. A. E. et al. (2016). 'Bridging the Simulations-Measurements Gap: State of the Art [Meeting Reports]'. In: *IEEE Antennas and Propagation Magazine* 58.6, pp. 12–14. DOI: 10.1109/MAP.2016.2610189.

Vinatier, F. et al. (2010). 'Radiotelemetry Unravels Movements of a Walking Insect Species in Heterogeneous Environments'. In: *Animal Behaviour* 80.2, pp. 221–229. DOI: 10.1016/j.anbehav.2010.04.022.

Wamba, S. F., A. Anand and L. Carter (2013). 'A Literature Review of RFID-Enabled Healthcare Applications and Issues'. In: *International Journal of Information Management* 33.5, pp. 875–891.

Warren, R. (2017). 'Optimising Radio Frequency Identification Systems for Monitoring Variation in Individual Honey Bee Behaviour'. Honours thesis. Hobart, Australia: University of Tasmania.

Weil, E. D. and S. Levchik (2004). 'A Review of Current Flame Retardant Systems for Epoxy Resins'. In: *Journal of Fire Sciences* 22.1, pp. 25–40. DOI: 10.1177/0734904104038107.

Weily, A. R., D. Ostry and M. E. Johnson (2015). 'Harmonic Radar Transponder for Microsensing Systems'. In: *2015 International Symposium on Antennas and Propagation (ISAP)*. 2015 International Symposium on Antennas and Propagation (ISAP), pp. 1–2.

Weisbrot, D. et al. (2003). 'Effects of Mobile Phone Radiation on Reproduction and Development in Drosophila Melanogaster'. In: *Journal of Cellular Biochemistry* 89.1, pp. 48–55. DOI: 10.1002/jcb.10480.

Wheeler, H. (1947). 'Fundamental Limitations of Small Antennas'. In: *Proceedings of the IRE* 35.12, pp. 1479–1484. DOI: 10.1109/JRPROC.1947.226199.

Williams, R. (2016). 'Swarm Sensing Modelling'. In: *CSIRO Data Access Portal*. DOI: 10.4225/08/57A7DE31147FA.

Wood, C. R. et al. (2009). 'Cloud-Radar Observations of Insects in the UK Convective Boundary Layer'. In: *Meteorological Applications* 16.4, pp. 491–500.

Woodgate, J. L. et al. (2016). 'Life-Long Radar Tracking of Bumblebees'. In: *PloS one* 11.8, e0160333.

Woodgate, J. L. et al. (2017). 'Continuous Radar Tracking Illustrates the Development of Multi-Destination Routes of Bumblebees'. In: *Scientific reports* 7.1, p. 17323.

Zeljami, K. et al. (2012). 'Characterization and Modeling of Schottky Diodes up to 110 GHz for Use in Both Flip-Chip and Wire-Bonded Assembled Environments'. In: *Progress In Electromagnetics Research* 131, pp. 457–475.

Zhang, C. et al. (2013). 'Open-Source 3D-Printable Optics Equipment'. In: *PloS one* 8.3, e59840.

Zhu, H. et al. (2011). 'Capability of Patch Antennas in a Portable Harmonic Radar System to Track Insects'. In: *Transactions of the ASABE* 54.1, pp. 355–362. DOI: 10/gfw2kk.

Zydlewski, G. B. et al. (2006). 'Remote Monitoring of Fish in Small Streams'. In: *Fisheries* 31.10, pp. 492–502. DOI: 10.1577/1548-8446(2006)31[492:RMOFIS]2.0.CO;2.